Structural traps and seals for expanding CO_2 storage in the northern Horda Platform, North Sea

Osmond, Johnathon L.[1]*, Mulrooney, Mark J.[1], Holden, Nora[1], Skurtveit, Elin[2,1], Jan Inge Faleide[1], and Alvar Braathen[1]

1) Department of Geosciences, University of Oslo, Sem Sælands vei 1 0371 Oslo, Norway
2) Integrated Geotechnology, Norwegian Geotechnical Institute, Sognsveien 72, 0806 Oslo, Norway
*Corresponding author (johnathon.osmond@gmail.com)

This manuscript is the preprint version submitted to the AAPG Bulletin for peer review in June 2021. Please note that this preprint version has undergone peer-reviewed after June 2021, but has yet to be formally accepted for publication. Subsequent versions of this manuscript have been peer-reviewed, and may have different content from this preprint version. Upon acceptance, a 'Published DOI' from the publisher will be provided, and later, a final preprint version of this manuscript will be available no earlier than 12 months after publication. Please contact the primary and corresponding author, Johnathon L. Osmond, for questions or comments related to the work.

Structural traps and seals for expanding CO_2 storage in the northern Horda Platform, North Sea

Osmond, J. L.[1]*, Mulrooney, M. J.[1], Holden, N.[1], Skurtveit, E.[2,1], J. I. Faleide[1], and A. Braathen[1]

1) University of Oslo

2) Norwegian Geotechnical Institute

*Corresponding author

Submitted to the AAPG Bulletin Thematic Set on Geological Controls on Carbon Subsurface Utilization and Storage

Key words: structural traps, North Sea, CCS, CO_2 storage, top seal, fault seal, saline aquifers, storage complex

Acknowledgements

This publication has been produced with support from the Norwegian CCS Research Centre (NCCS) under the Centres for Environment-friendly Energy Research (FME) in Norway. The authors acknowledge the following partners for their contributions: Aker Solutions, Ansaldo Energia, CoorsTek Membrane Sciences, EMGS, Gassco, Krohne, Larvik Shipping, Lundin, Norcem, Norwegian Oil and Gas, Quad Geometrics, TotalEnergies, Vår Energi, and the Research Council of Norway (257579/E20). The workflows herein were conducted in collaboration with the Northern Lights project (Equinor, TotalEnergies, and Shell). We gratefully acknowledge Schlumberger for the provision of academic licenses for the Petrel E&P Software Platform and Petroleum Experts for the provision of academic licenses for the Move Software

Suite. Additional thanks are directed to the 3D seismic data providers, CGG, and Equinor for contributing proprietary well data. The Norwegian Petroleum Directorate contributed other data. The authors also wish to thank reviewers for critically reading the manuscript.

Abstract

The maturation of geological CCS along the Norwegian Continental Shelf is ongoing in the Norwegian North Sea, however, more storage sites are needed to reach climate mitigation goals by 2050. In order to augment the Aurora site and expand CO_2 storage in the northern Horda Platform, regional traps and seals must be assessed to better understand the area's potential. Here, we leverage wellbore and seismic data to map storage aquifers, identify structural traps, and assess possible top and fault seals associated with Lower and Upper Jurassic storage complexes in four major fault blocks. With respect to trap and seal, our results maintain that both prospective intervals represent viable CO_2 storage options in various locations of each fault block. Mapping, modeling, and formation pressure analyses indicate that top seals are present across the entire study area, and are sufficiently thick over the majority of structural traps. Across-fault juxtaposition seals are abundant, but dominate the Upper Jurassic storage complexes. Lower Jurassic aquifers, however, are often upthrown against Upper Jurassic aquifers, but apparent across fault pressure differentials and moderate to high shale gouge ratio values correlate, suggesting fault rock membrane seal presence. Zones of aquifer self-juxtaposition, however, are likely areas of poor seal along faults. Overall, our results provide added support that the northern Horda Platform represents a promising location for expanding CO_2 storage in the North Sea, carrying the potential to become a future injection hub for CCS in northern Europe.

Introduction

The implementation of subsurface geological CCS and CCUS technologies is recognized as a necessary step towards significantly reducing global carbon dioxide emissions by the year 2050 (IPCC, 2014; IEA, 2015; IPCC, 2018). Among the many other facets of developing a CCS or CCUS operation, subsurface geological characterization represents a critical part of the technical work involved. Much like play elements in petroleum geology (i.e., Magoon and Dow, 1994), geological elements of a CO_2 storage complex must be established in order to advance the geological concept of a given project. Here, we define a CO_2 storage complex as an interval of rock comprised of both storage formations (saline aquifers herein) and corresponding seal formations, where either can be the sum of multiple formations, if applicable. Over time, geological sequestration of CO_2 is achieved via four trapping mechanisms, including structural (i.e., both structural and stratigraphic), residual, dissolution, and mineral trapping (i.e., IPCC, 2005; Ringrose et al., 2021). While only representing one facet of the process, structural traps specifically are easily mappable, and lend themselves to predictable migration pathways and accumulation points. By analogy, structural traps also contain the majority of global hydrocarbon accumulations (USGS, 2000), many of which are faulted, implying that such lateral seals can be effective. Faults can provide lateral seals simply by way of juxtaposing low-permeability sealing formations onto higher-permeability storage formations (i.e., Allan, 1989). Additionally, the fault rock itself can act as a membrane seal for across-fault migration (Watts, 1987; Fisher and Knipe, 2001), which is most important where faults self-juxtapose the storage formation or displace the storage formation onto another porous and permeable formation. Generally speaking, traps overlain by thin seals or rely on fault rock membrane seal for containment of injected CO_2 are perceived as less favorable than those with thick top seals and faults providing sizeable low-permeability juxtapositions against the storage formation, but the former can present significant storage potential.

Along the Norwegian Continental Shelf, successful CO_2 storage associated with hydrocarbon production has taken place since 1996 (i.e., Sleipner field; Furre et al. 2017), but a novel full CCS value-chain (sequestration only) is scheduled to commence in 2024 (NMPE, 2020). This value-chain has been partitioned into two primary segments, where industrially-sourced CO_2 from East Norway will be captured and transported via marine vessel to a processing center in West Norway (Naturgassparken) under project Longship. Thereafter, the operators of the Northern Lights JV DA (Equinor, Shell, and Total Energies) will deliver the processed CO_2 offshore via submarine pipeline to an injection site in the northern Horda Platform area of the North Sea (Figure 1). More specifically, injection of supercritical CO_2 will take place in a siliciclastic Lower Jurassic storage complex at the Aurora site via verification well 31/5-7 (also known as Eos) just south of Troll West and within the EL001 exploitation license area, with northward up-dip migration through the saline aquifer occurring over time (e.g., Furre et al., 2019; 2020). The total storage potential of the aquifer in and around this locality is estimated to be 1.78 Gt (NPD, 2011), and the initial anticipated injection rate at the Aurora site is approximately 1.5 Mt/a, but will be increased to 5 Mt/a or more after the initial project phase (NMPE, 2020). While the concept for injection and monitoring within the Lower Jurassic storage complex at Aurora has been well-established by operators (e.g., Furre et al., 2020), less is understood about its potential in other areas within the region. Above this Lower Jurassic storage complex, hydrocarbon accumulations, such as the Troll field, are located in faulted Upper

Jurassic sandstone traps capped by proven seals (Spencer and Larsen, 1990) (see Figure 1). Therefore, Upper Jurassic aquifers represent a second possible CO_2 storage complex, but since the existing fields are capable of producing over several decades (e.g., Gudmestad, 2019), uncharged structural traps in the region may offer more immediate storage opportunities. The upper-most formations of this interval is encountered throughout the northern Horda Platform and areas to the north, and has an estimated total storage capacity of nearly 18 Gt (NPD, 2011). Unfortunately, only limited work has been done to advance the storage concept, with the exception of a few recent structural, seismological, and petrophysical studies (e.g., Mulrooney et al., 2020; Osmond et al., 2020; Rahman et al., 2020; Fawad et al., 2021a, b; Wu et al,. 2021a).

Despite the development of the Aurora site, which indeed, is a sizeable project, many more locations must be assessed and matured into storage sites to upscale CCS operations and reach global climate mitigation targets (GCCSI, 2020; Zahasky and Krevor, 2020). With that in mind, the developing infrastructure at the Aurora site could prove strategic for expanding CCS activity in the northern Horda Platform. Before expansion can take place, though, the subsurface geology will need to be evaluated further, where CO_2 storage complexes are characterized and storage prospects are identified. In an effort to contribute towards this task, we present the Lower and Upper storage complexes, map aquifers and corresponding structural traps, and assess top and lateral seal presence in order to demonstrate additional CO_2 storage prospectivity within the northern Horda Platform beyond the Aurora storage site. We utilize data from a high quality 3D seismic reflector survey and newly-drilled wellbores to interpret and map key stratigraphic horizons and faults in the region. Storage aquifer and seal presence is determined by qualitative analyses of wellbore data and thickness mapping based on seismic interpretations. We then go on to define structural traps within four major fault blocks located in the study area. Finally, fault and inter-formational seal presence for three thick-skinned fault zones and their corresponding fault blocks are assessed on the basis of across-fault juxtaposition relationships, formation pressure data, and fault rock membrane seal analysis in order to qualify the two storage complexes across the four major fault blocks.

Geological setting

Regional structural and stratigraphic framework

The Horda Platform is a roughly 30,000 km^2 Mesozoic sedimentary depocenter located off the coast of West Norway in the northern North Sea Rift Basin (Glennie, 1987; Ziegler, 1990) (Figures 1, 2A). The north–south trending platform is a structural high bounded by the Viking Graben (e.g., Badley et al., 1988; Ziegler, 1990; Odinsen et al., 2000) to the west, the Øygarden Fault Zone (also referred as Øygarden Fault Complex; e.g., Færseth et al., 1995) to the east, the southern extent of the Stord Basin (e.g., Jarsve et al., 2014a; Fazlikhani et al., 2020) to the south, as well as to the north along the Uer and Lomre terraces (e.g., Briseid et al., 1998; Phillips et al., 2019; Zhong et al., 2020; Tillmans et al., 2021). After terrane accretion resulting from both the Caledonian (460–400 Ma) and Variscan (400–300) orogenies (Ziegler, 1975, 1982; Frost et al., 1981; Gee et al., 2008), followed by gravitational collapse later in the Devonian (e.g., Norton, 1986; Fossen,1992; Fossen and Hurich, 2005; Vetti and Fossen, 2012; Gabrielsen et al., 2015; Fossen et al., 2017; Wiest et al., 2020), the North Sea Rift Basin formed as a result of multiple phases of rift activity that took place throughout the Mesozoic and into the Early Cenozoic Era (Glennie, 1987; Ziegler, 1990; Bartholomew et al., 1993; Lepercq, et al. 1996; Odinsen, et al., 2000; Bell et al., 2014; Phillips et al., 2019). A Permian-Triassic rift phase associated with east–

west extension resulted in the formation of large, half-grabens bounded by thick-skinned, north–south oriented normal faults with listric geometries (e.g., Steel and Ryseth, 1990; Færseth et al., 1996; Fazlikhani et al., 2017) (Figures 1, 2A, 3). The Troll, Svartalv, Tusse, Vette, and Øygarden fault zones bound prominent fault blocks of the northern Horda Platform, and demarcate areas of focus for our study. Non-marine deposition of the Hegre Group (Vollset and Doré, 1984; Larvik, 2006) (Figure 2B) took place throughout this major pulse of extension, forming syn-rift siliciclastic wedges up to 3 km thick within the Troll, Svartalv, Tusse, and Smeaheia fault blocks, which progressively deepen to the west (Steel and Ryseth, 1990; Ravnås et al., 2000; Jarsve et al., 2014a; Würtzen et al., in review). Towards the end of the Triassic and into the Jurassic Period, the depositional environment gradually transitioned towards a marginal marine setting as rifting activity waned and the Statfjord Group was deposited (e.g., Røe and Steel, 1985; Stewart et al., 1995; Lervik, 2006) (Figure 2B). In the northern Horda Platform, fluvial-deltaic Dunlin (e.g., Marjanac and Steel, 1997; Chamock et al., 2001) and Brent (e.g., Helland-Hansen et al., 1992; Fjellanger et al., 1996) groups characterize the Early to Middle Jurassic sedimentary record, exhibiting only minor fault influence during a period of post-rift thermal subsidence (e.g., Bartholomew et al., 1993; Bell et al., 2014; Whipp et al., 2014) (Figure 2B, 3B).

A second major phase of rifting transpired from the Late Jurassic through Early Cretaceous associated with cooling and deflation of the North Sea dome (e.g., Underhill and Partington, 1993; Phillips et al., 2019), along with far-field stress perturbations from rifting in the North Atlantic. While thick-skinned normal faults inherited from the Permian-Triassic rift phase were reactivated, slip rates and displacements along these faults were lower during the Late Jurassic through Early Cretaceous phase (Odinsen et al., 2000; Bell et al., 2014; Phillips et al., 2019; Fazlikhani et al., 2020). Furthermore, both northeast–southwest and northwest–southeast trending thin-skinned faults with displacements under 100 m formed oblique to the dominant north–south trending structures (Figure 3B) (Whipp et al., 2014; Duffy et al., 2015; Deng et al., 2017; Mulrooney et al., 2020). A fully marine depositional environment prevailed during much of the second rift phase (e.g., Nøttvedt et al., 1995; Stewart et al., 1995), resulting in the deposition of the siliciclastic Viking Group (e.g., Vollset and Doré, 1984; Sneider et al., 1995; Stewart et al., 1995; Husmo et al., 2002), and later, the mixed siliciclastic and carbonate sedimentary successions of the Cromer Knoll and Shetland groups (e.g., Isaksen and Tonstad, 1989; Rattey and Hayward, 1993; Bugge et al., 2001; Gradstein and Waters, 2016) (Figures 2B, 3B). Subsurface interpretation and modeling suggests that the footwall crests of tilted fault blocks were often subaerially exposed (e.g., Rattey and Hayward, 1993; Færseth, 1996; Gabrielsen et al., 2001) as syn-rift deposition occurred below sea-level in hanging-wall depocenters (e.g., Ravnås et al., 2000; Whipp et al., 2014; Duffy et al., 2015), and leading to the formation of an archipelago in the northern North Sea until the end of the Early Cretaceous (Roberts et al., 2019). More broadly, Jurassic–Cretaceous syn-rift to post-rift events led to the erosion of local structural highs and the formation of various types of onlap relationships and unconformities throughout the northern North Sea (e.g., Rawson and Riley, 1982; Yielding, 1990; Kyrkjebø et al., 2004). While still often referred to as a single Base Cretaceous Unconformity (i.e., BCU; Fyfe et al., 1981; Rawson and Riley, 1982), the term North Sea Unconformity Complex (NSUC) proposed by Kyrkjebø and others (2004) is likely more accurate given its time-transgressive and heterogeneous nature, and because it does not represent a single event boundary between Jurassic and Cretaceous strata.

In much of the northern North Sea, rifting ceased by end of the Early Cretaceous (e.g., Færseth, 1996; Coward et al., 2003; Bell et al., 2014; Phillips et al., 2019), however, displacement continued to accrue along many faults during the late Paleocene or possibly early Eocene epochs (Bell et al., 2014; Whipp et al., 2014; Mulrooney et al., 2020) (Figure 3B), primarily as a result of thermal subsidence and compaction of sedimentary deposits, but possibly also due to local or far-field stress perturbations. Marine conditions dominated during the Paleogene and Neogene history of the northern Horda Platform area (e.g., Jordt et al., 2000), where westward-dipping, siliciclastic sediments of the Rogaland and Hordaland groups (e.g., Isaksen and Tonstad, 1989; Eidvin and Rundberg, 2007; Brunstad et al., 2013) were deposited into a thermally subsiding basin (Faleide et al., 2002; Anell et al., 2012; Jarsve et al., 2014b) (Figures 2B, 3B). Polygonal fault systems have been observed and described within much of the Cenozoic interval of the northern North Sea (e.g., Clausen et al., 1999; Wrona et al., 2017), and are thought to have nucleated during in the Eocene to early Oligocene. Within the northern Horda Platform, these are generally confined to the Upper Cretaceous through middle Miocene stratigraphy (Wrona et al., 2017; Mulrooney et al., 2020), but occasionally displace early glacial to marine Quaternary deposits towards the base of the Nordland Group (e.g. Eidvin and Rundberg, 2007; Eidvin et al., 2014) (Figure 2B) or link with deeper faults of tectonic origin (Figure 3B). Regardless of location, no faults in the region displace the Quaternary-aged Upper Regional Unconformity (URU; e.g., Sejrup et al., 1995; Ottesen et al., 2018) surface, and no discernable faulting has been observed above it, indicating a lack of such deformation since the early Pleistocene (Sejrup et al., 1995) (Figures 2B, 3B). Pockmarks have been documented at the seafloor surface, which have been attributed to the destabilized methane hydrates during the last deglaciation period over

10,000 years ago (Forsberg et al., 2007; Mazzini et al., 2016, 2017), but no correlation to underlying geologic features has been made to date.

Jurassic CO_2 storage complexes

Hydrocarbon exploration in northern Horda Platform area has provided considerable subsurface data and knowledge (i.e., Knag et al., 1995; Kombrink and Patruno, 2020) that has been leveraged towards evaluating regional CO_2 storage potential (e.g., NPD, 2011). Two suitable storage complexes have previously been identified (NPD, 2011; Furre et al., 2019), and are our focus herein (Figure 2B, 3C). The first is the Lower Jurassic storage complex, which is comprised entirely of Dunlin Group formations (Vollset and Doré, 1984; Marjanac and Steel, 1997; Chamock et al., 2001). Sandstones of the Johansen Formation are of good to excellent reservoir quality (Bergmo et al., 2009; Sundal et al., 2016), and are envisaged as the principal storage aquifer at the Aurora injection site (Furre et al., 2019, 2020). However, another suitable Lower Jurassic storage aquifer is represented by the Cook Formation sandstones upsection, but is separated from the underlying Johansen Formation by Amundsen Formation marine siltstones and mudstones (Amundsen Formation unlabeled, but with minor demarcations in Figure 2). The Amundsen Formation represents the distal time equivalent formation to the Johansen proximal (e.g., Vollset and Doré, 1984; Marjanac and Steel, 1996; Sundal et al., 2016). In the northern Horda Platform, it is present as a lower unit between the Johansen Formation and Statfjord Group, and an upper unit between the Johansen and Cook formations (Figure 2B). However, the upper Amundsen and Cook units become absent in the eastern side of the northern Horda Platform (e.g., Sundal et al., 2016), and are often too thin to map using seismic surveys. For the sake of practicality, we amalgamate the Amundsen, Johansen, and Cook formations into the gross storage aquifer of the Lower Jurassic storage complex (see Figures 2B, 3B, 3C). Above this gross storage aquifer lies the Drake Formation, of which its lower marine shales and mudstones will provide the primary seal for injected CO_2 at Aurora, but it is apparent that the upper part of the Drake formation coarsens upward towards the boundary between it and the Brent Group sandstones and siltstones (Figure 2B) (e.g., Steel, 1993; Marjanac and Steel, 1997; Holden, 2021).

Above the Lower Jurassic storage complex and Brent Group lies the prospective Upper Jurassic storage complex (Figures 2B, 3C). The Viking Group hosts a set of stacked deltaic sandstone formations; the Krossfjord, Fensfjord, and Sognefjord formations, while distal, fine-grained equivalents of the Heather Formation inter-tongue between them (e.g., Dreyer et al., 2005; Holgate et al., 2013; Patruno et al., 2015) (Heather Formation unlabeled, but with minor demarcations in Figure 2). Hydrocarbon accumulations occur within Sognefjord and Fensfjord formations in the Troll (East and West), Brage, and Oseberg fields (e.g., Gray, 1987; Nipen, 1987; Bolle, 1992; Hagen and Kvalheim, 1992; Høye et al., 1994; Johnsen et al., 1995). Heather Formation lithologies are too fine-grained for CO_2 storage, but are not readily mappable from seismic or wellbore data. Therefore, we define the gross Upper Jurassic storage aquifer to be confined between the top of the Brent Group (i.e., base Heather or Krossfjord Formation) to the base of the Draupne Formation (i.e., top Heather or Sognefjord Formation). Above this gross storage aquifer, the Draupne Formation mudstones and shales at the top of the Viking Group represents the primary seal. Both Troll East and West fields are sealed by the Draupne formation, however, areas along their structural crests are eroded, requiring the marls and calcareous mudstones of the Lower Cretaceous Cromer Knoll and Upper Cretaceous Shetland groups, as well as the lower part of the Paleocene Rogaland Group (Våle and Lista formations) (e.g., Martinsen, et al., 2005; Dmitrieva et al., 2012, 2018) to provide the seal (Spenser and Larsen, 1990; Bolle, 1992; Osmond et al., 2020). Consequently, the gross seal is comprised of the Draupne through Lista formations, where the Cretaceous interval is considered the secondary seal, and the Våle and Lista formations as a tertiary seal. It must be noted that since the exact position of the top Cromer Knoll Group reflector has little bearing on our analysis of Upper Jurassic seals herein, we instead have interpreted a near-top Cromer Knoll Group seismic horizon correlating with the top of the Svarte Formation at the base of the Shetland Group, similar to Wu and others (2021a), due to its high reflector quality. With respect to the Brent and Statfjord groups, we do not consider them to offer viable storage complexes at this time, as no thick seal of regional significance has been identified immediately above potential storage aquifers. Consequently, we classify them here as intermediate aquifers.

Data and methodology

Dataset

The data available for our study of potential seals for CO_2 storage in the northern Horda Platform come in the form of a 3D seismic reflection survey and wellbore penetrations (Figure 1). The seismic data is a subset of the CGG NVG prestack depth-migrated 3D seismic data acquired in 2016, and later reprocessed in 2018**.** The volume consists of 5832.3 km^2 of data, imaging depths from 0–20 km below sea level**,** and is characterized by a zero-phase wavelet and SEG normal polarity (increase in acoustic impedance corresponding to a reflection peak)**.** The vertical image resolution is roughly 5–10 m within the Jurassic through Paleocene interval of interest, whereas the horizontal resolution is limited by the 37.5 m sub-sample line spacing, as it is larger than the migrated Fresnel zone for the survey. Inline and cross-line bin size and line spacing are 12.5 m and 18.75 m, respectively. Inlines are oriented north–south and cross-lines are oriented east–west, with cross-lines approximately orthogonal to large block-bounding faults (e.g., Vette Fault Zone). Most well data, including locations, trajectories, formation tops, formation pressure measurements, completion reports, and digital log curves were acquired online from the Norwegian Petroleum Directorate (NPD) Factpages and DISKOS data repository. As of April 2021, a total of 106 exploration wellbores have been drilled within the outline of the seismic data used in this study, including sidetracks. From the total, 50 wells were used to aid interpretation or provide modeling constraints due to their position within the Horda Platform and along its borders and penetration depth. For the planned injection well at Aurora (31/5-7), data is publicly available courtesy of the Northern Lights JV DA, and is hosted on the Equinor ASA website. However, the recent exploration well 32/4-3 S currently lacks full public access to data via the Diskos repository, and data was provided directly from operators.

Subsurface data interpretation and mapping

Mapped subsurface geological features provide the backbone for the geomodeling inputs, as well as trap and seal analyses performed herein. Interpretation of subsurface data was performed within a 4317.5 km^2 study area of the northern North Sea (Figure 1). The boundaries of the study area were chosen within the limits of the available 3D seismic data coverage, but were further constrained to the areal extent of the northern Horda Platform. Our analysis excludes areas north of the northernmost boundary of the Smeaheia fault block as defined by Mulrooney and others (2020), north of the Horda Platform boundary with the Uer and Lomre terraces along the Horda North Fault Zone named by Zhong and others (2020), the east–west striking segment of the Vette

Fault Zone (i.e., Bell et al., 2014) and west–northwest of the Troll Fault Zone (i.e., Whipp et al., 2014) as the eastern and southern extents of the seismic data. Seismic horizons were interpreted at survey cross-lines 250 m apart, quality-controlled using inlines and arbitrary lines, then autotracked using a 0.5 seed confidence using Petrel E&P software. Reflector picks are based on well top intersections, synthetic seismograms, and picks indicated within operator well reports. In a few cases, operator well tops obtained through the Diskos repository were adjusted when inconsistencies between datasets or different locations were encountered. These adjustments were constrained by biostratigraphic data, well log responses, and seismic reflector correlations, and although such cases were uncommon, a few were significant (e.g., 32/2-1). Faults were also interpreted manually at a 250 m cross-line spacing in order to produce a network of fault sticks for each fault and capture the essential geometry of multiple regional faults at length scales over tens of kilometers. The variance seismic attribute (Randen and Sønneland, 2005) was calculated throughout the entire seismic volume, and values were extracted along mapped horizons in order to assist with fault and displaced seismic reflector mapping. After completing the interpretation and mapping of key subsurface features, the products could then be utilized for geomodeling.

Geomodel construction

Geomodeling was imperative for undertaking the trap and seal analyses described in later sections. Autotracked horizons were converted to gridded surfaces with 50 by 50 m cells using the convergent interpolation method in Petrel in order to finalize structural maps and perform area, thickness, and gross-rock-volume (GRV) calculations. Fault interpretation sticks, raw horizon cross-line interpretations, gridded surfaces, and well data were then imported into the Move software suite (PETEX) for further input conditioning and subsequent geomodeling.

Triangular mesh surfaces were generated from fault interpretation sticks resampled at 50 m along the length of each fault stick using the Delaunay triangulation method. Seal analyses performed in this study required hanging-wall and footwall cutoff inputs, and were derived using the same method implemented by Mulrooney and colleagues (2020). That is, horizon cutoffs were mapped manually along fault terminations of the raw cross-line horizon inputs, which were then projected laterally onto the associated fault mesh, producing the finalized horizon cutoff polyline. This an attempt to honor the input data and best-represent in situ cutoff geometries, particularly in areas where horizon dip angle exceeds 45° or where cutoff geometry is affected by poor seismic data quality. Occasionally, cutoffs were edited manually where the method described above did not accurately capture the geometry of the surface after manual inspection, including at areas of discernible displacement along intersecting or branching faults.

Trap and seal analyses

Structural traps were identified manually in Petrel for both the top Lower Jurassic and Upper Jurassic aquifer surfaces (i.e., aquifer-top seal interface) using an upward-moving horizontal plane (i.e., depth slice) at 5 m increments. For simplicity, it was assumed that that fluids could move freely across faults at self-juxtaposed contacts. The only exceptions include hanging-wall traps along the Øygarden Fault Zone, which were mapped assuming impermeable lateral seal along it, regardless of footwall lithologies. Up-fault migration potential was disregarded during trap mapping, but is briefly discussed in a later section. Relevant top seals above the trap were considered impermeable, and aquifer heterogeneity or potential bottom seals were ignored. No maximum trap size was enforced, but the areal extent of a given trap was restricted to the Troll, Svartalv, Tusse, or Smeaheia fault block (Figures 1, 3). The Troll field, however, represents a structural trap that was filled to its spill point before production commenced (Gray, 1987; Bolle, 1992; Sales, 1997), and the single closure area was mapped across multiple fault blocks at an average hydrocarbon-water contact of -1555 m TVDSS. Practical criteria were placed on minimum trap closure height and closure area, those being >0.1 m (near well log resolution) and >0.01 km^2 (arbitrary), respectively. If the maximum trap closure area extended beyond the boundary of the 3D seismic dataset, the apparent closure area represented by the deepest available closed contour was mapped instead.

Storage formation and top seal presence was determined by mapping their gross isochore thickness across the study area, but was limited to the primary and secondary seals since the Paleocene tertiary seal is only required for sealing parts of Troll (e.g., Spencer and Larsen, 1990; Osmond et al., 2020) (e.g., Figure 3), which remains in production and is not viable CO_2 storage target some time after 2050 (Gudmestad, 2019; Lothe et al., 2019). For thickness map generation, the upper and lower input surfaces were first smoothed in a single iteration using a filter width of two grid cells, then an isochore calculation was performed to create an isochore grid of 50 by 50 m cells using Petrel. We conducted inter-formational and fault seal analyses in the northern Horda Platform primarily using the PETEX Move Fault Analysis application. Allan diagrams (Allan, 1989) were used to visualize juxtaposed stratigraphic units and fault seal properties along key fault zones. In general, traps where the storage aquifer is juxtaposed entirely against down-dropped sealing formations are optimal. However, faults have been suggested to provide baffles or barriers to fluid migration due to their fault rock composition (i.e., Pei et al., 2015), which is important when permeable rocks are juxtaposed against one another (i.e., aquifer-aquifer juxtapositions). Where available, pressure measurements from repeat formation tests (RFT) were used to identify inter-formational pressure differences between aquifers (i.e., Watts, 1987), but also to infer fault rock seal presence if an across-fault pressure differential (AFPD) was observed between blocks (e.g., Bretan et al., 2003). It is virtually infeasible to predict fault seal capacity using AFPD between two saline aquifers, as the single-phase flow of brine across a fault is governed by Darcy Law and fault rock permeability, and is not strictly related to capillary-limited flow of a non-wetting phase fluid (i.e., CO_2) (Watts, 1987; Yielding et al., 2010), especially at production timescales (e.g., Wibberley, 2017). However, Bretan and others (2003), with similar results to Harris et al. (2002), suggested that AFPD between two saline aquifers can represent a hydraulic resistance (i.e., hydrodynamic) seal (i.e., Heum, 1996) in the presence of fine-grained fault rock with low permeabilities. In an attempt to consider grain size and predict fault rock membrane seal presence, we utilize the shale gouge method (SGR; Yielding et al., 1997; Freeman et al., 1998), which has been presented in many studies to explain or predict instances of perceived subsurface fault rock seal due to fine-grained fault rock for hydrocarbon (e.g., Lyon et al., 2005; van Ojik et al., 2020), groundwater (e.g., Bense and Van Balen, 2004), and CO_2 storage systems (e.g., Bretan et al., 2011; Karolytė et al., 2020). Yielding (2002) provided empirical evidence from the North Sea suggesting that SGR values >0.15–0.2 correlated with areas along faults known to seal hydrocarbons, and 0.15 is used herein as a minimum threshold value for indicating areas of potential fault rock membrane seal. The volume of shale (V_{sh}) parameter for this study was sourced from gamma-ray (GR) log curves by visually interpreting sand-shale cutoff values for each well, and employing a linear relationship derive a V_{sh} log (i.e., GRI; Asquith and Krygowski, 2004). Values for the throw parameter were derived from displacement calculations based on the footwall and hanging-wall cutoffs from the geomodel.

Storage aquifer and seal mapping

Gross aquifer thickness

Wellbore penetrations within the northern Horda Platform study area provide constrains on the properties of potential Jurassic storage aquifers (Figure 4). In general, low GR readings indicate that sandstones within both the Lower and Upper Jurassic aquifers are present. The gross Lower Jurassic storage aquifer gradually thins to the east, with blocky gamma-ray log motifs transitioning into an upward-coarsening pattern. Even as Amundsen and Cook formations thin and are no longer present west of well 31/6-2, sandstones of the Johansen Formation persist towards the eastern side of the Smeaheia fault block. For the gross Upper Jurassic storage aquifer, logs show an apparent heterogeneous distribution of Krossfjord, Fensfjord, and Sognefjord Formation sandstone deposits throughout the study area, but sandstone quality is likely sufficient for CO_2 injection, especially in the upper two formations. Stemming from our seismic interpretation, the top and base surfaces for both Lower and Upper Jurassic CO_2 storage aquifers were used to derive isochore thickness maps (Figure 5). The gross Lower Jurassic storage aquifer thickness map generally thickens from east to west to nearly 270 m within the northern Horda Platform (Figure 5A). On the eastern edge of the Tusse fault block and most of the Smeaheia fault block, gross aquifer thickness remains under 50 m, particularly along the Vette Fault Zone and towards the hanging wall of the Øygarden Fault Zone. In contrast, areas within much of the Tusse fault block and westward are characterized by Lower Jurassic aquifer thicknesses well above 50 m, and approach 200 m within the EL001 exploitation license. Seismic mapping of the Upper Jurassic CO_2 storage aquifer exhibits a different isochore thickness pattern than the Lower Jurassic aquifer (Figure 5B). Overall, gross thickness varies between about 200 and 550 m throughout much of the study area, with the exception of Horda North and Troll fault zone hanging walls. East of the greater Øygarden Fault Zone, however, thickness decreases considerably where much of the Jurassic and Cretaceous stratigraphy is truncated by the URU. Moreover, minor amounts of the Upper Jurassic storage aquifer truncated by the NSUC.

Top aquifer structure

The interface between a storage aquifer and overlying seal represents a critical barrier for retaining buoyant fluids in the subsurface, and provides constraints over potential CO_2 migration pathways, barriers and accumulation points. Maps of the top Lower and Upper Jurassic CO_2 storage aquifers in the northern Horda Platform shows that the general structural architecture of the two intervals is fairly complementary (Figure 6). A westward down-stepping of structural relief towards the Viking Graben is evident from both surfaces, with the deepest areas located in the Lomre and Uer terraces, as well as towards the southwest near the northern Stord Basin. Maps generated from seismic variance attribute values extracted along the two surfaces highlight faults displacing the Jurassic storage aquifers (Figure 7). Thick-skinned, north–south striking normal faults bounding the major fault blocks are the most prominent structural features, with maximum displacement ranging between 150 m and approximately 1200 m (e.g., Figures 3, 6), agreeing with the results of Bell and others (2014). Smaller-scale faults, particularly ones with maximum displacements under 50 m (i.e., Whipp et al., 2014; Wu et al., 2021a), are ubiquitous throughout the study area, but more cryptic without the aid of the variance attribute maps (Figure 7). For more details on the distribution, geometry, and structural evolution of the faults within the study area, we direct the reader to the work of previous authors (e.g., Bell et al., 2014; Whipp et al., 2014; Duffy et al., 2015; Deng et al., 2017; Mulrooney et al., 2020; Holden, 2021; Wu et al., 2021).

Gross seal thickness

The sealing lithofacies above both Lower and Upper Jurassic storage complexes have been encountered in many exploration wellbores within the northern Horda Platform (Figure 4). Gamma-ray log readings show that the lower Drake Formation is dominated by fine-grained rocks, then transitions into an upper part with either serrated or upward-coarsening motifs, sometimes resembling the overlying Brent Group deposits (e.g., Holden, 2021). Draupne mudstones and shales are also prevalent within the study area, although intra-formational sandstone-rich intervals have occasionally been encountered (e.g., 31/6-2; Figure 4). Some wellbores drilled on footwall crests of major the fault zones show that the Draupne Formation along structural highs is missing, ergo, Cretaceous Cromer Knoll and Shetland Group deposits cumulatively serve as a secondary seal (e.g., Spenser and Larson, 1990; Bolle, 1992; Osmond et al., 2020). Cretaceous formations are, more heterolithic and carbonate-rich in the northern Horda Platform compared to the underlying stratigraphy (e.g., Gradstein and Waters, 2016; Wu et al., 2021). Gamma-ray readings often show an overall upward-coarsening trend for the Cromer Knoll Group and overlying Svarte Formation, but along footwall crests, the lower fine-grained units onlap, and are also missing in some localities (e.g., 31/6-1 and 32/4-1 T2; Figure 4). Shetland Group gamma-ray log readings show a similar pattern above the Svarte Formation carbonates, however, with lower overall values compared to the Cromer Knoll Group owing to a larger proportion of deposits containing carbonate-rich material. On the eastern side of the Smeaheia fault block, Cretaceous intervals are eroded by the URU (i.e., 32/2-1; Figures 3, 4, 8).

In areas above the Troll field where no other sealing formation is present due to erosion or non-deposition, sandstones and marls of the Våle Formation (where present), or more commonly fine-grained mudstones of the Paleocene Lista Formation act as a tertiary seal. Gamma-ray responses within this interval are fairly consistent in character (see Figure 4), but it is also eroded by the URU just east of the Vette Fault Zone (e.g., Mulrooney, et al., 2020; Wu et al., 2021a).

Thickness of the Lower Jurassic Drake Formation decreases from just under 215 m to nearly zero in the northeast direction, with thicknesses around 175 m around the developing Aurora CO_2 storage site (Figure 8A). At this time, inadequate seismic resolution and lack of wellbore penetrations makes it challenging to determine with certainty any stratigraphic termination of the Drake Formation in the northern part of the Smeaheia fault block and footwall of the Øygarden Fault Zone. Locations with thicker deposits along fault hanging walls are few, modest, and are only observed in the west and southwest parts of the study area, as noted by Deng et al. (2017). The thickness map for the gross Upper Jurassic seal interval lends itself to observations much different than those from the Lower Jurassic seal (Figure 8B). Draupne Formation through Shetland Group thickness is 0–1250 m, where thin areas reside along the footwall crests of thick-skinned, north–south trending faults. The opposite holds true, in general, along the hanging walls of such faults, where the thick portions of the seal interval are located, consistent with syn-rift deposits (e.g., Prosser, 1993; Gawthorpe and Leeder, 2000). The thickest of these deposits are located along the Vette Fault Zone and the southern part of the Tusse Fault Zone, as also observed by others (e.g., Bell et al., 2014; Duffy et al., 2015). To the west, areas of zero seal thickness above the Troll West field in the Troll and Svartalv fault blocks are supplemented above by the unmapped Våle and Lista formations.

Structural trap mapping

Structural traps can serve as potential storage locations or intermediate accumulation points of CO_2 along its migration route away from the injection wellbore. The majority of structural traps within the northern Horda Platform study area are fault-bound, residing on the footwall side of normal faults of various sizes (Figures 2A, B). Qualitatively, the density of traps mapped for both Lower and Upper Jurassic storage complexes appears higher in the northern half of the study area, and trends in a northwest–southeast direction. Fifty Lower Jurassic traps were identified, with more located in the Svartalv and Tusse fault blocks comparted to the Troll and Smeaheia blocks. In contrast to the number of Lower Jurassic traps, only 28 Upper Jurassic traps were identified using the mapping criteria. This difference is attributed mostly to the Troll field accumulation, as an exception to the criteria, being treated as a single trap and reducing the overall number due to its significant size. Nevertheless, many smaller traps are located in northern Tusse fault block, and along the faulted borders of the Smeaheia fault block. Lower and Upper Jurassic trap outlines laid over their respective gross seal thickness maps highlight traps with thin or possibly absent seals above them (Figures 9C, D). The Lower Jurassic Drake Formation maintains a thickness >50 m above most traps within the study area, but the northern part of Tusse and Smeaheia fault blocks appear less favorable, as the top seal may not even be present above the Cook/Johansen aquifer. Above the Upper Jurassic Viking Group storage aquifer, many of the traps are often sufficiently capped by the Draupne Formation, as well as Cromer Knoll and Shetland groups. However, thin areas are prevalent to the west, stretching from Troll West to the Brage field. On the crests of the northern Troll, Svartalv, and Tusse fault blocks, areas of zero thickness (confirmed by well data) are located above the Troll accumulation, meaning that the Våle and Lista Formation marls and mudstones (tertiary seal) represent the final stratigraphic barrier.

Closure height and area data generally plot in a linear trend in log-log space for both Lower and Upper Jurassic traps, although a few outliers are evident (Figure 10A). Closure area for Lower Jurassic traps ranges between approximately 0.18 and 642.48 km^2, while closure height among the mapped traps varied from 6.8 to 405.3 m. Upper Jurassic closure area values are between 0.07 km^2 and 446.92 km^2, while minimum and maximum closure height is 1.4 and 446.9 m, respectively. Values of GRV calculated between the top storage aquifer surface and the trap base within the closure area increase from roughly 3,000 m^3 to nearly 17,450,000,000 m^3 for the Lower Jurassic traps, and from about 488,300 m^3 to 53,920,000,000 m^3 for the Upper Jurassic traps (Figure 10B). Again, the largest trap is that representing the Troll field in the Upper Jurassic section, but most trap GRV values fall between 1,000,000 and 100,000,000 m^3. However, these traps are faulted, requiring lateral seals, and therefore, demand characterization and an assessment of their fault seal potential.

Fault and inter-formational seal analyses

Across-fault juxtaposition

Displacement along faults can form lateral seals where sealing formations are juxtaposed against a saline aquifer. The majority of mapped traps in the northern Horda Platform are located along the footwall side of normal faults. With respect to a storage aquifer in the footwall block, five specific juxtaposition scenarios are possible (Figures 11–13): (1) self-juxtaposition of the storage aquifer, (2) juxtaposition against a sealing formation (i.e., the primary, secondary, or tertiary) immediately above the storage aquifer, (3) juxtaposition against an aquifer upsection (i.e., an intermediate aquifer or the Upper Jurassic storage aquifer), (4) juxtaposition against a sealing formation associated with the Upper Jurassic storage complex, and (5) juxtaposition against the stratigraphic overburden beyond the Upper Jurassic storage complex. Juxtaposition scenarios 2 and 4 imply that juxtaposition seal is achieved, while scenarios 1, 3, and 5 imply that a fault rock membrane seal is necessary in order to retain CO_2 column. The juxtaposition scenario number attributed to a given trap is governed by fault displacement and stratigraphic thickness of the individual formations above of the storage formation. For the Lower Jurassic storage aquifer, all five scenarios are feasible, however, only 1–4 are observed within the study area. Contrastingly, scenarios 1, 2, and 5 are theoretically possible, but only 1 and 2 are observed. Serial seismic cross-sections distributed lattitudinally across the study area show that mapped Lower and Upper Jurassic traps are bounded by at least one fault (i.e., 3-way closure), but are often intersected by several other faults (Figures 11–13). Most intra-trap faults are characterized by scenarios 1 or 2, but along some Lower Jurassic traps, displacement is occasionally great enough that juxtaposition scenario 3 is realized. Trap-bounding faults, however, are often large enough that scenarios 1–4 are observed along several Lower Jurassic traps, particularly when bounded by the largest, block-bounding faults (e.g., the Tusse Fault Zone). Upper Jurassic traps, though, are characterized by faults in which only the first and second juxtaposition scenario are observed (no overburden juxtapositions), and therefore, do not require the fault rock to act as a membrane seal for much of the trap.

Faults with the greatest displacement bound the largest traps within the study area (Figure 9, 11–13). Naturally, juxtaposition scenarios can change horizontally along the length of a fault and any traps bounded by it. That is, different juxtaposition relationships characterize the fault-bounded area of the trap. Allan diagrams (i.e., Allan, 1989) constructed for the Svartalv, Tusse, and Vette fault zones were filtered to illustrate the specific units juxtaposed against Lower and Upper Jurassic storage aquifers in their respective footwall blocks (i.e., eastern blocks) (Figure 14). For the Svartalv Fault Zone (Figure 14A), mapping indicates that much of the Lower Jurassic storage aquifer is juxtaposed against either an intermediate aquifer or the overlying Upper Jurassic storage aquifer (scenario 3). Lower Jurassic traps overlain onto the diagram tend to be located at these aquifer-aquifer juxtapositions, meaning that they would require fault rock membrane seals to retain CO_2 columns. Upper Jurassic sandstones in the footwall block of the Svartalv Fault Zone are charged with oil and gas (Troll West field), where fault displacement and thinning of the sealing formations have placed the sandstones up against the tertiary seal interval at the very crest of the trap. With exception of the northern-most part, Scenario 3 juxtapositions are observed along nearly the entire length of the Tusse Fault Zone footwall at the Lower Jurassic aquifer level, where the central and southern areas are in contact with Upper Jurassic storage aquifer (Figure 14B). Similarly to the Svartalv Fault Zone, the Troll East hydrocarbon accumulation resides within the Upper Jurassic Viking Group sandstones, which are mainly sealed by a thick secondary seal interval and tertiary seal interval in the hanging-wall block. It must be noted that 3D seismic data coverage terminates before reaching the southern tip of the Tusse Fault Zone, making the model incomplete, yet inconsequential with respect to the topics addressed herein. Allan diagrams were constructed for two southern segments of the Vette Fault Zone (Figure 14C) in order to consider juxtapositions with established CO_2 storage prospects, as well as a recently-drilled, nearby well (32/4-3 S) discussed in the next section. For Vette Fault Zone segment 1, no traps are present in the footwall block, but a key observation is that the

Lower Jurassic storage aquifer is completely juxtaposed against the Upper Jurassic aquifer in the hanging-wall block (scenario 3). In segment 2 of the Vette Fault Zone, displacement has down-dropped the primary and secondary seals of the Upper Jurassic storage complex so that they are in contact with the entire Lower Jurassic trap on the footwall side (scenario 4). Higher in the stratigraphy, the second Vette Fault Zone segment hosts the Alpha CO_2 prospect (e.g., Goldsmith, 2000; Lauritsen et al., 2018; Mulrooney et al., 2018; 2020), in which the footwall trap is characterized by a scenario 2 juxtaposition, much like the other Upper Jurassic traps in the northern Horda Platform (e.g., Figures 2, 11–13, 14C).

Inter-formational and across-fault pressure differential

Within the northern Horda Platform study area, three wellbore penetrations with RFT pressure data were available for identifying potential inter-formational and fault pressure seals between aquifers (Figure 15). Wellbores 31/5-7, 31/3-4, and 32/4-3 S were drilled in the Svartalv, Tusse, and Smeaheia fault blocks, and completed in 2020, 2013, and 2019, respectively. The Lower and Upper Jurassic storage aquifers showed in situ hydrostatic pressure conditions before production of the nearby Brage field began in 1993, and the Troll fields in 1995 (see Figure 1 for locations) in mainly Upper Jurassic reservoirs. For some time, it was postulated that ongoing production in areas west of the Smeaheia fault block was reducing formation pressure in its equivalent intervals via several relay ramps along the Vette Fault Zone and around its termination south of the study area (e.g., Lauritsen et al., 2018; Riis, 2018; Lothe et al., 2019; Mulrooney et al., 2020; Orsini et al., 2020), or was effecting the pressure conditions within the Lower Jurassic interval. Since the RFT data from these three wells are substantial and were acquired after the start of production at Troll, it is now possible to utilize them for assessing depletion, variations of inter-formational pressure, and AFPD for the Tusse and Vette fault zones given that data from displaced Lower and Upper Jurassic storage complexes are available on both their footwall and hanging-wall sides. For the Svartalv fault block, aquifer pressure from the latest wellbore (31/5-7) remains essentially hydrostatic (ρ_w = 1.03 g/cm3) within the Lower Jurassic Dunlin Group (Figure 15). Above the Drake Formation seal, pressure decreases by roughly 6 bar (leftward separation from the hydrostatic trend), indicating signs of aquifer depletion within the Brent Group. As expected, Upper Jurassic aquifer pressure depletion is documented by the RFT data in the Svartalv fault block, but is divided into a lower and upper zone. The lower zone is comprised of Krossfjord, Fensfjord, and Heather formations with an average pressure depletion of nearly 18 bar, whereas depletion in the upper Sognefjord Formation zone is even greater, reaching almost 32 bar below hydrostatic. Unfortunately, no recent RFT data was available below the Lower Jurassic storage complex, but measurements from the Tusse fault block show three important details. The first is that maximum measured depletion is approximately 27 bar from hydrostatic, which is 5 bar lower than the highest Upper Jurassic measurements in the Svartalv fault block. The second detail is that RFT points from the gross Viking Group sandstone aquifer exhibit a fairly uniform depletion trend averaging about 26 bar with depth, and with values differing by only about 4 bar relative to one another. Lastly, formation pressure data points collected from the upper-most tertiary seal in well 31/3-4 indicate that pressure conditions within testable coarse-grained intervals of the Lista Formation (e.g., Dmitrieva et al., 2012, 2018) are slightly higher than hydrostatic (i.e., overpressured). Even more interesting are the results from RFT tests conducted through wellbore 32/4-3 S in the Smeaheia fault block east of the producing Troll fields, which have also been reported recently by Wu and colleagues (2021a). Similar to the trends observed in the Svartalv block, Triassic and Lower Jurassic formation pressures appear to have remained at or near hydrostatic. From the Brent intermediate aquifer and up, however, formation pressure values decrease markedly, mimicking what is observed in the Svartalv fault block. Including those from the Brent Group, pressure depletion within the lower zone of the gross Upper Jurassic storage aquifer is greater than 10 bar through the midpoint of the Fensfjord Formation. Upsection in the Fensfjord Formation, the pressure decreases more than 14 bar until the base of the Draupne primary seal.

Permeable storage formations that are juxtaposed against one another (scenarios 1 and 3; e.g. Figures 3, 11–14) represent potential zones of across-fault fluid flow and pressure transfer if no fault rock membrane seals prevail. The three wellbores corresponding to the available RFT data in each fault block are too far from one another (~39.5–56.6 km) for direct comparison of their pressure points with depth or between more detailed stratigraphic units across the Tusse and Vette fault zones (Figure 15). We, therefore, have taken a more qualitative approach towards using the RFT data and assessing AFPD for seal analysis herein. Along the Tusse Fault Zone, the Lower Jurassic storage aquifer in the footwall is juxtaposed against Middle Jurassic intermediate and Upper Jurassic storage aquifers in the hanging wall (scenario 3; e.g., Figures 2, 3, 12, 14B, 15), placing depleted aquifers in fault contact with the Dunlin Group aquifers. Again, there are no recent RFT measurements available below the Upper Jurassic interval in the Tusse fault block to determine pressure conditions within Lower Jurassic strata. Regardless, similar juxtaposition scenarios are found along the Vette Fault Zone (e.g., Figures 12, 13, 14C, 15), providing a key observation with respect to potential fault rock membrane seal presence. Here, Lower Jurassic sandstones in the Smeaheia block are at or near hydrostatic pressure conditions, despite being juxtaposed against Upper Jurassic sandstones showing significant depletion, overall, representing a potential AFPD of 25 bar. For reference, the nearest production well (not shown) from 32/4-3 S is about 28 km away in the southeastern part of the Troll East field. Self-juxtaposition (scenario 1) of the depleted Upper Jurassic storage aquifer interval occurs along both the Tusse and Vette fault zones, as well as the Svartalv Fault Zone (e.g., Figures 11–15). Based on all measurements from wellbores 31/5-7 and 31/3-4, across-fault pressure differential appears to be as high as 7 bar across the Tusse Fault Zone, but could be under 4 bar where the top part of the Upper Jurassic storage aquifer (Sognefjord Formation) is self-juxtaposed. Between wellbores 31/3-4 and 32/4-3 S, we observe potential AFPD values between roughly 10 and 15 bar.

Shale gouge ratio

Areas of aquifer-aquifer juxtaposition along faults (scenarios 1 and 3) require a fault rock membrane seal mechanism in order to retain CO_2 columns. These juxtaposition scenarios represent high-risk lateral seals because there is uncertainty that low-permeability fault rock is continuously present along the fault zone of interest (i.e., Childs et al., 2007). Indeed, many instances of aquifer-aquifer juxtaposition are observed at footwall traps inside the northern Horda Platform study area (Figures 3, 11–14), including those found along the large Svartalv, Tusse, and Vette fault zones. We used the SGR method for predicting fault rock membrane seal presence for these three faults. If the empirical relationship demonstrated by Yielding (2002) holds true in the northern Horda Platform, areas with SGR values under 0.15 are of critical interest with respect to CO_2 containment. This is especially important where RFT measurements also suggest that there is a lack in across-fault pressure communication (i.e., highest AFPD; Figure 15).

Our SGR modeling results for the Svartalv, Tusse, and Vette fault zones are expressed as Allan diagrams in Figure 16. In general, areas where the footwall aquifers are juxtaposed against seals (scenarios 2 and 4) are associated with SGR values >0.2, and are not reported here in greater detail. The Svartalv Fault Zone SGR model (Figure 16A) at the Lower Jurassic level shows two dominant value ranges. At self-juxtaposed zones, SGR values are mainly <0.15, but where the Dunlin Group storage aquifer is juxtaposed against the overlying Brent and Viking group aquifers, corresponding SGR values range between 0.2 and 0.3, including along all mapped traps bounded by the Svartalv Fault Zone. Upsection, areas of Upper Jurassic storage aquifer self-juxtaposition are prevalent along the Svartalv Fault Zone, and many are associated with calculated SGR values <0.15. The area corresponding to the Troll hydrocarbon accumulation also exhibits low SGR values in the northern part of the Svartalv Fault Zone. Furthermore, hydrocarbon-water contacts (HWC's) associated with the Troll hydrocarbon accumulation are essentially continuous across the Svartalv Fault Zone, rather than at significantly different depths in each block. Similar observations are made along the Tusse Fault Zone (Figure 16B). Poor SGR values (<0.15) correlate with areas of Lower Jurassic storage aquifer self-juxtaposition, whereas areas in which it is juxtaposed with overlying aquifers correlate with values >0.4, particularly to the north. Results from the Tusse Fault Zone SGR model can also be correlated with relatively low AFPD (Figure 15), as the Upper Jurassic CO_2 storage aquifer is characterized by SGR values ranging from 0 to just over 0.3 at areas of self-juxtaposition. Moreover, the northern sector of the Troll hydrocarbon accumulation is associated with a fairly even HWC across the Tusse Fault Zone, and is in fault contact with SGR values <0.15. The SGR results pertaining to the two Vette fault zone segments (Figure 16C) are more complete than the results from Mulrooney et al. (2018), and when combined with AFPD observations (Figure 15), provide the most robust set of observations for fault rock membrane seal assessment in the northern Horda Platform study area. This is best-highlighted where Lower Jurassic storage aquifers are juxtaposed with Middle Jurassic intermediate and Upper Jurassic storage aquifers, especially in fault segment 1 closest to wellbore 32/4-3 S on the footwall side. SGR values at this depth along segment 1 are >0.15, and exceed 0.4. In general, a similar result is exhibited in the second segment of the Vette Fault Zone, although a relatively minor zone with values under 0.15 is located to the north. However, this low-value zone is less relevant for the mapped Lower Jurassic storage trap just to the south along segment 2, where SGR is well above 0.3. High AFPD is observed between the Lower Jurassic storage aquifer in the Smeaheia block (hydrostatic) and the Upper Jurassic storage aquifer in the Tusse fault block (depleted). A large proportion of the Upper Jurassic storage aquifer is juxtaposed against its primary and secondary seal units along the footwall of the Vette Fault Zone (scenario 2), which is relevant for traps like the Alpha prospect. As observed along the Svartalv and Tusse fault zones, areas of self-juxtaposition (scenario 1) are largely associated with SGR values <0.15. Relatively low apparent AFPD stemming from 31/3-4 and 32/4-3 S RFT data (Figure 15) correlate well, once again, with these low SGR zones.

Discussion

Storage aquifer and top seal presence

A set of key storage aquifer and top seal attributes for Lower and Upper Jurassic CO_2 storage complexes in the northern Horda Platform is compiled in Table 1, and are discussed in the context of their presence within the four major fault blocks analyzed herein. For the Lower Jurassic storage complex, storage aquifers appear present across all the fault blocks, but the gross thickness thins considerably along the eastern Tusse block and much of Smeaheia block (Figure 5A) as both Amundsen and Cook formations become absent eastward. There is some uncertainty, however, related to the presence of Johansen sandstones in areas close to the Øygarden Fault Zone. For instance, seismic reflectors mapped across the study area do not correlate well with operator tops from well 32/2-1 and 32/4-1 T2 at this depth (Figure 4), but are consistent with data from the latest well, 32/4-3 S. Moreover, there are currently no wellbore penetrations in the northern Smeaheia block and the vertical seismic resolution (~10 m) makes it difficult to determine areas lacking the storage aquifer. Despite these concerns, we assume that seismic reflectors are reliable representations of formation boundaries, and within the constraints of the available well data, alternative formation interpretations were possible and adopted. This reinterpretation of the Johansen Formation in the eastern Smeaheia fault block is at odds with those from Husmo et al. (2003) and Sundal et al. (2016), who suggested the formation is absent. They mainly based their analyses on wellbore data, but did not benefit from recent data from 32/4-3 S or thorough novel 3D seismic data coverage within the block as we do here. Nevertheless, areas where the Lower Jurassic storage aquifer is under 50 m thick are relatively small, and therefore, its CO_2 storage potential is likely influenced more by aquifer facies variations and top seal presence.

The thickness of the Drake Formation is substantial across the Troll and Svartalv fault blocks, but remains above 50 m only in the southern Tusse and Smeaheia blocks (Figure 8A). For similar reasons as the Lower Jurassic storage aquifer, it remains uncertain whether the Drake Formation is present in several parts of the study area, and our interpretation is different from Sundal et al. (2016) and well 32/2-1 operators. That said, mapping of continuous reflectors indicates that the interval is <25 m thick only in the middle of the Smeaheia fault block and the footwall side of the Øygarden Fault Zone where no structural traps are present (Figure 9C). However, if present, thinner seals do not necessarily equate to poorer seal capacity (i.e., Downey, 1984, 1994). Formation pressure from the Svartalv and Smeaheia fault blocks indicated that the Drake Formation provides a pressure barrier between the Lower Jurassic and Middle Jurassic aquifers (Figure 15) (Wu et al., 2021a). This observation cannot be corroborated within the Troll and Tusse fault blocks due to the lack of recent wellbore penetrations down to the Lower Jurassic interval, but it is within reason to cautiously infer that the Drake Formation would perform in a similar fashion within the untested fault blocks. A more detailed characterization of facies variations within the Drake Formation is carried out in the future, particularly with respect to the upper and lower Drake Formation units (Figure 2B) (e.g., Holden, 2021; Wu et al., 2021a).

The presence of the Upper Jurassic Viking Group storage aquifers is much more certain throughout the northern Horda Platform. Gross thickness is consistently >200 m in all four major fault blocks with the only exception being along the Troll Fault Zone footwall where the interval is heavily eroded as a result of events forming North Sea Unconformity Complex (Figure 5B). It is assumed that uppermost Fensfjord and Sognefjord formations are of good quality for CO_2 storage based on previous studies (e.g., Goldsmith, 2000; Holgate et al., 2013; Patruno et al., 2015; Fawad et al., 2021a) and production from hydrocarbon accumulations in the region. Therefore, CO_2 storage locations within the study area are unlikely to be limited by aquifer presence, but rather other factors, such as potential seals or the inter-tonguing of the finer-grained Heather Formation (e.g., Stewart et al., 1995).

Top seal presence varies in the norther Horda Platform area in that required units (primary, secondary, or tertiary) are different in each major fault block for the Upper Jurassic storage complex (Table 1). All three top seal units are required to seal the envisaged storage aquifer in the Troll and Svartalv blocks, whereas only the primary and secondary units are for the Tusse and Smeaheia blocks (e.g., Figure 11). The Draupne Formation, as well as Cromer Knoll and Shetland groups onlap structural highs and footwall crests (e.g., Whipp et al., 2014), and show evidence of both non-deposition and truncation against the North Sea Unconformity Complex (i.e., Kyrkjebø et al., 2004). Total thickness of the combined primary and secondary seal intervals varies considerably between the different fault blocks, where maximum thickness is least in the Troll block and greatest in the Tusse block (Figure 8B). Minimum thickness in the Smeaheia fault block, however, is greatest compared to the other three. While the primary and secondary seal units are often present above the Viking Group sandstone aquifers, a detailed understanding of vertical and horizontal facies changes within these units has yet to be undertaken, and would contribute mightily towards derisking their seal potential in the context of CO_2 storage. We did not map the Paleocene Våle and Lista formations here, but work by Dmitrieva and others (2018) indicates that the gross Rogaland Group thickness exceeds 100 meters where the older seals are missing. While they did not map the two lower-most formations, their seal potential is evident given the size and presence of the Troll West hydrocarbon accumulation, which is >200 meters in column height (e.g., Figures 11, 12). Only the Tusse fault block contains recent RFT data that suggests a top seal pressure barrier between the depleted Upper Jurassic storage aquifer and the slightly overpressured post-Paleocene stratigraphic overburden (Figure 15). This difference in formation pressure is not surprising given that there is nearly 300 meters of sealing lithologies between the upper and lower points of measurement, however, readings from the Lista Formation may not be truly indicative of pressure seal presence, and more data from future wellbores are required from the gross Upper Jurassic seal interval and stratigraphic overburden are required.

Structural traps

The total number of Lower and Upper Jurassic structural traps and their combined GRV are summarized for each four major fault block in Table 1. Lower Jurassic structural traps are more numerous in the Svartalv, Tusse, and Smeaheia fault blocks (see Figures 9A, 9C), but total trap GRV in the Tusse fault block is one or two orders of magnitude larger than the other three. The extent of the giant fill-to-spill closure of the Troll hydrocarbon accumulation spans across three out of the four major fault blocks, reducing the total amount of traps in the western half of the study area (see Figures 9B, 9C). Aside from the Troll trap, no sizeable traps were mapped in the Troll and Svartalv blocks, whereas the Tusse and Smeaheia blocks contain 12 or more. The since the extent of the Troll trap is shared between three fault blocks, the total GRV for the Troll and Tusse blocks is equal to the GRV of the trap. In the Tusse block, this same GRV value is also combined with those from the other 15 mapped traps in the block. The total trap GRV of the Tusse block is an order of magnitude larger than that of the Smeaheia fault block, but is similar in value if the Troll trap is discounted. The overall structural trap GRV for the Upper Jurassic storage complex is lower than the Upper Jurassic, and are approximately 2.74×10^{10} and 2.50×10^{10} m^3, respectively.

Considering their size, the prospectivity of Lower and Upper Jurassic structural traps located within the northern Horda varies significantly. Several relatively large traps were identified, mainly in the footwall sides of large, block-bounding faults (e.g., the Tusse Fault Zone), but most traps are fairly small, and would make poor individual CO_2 storage targets (Figures 9A, C, 10). Nevertheless, while the largest traps are most attractive targets, the smaller traps could be utilized as local accumulation points along the up-dip migration path towards a larger trap, for instance, in the norther Tusse fault block (Figure 9). Our analysis did not consider other effective CO_2 trapping mechanisms (i.e., Ringrose et al., 2021), such as mineral trapping (e.g., Sundal and Hellevang, 2019), which combined with migration through the smaller traps, would make storage more efficient. Furthermore, we did not advance our calculation of trap GRV into more detailed storage capacity estimates for each trap because we lacked the information necessary to conveniently derive such figures for specific traps. Therefore, additional work that accounts for the other strapping mechanisms and storage capacity is required in order to fully evaluate the potential of the structural traps mapped herein.

Fault seal presence

Faults control the distribution of traps in the northern Horda Platform, and the containment of potential CO_2 columns is dependent on their ability to provide lateral seals. From our results, we have summarized juxtaposition types, relative AFPD, and minimum SGR values for three thick-skinned fault zones (four segments) in Table 2, which may also be applied to other faults in the study area in a generalized manner. With respect to the footwall block, displacement of the Lower Jurassic storage aquifer has resulted in juxtaposition scenarios 1–3 or 1–4 (see Across-fault juxtaposition for explanation) (Figure 14). That is, traps along these large faults generally require some fault membrane seal potential in order retain a CO_2 column because the Lower Jurassic aquifers are juxtaposed against Middle or Upper Jurassic aquifers in the hanging wall (scenario 3). This will be true for any other faulted traps in the study area in which displacement is greater than the Drake Formation thickness, especially in the northeastern part of the study area (Figure 8A). Exceptions include where displacement is small enough that the fault creates a juxtaposition seal with the Drake Formation (scenario 2) or, more rarely, where the displacement is great enough to create a juxtaposition seal with the Draupne Formation or Cromer Knoll Group seals (scenario 4, e.g., Vette Fault Zone segment 2; Figure 14C). With respect to scenario 4, Upper Jurassic–Paleocene seal units are proven lateral seals for the Troll hydrocarbon accumulations along large faults, such as the Tusse Fault Zone (e.g., Figures 3, 11–14), but are unproven east of the field. We have assumed that any areas exhibiting scenarios 2 and 4 would serve as across-fault migration seals, but as noted earlier, unfavorable vertical and lateral facies changes into higher-permeability lithologies may impact the lateral potential of the hanging-wall stratigraphy (i.e., primary, secondary, and tertiary seals). Therefore, caution should be taken until more detailed studies can characterize regional facies variations within these intervals.

Where aquifer-aquifer juxtapositions are present (scenarios 1 and 3), data from RFT measurements and SGR model results provide a means to explore potential fault membrane seals for the Lower Jurassic storage complex in the northern Horda Platform (Table 2). Across-fault pressure differential is not determinable for juxtaposition scenario 1, and SGR values are <0.15 for all modeled fault zones (Figure 15, 16). In contrast, while AFPD is undeterminable for other faults, it is relatively high (>20 bar) for the Vette Fault Zone segments along areas exhibiting juxtaposition scenario 3, and SGR values are generally greater than the 0.15 threshold suggested by Yielding (2002), within only a small localized zone <0.15 in the northern part of the second Vette Fault Zone segment. If high AFPD are related to the presence of low-permeability fault rocks, and SGR values >0.15 are indicative of fault zones possessing fine-grained rocks, then their agreement is a positive result with respect to scenario 3 fault seal potential. New wellbore data down through the Lower Jurassic interval are needed within the Troll and Tusse fault blocks in order to demonstrate AFPD across the Svartalv and Tusse fault blocks, but the results from their respective SGR models are similar to those from the Vette fault zone segments, suggesting that the Lower Jurassic storage aquifer may still enjoy hydrostatic pressure conditions and that an AFPD would be observed.

Fault seal attributes for the Upper Jurassic storage complex differ from those of for the Lower Jurassic (Table 2). Firstly, the range of observed juxtaposition scenarios is limited to scenarios 1 and 2 for all faults in the northern Horda Platform, including those modeled in Figure 14. Again, areas exhibiting scenario 2 are assumed to provide across-fault juxtaposition seals throughout the study area with the caveat that there are no detrimental facies changes in locations away from the Troll field, though primary, secondary, and tertiary units indeed provide lateral seals for the field itself (e.g., Figures 3, 11, 14A, B). The Upper Jurassic storage aquifers within the Svartalv, Troll, Smeaheia, and presumably Troll fault blocks are pressure-depleted (Figure 15). While no pressure communication across the Svartalv and Tusse faults zones is necessary to explain this observation, depletion in the Smeaheia block has occurred in the absence of production, and it is more likely that moderate (> 5 bar) pressure communication occurs across the Vette Fault Zone rather than the pressure front migrating around the very southern tip of the fault zone and back northward (i.e., as a no flow boundary) (Riis, 2018). However, simulation results from Lothe et al. (2021) suggested that the Vette Fault Zone maintains some pressure seal potential. This agrees with the results from our SGR modeling, as areas exhibiting scenario 1 are associated with values <0.15, but >0 for all three modeled faults (Figure 16). It remains evident, though, that over geological timescales, the Svartalv and Tusse fault zones do not provide fault rock membrane seals where juxtaposition scenario 1 persists since the Troll HWC is nearly at the same depth on both sides of each fault (e.g., Figures 3, 11–13) (Horstad and Larter, 1997), but could over production timescales (e.g., Wibberley et al., 2017). Moreover, the contact was tilted westward sometime in the Neogene (Riis, 1996; Faleide et al., 2002), and the estimated paleo-HWC based on residual oil zones observed in cores was also relatively level across fault zones (e.g., Horstad and Larter, 1997), even though it was geometrically a taller trap (e.g., Bergmo et al., 2018). If the HWC has been level both before and after the tilting of strata on the flanks of the Horda Platform, then possibly fault rock seal at Upper Jurassic storage aquifer self-juxtapositions is poor over geological timescales, but such an observation is not conclusive (e.g., Fisher et al., 2001). Although more deeply buried, we can only assume similar across-fault flow behavior along self-juxtapositions of the Lower Jurassic storage aquifer given the results from out SGR analysis until more data becomes available.

Aside from the robustness of out interpretation and geomodeling, our analysis relies heavily on the relationship between AFPD and SGR at aquifer-aquifer juxtapositions. That is, we infer that zones with high AFPD (>20 bar) and SGR (>0.15) qualitatively represent areas of fault membrane seal. Yielding and others (2010) stressed that AFPD measured between aquifers is a function of the hydrodynamic behavior of a fault zones, rather than its seal capacity via capillary-based mechanisms. The AFPD observed from data in the northern Horda Platform herein are then a function of fault rock permeability, thickness, and the flow rate (Yielding et al., 2010). However, permeability decreases with decreases in grain size, especially as fine-grained material, such as clay minerals from mudstones or shales within the hostrock stratigraphy is entrained within the fault rock, and has been previously linked to increasing SGR (Sperrevik et al., 2002; Yielding et al., 2010). The empirical SGR threshold suggested by Yielding (2002) was derived partially by nearby fields in the North Sea (e.g., Brage; see Figure 1), and has widely been used by subsequent authors successfully to demonstrate fault seal capacity (e.g., Lyon et al., 2005). Increasing SGR has also been shown to positively correlate with AFPD between aquifers (Harris et al., 2002; Bretan et al., 2003). Therefore, we maintain that the qualitative relationship between aquifer-aquifer AFPD and SGR is indicative of fault seal presence to some degree. With regards to fault seal capacity, previous work by Bretan and others (2011) suggested that a portion of the Svartalv Fault Zone we analyzed could retain a CO_2 column in excess of 100 m based on the methodology described by Bretan et al. (2003) modified for a CO_2 density of 0.67 g/cm^3. While this was a meaningful contribution that could be corroborated and supplemented by our fault models (Figure 16), we purposefully avoided carrying out an estimation of retainable CO_2 columns. This is mainly because we lack the necessary data to confidently do so in light of recent literature that has shown the importance and sensitivity that fault rock and brine-CO_2 system properties have on membrane seal capacity, particularly in the absence of CO_2 storage sites, which could eventually provide empirical calibrations (e.g., Miocic et al., 2019; Karolytė et al., 2020). It is hoped that, in time, stronger relationships between fault rock and brine-CO_2 properties are established, and more reliable means of predicating fault seal capacity are developed, as it will be necessary for new CO_2 storage sites where faults are present, both regionally and globally.

In the Smeaheia fault block, several traps large were mapped in the Lower and Upper Jurassic levels that are juxtaposed along the Øygarden Fault Zone hanging wall (e.g., Figures 9, 12). At present, there is no established method to reliably assess or predict fault seal where siliciclastic deposits have been sheared and juxtaposed against igneous or metamorphic basement rock. However, it is to be expected that both chemical and mechanical processes both positively and negatively contribute to the sealing potential of such a basin-bounding fault zone (e.g., Kristensen et al., 2016). While a smaller fault zone, Fossen and others (1997) described fault rocks from the Bjorøy Fault Zone intersected by the Bjorøy Tunnel onshore in the Bergen area (see Figure 1) as possessing non-cohesive, sandy fault gouge, where Upper Jurassic sandstones and conglomerates are juxtaposed against Paleozoic gneisses. They, along with Wu et al. (2021b) also reported pressure solution or quartz cementation within the hostrock sandstone with permeabilities ranging from 1 to 50 mD, potentially due to interactions with hydrothermally sourced fluids from the fault zone, but no such observation has been observed from offshore wellbores, such as 32/2-1 (Figures 3, 4). In the worst case, CO_2 injected into Øygarden Fault Zone hanging-wall traps would either migrate as a free gas (<800 m TVDSS; i.e., Bachu, 2003) up the Øygarden Fault Zone itself, or flow into footwall basement rocks and migrate up fractures or intra-block faults, such as those interpreted by Torabi and colleagues (2018), Bjerkeli (2019), Mulrooney and colleagues (2020), or the authors herein (Figures 3, 7, 11, 12). Even though fine-grained Jurassic seal units may be present above the basement rock in the footwall block, strata dip to the west, which would encourage eastward migration up towards the URU surface, and ultimately to the seafloor. Overall, the mapped hanging-wall traps along the Øygarden Fault Zone are deemed too risky for CO_2 storage until these issues can be thoroughly and confidently be addressed.

Additional considerations

While the results associated to trap and seal presence within the northern Horda Platform assessed herein were favorable, several other factors should also be considered with respect to CO_2 containment. For instance, we did not undertake an in situ or induced mechanical top seal failure, however, no pervasive fracturing has been reported within the Lower and Upper Jurassic top seal intervals to date, and recent petrophysical and geophysical studies suggest that both possess adequate seal integrity (e.g., Rahman et al., 2020; Fawad et al., 2021b). Another important derisking measure is to evaluate the reactivation potential for preexisting faults, as this can generally lead to the breach of potential seals (e.g., Jones and Hillis, 2003; Lyon et al., 2005; Osmond and Meckel, 2020). Bretan et al. (2011), Skurtveit et al. (2018), Rahman et al., (2021) concluded that faults, including segments of the Svartalv, Tusse, and Vette fault zones, show low risk for reactivation due to increased pore pressure resulting from CO_2 injection in a normal stress regime, but more detailed and site-specific work is recommended. To date, up-fault migration remains difficult to assess without sophisticated modeling approaches (e.g., Fredman et al., 2007) or rather serendipitous datasets and observations more common in outcrop analogs (e.g., Naruk et al., 2019; Miocic et al., 2020). Considering the in situ conditions, one might expect vertical pressure communication across the Drake Formation via through-going faults within the Svartalv and Smeaheia blocks, but such an observation is not apparent from RFT measurements (Figure 15). Furthermore, no significant hydrocarbon shows have been encountered above the Upper Jurassic accumulations. However, if seafloor pockmarks have been sourced thermogenically (e.g., Forsberg et al., 2007; Hovland, 2007), then the observation suggests that any substantial volume of CO_2 escaping into the Cenozoic and Quaternary stratigraphic overburden from Jurassic aquifers could utilize up-fault pathways (e.g., polygonal faults), and eventually reach the surface. Leakage through wellbores presents another risk towards retaining injected CO_2 in the subsurface (i.e., Bachu and Celia, 2009). Details, such as the aquifer pressure conditions, wellbore age, casing and cement material, plugging method, and other parameters play a role in possible leakage up wellbores (Ide et al., 2006), but were not studied herein. In the northern Horda Platform, fewer wells have been drilled down to the Lower Jurassic storage aquifer compared to the Upper Jurassic, reducing the risk of interaction in that interval. Also, the overall well density within the study area is highest within the area of known hydrocarbon discoveries, such as Troll. Assuming the careful drilling and completion of future injection wells and the utilization of structural closures mapped herein, injection locations can be planned in such a way that the CO_2 plume could avoid preexisting wellbores along a migration route towards a final trap, as envisaged at the Aurora site (Furre et al., 2020; Holden, 2021) (e.g., Figures 6A, 12B)

Regional CO_2 storage implications

The primary goal of this work is to, from a trap and seal perspective, highlight areas demonstrating favorable CO_2 storage potential in the northern Horda Platform. Development of the Aurora storage site within the Svartalv Fault Block could provide a critical stepping-stone for CCS in offshore Norway and northern Europe in that the incoming infrastructure and subsurface geological knowledge could be leveraged towards forming a future CO_2 storage hub (e.g., Lothe et al., 2019; Meckel et al., 2021). In general, our results indicate that traps and seals are viable with respect to both the Lower and Upper Jurassic storage complexes in all four major fault blocks within the study area (Tables 1, 2), and can be used to speculate over of the eight options.

For the Lower Jurassic, the Troll and Tusse fault blocks are attractive locations for storage given the presence of thick aquifers, large traps, and the likelihood of present seals (Figure 9A, C). Moreover, their geological attributes resemble those of the Aurora site, and a similar development strategy could be employed. Lower Jurassic prospectivity in the Smeaheia block is deemed riskier given that there remains uncertainty in aquifer and seal presence, as well as quality, in addition to the risk of up-dip leaking towards the Øygarden Fault Zone (i.e., Mulrooney et al., 2020). However, the Smeaheia block may represent the most attractive location for immediate CO_2 storage once success at Aurora is established. This is mainly because there is no risk of contamination of Troll or other producing fields to the west, but also because aquifers and seals are fairly well-understood, and several sizable traps are available for storage, but primarily on more eastern sides of the fault block (Figure 9B, D). Ideally, all eight options within the study area could contribute in some way towards a hypothetical storage hub in the region with more localized geological characterization, strategic developmental concepts, and CCS maturation at even fraction of what has taken place historically within the hydrocarbon industry (e.g., Ringrose and Meckel, 2019; Ringrose et al., 2021). Ultimately, ongoing and continued progress towards building CCS projects in the North Sea will inevitably contribute to reducing CO_2 emissions and reaching global climate mitigation.

Conclusions

Sequestration of CO_2 is scheduled to begin in 2024 along the Norwegian Continental shelf at the Aurora site in the North Sea, but more locations are needed to upscale CCS as a climate mitigation strategy. Ahead of confirming the technical success of injection and sequestration operations at Aurora, a regional assessment of structural trap and seal presence has been performed herein, as the northern Horda Platform represents a potential CO_2 storage hub for northern Europe. Lower and Upper Jurassic storage complexes show potential, comprised of siliciclastic saline aquifers and mixed siliciclastic and carbonate-rich seals, and we focused our analysis within the Troll, Svartalv, Tusse, and Smeaheia fault blocks. The primary findings and conclusions of this study are summarized as follows:

- Both Lower and Upper storage aquifers are generally present throughout the study area, although Lower Jurassic aquifer thickness decreases to <50 m to the east (e.g., the Smeaheia block).
- Mapping of Lower Jurassic mudstones and shales suggests that top seals are present throughout much of the study area, but thin considerably in the northern parts of both the Tusse and Smeaheia fault blocks. Except in the northern sectors of the Troll and Svartalv fault blocks, primary and secondary seals for the Upper Jurassic storage complex appear sufficiently thick, and are further supported by a tertiary seal interval where others are absent.
- Tens of structural traps mapped herein could be utilized for containing injected CO_2, the largest of which are generally located in the footwall of the thick-skinned, N–S trending normal faults. The area defined by the Troll hydrocarbon accumulation, however, restricts the amount of structural traps available for immediate CO_2 storage within the Upper Jurassic storage aquifer, whereas traps in the Smeaheia fault block eliminate the risk of field contamination.
- Lateral seal via across-fault juxtaposition of sealing formations in the hanging wall against storage aquifers in the footwall is uncommon along the largest of mapped Lower

Jurassic faults. Contrastingly, Upper Jurassic traps are nearly all characterized by potential across-fault juxtaposition seals.

- Formation pressure measurements from Svartalv, Tusse, and Smeaheia fault blocks show depletion has occurred within the Middle Jurassic intermediate and Upper Jurassic storage aquifers due to production from nearby hydrocarbon fields in the same interval, but the Lower Jurassic seal unit provides an inter-formational seal between Lower Jurassic and Middle Jurassic aquifers.
- Across-fault pressure differentials (AFPD) are observed where depleted Upper Jurassic aquifers in the hanging wall are juxtaposed against the Lower Jurassic aquifers, suggesting some permeability and pressure seal (hydrodynamic) exists along faults, such as the Vette Fault Zone. Juxtapositions with observed AFPD correlate with shale gouge ratio (SGR) values >0.15, hinting that perhaps the apparent hydrodynamic fault seals are also indicative of fault rock membrane seals. Moreover, similar SGR results are shared between all modeled faults and suggests such seals are present throughout the study area where the Lower Jurassic aquifers are supposed against Upper Jurassic ones. Results and observations at elf-juxtapositions of the Upper Jurassic storage aquifer imply poor seal potential at those contacts, and is also assumed for similar situations within the Lower Jurassic storage complex.

Within the context of trap and seal, the results herein ultimately suggest that the containment of injected CO_2 within both Lower and Upper Jurassic storage complexes is, indeed, feasible across the four analyzed fault blocks off the coast of Norway. Therefore, we find that the northern Horda Platform remains a promising location for the continued development of CCS in the North Sea, carrying the potential to become a CO_2 storage hub for northern Europe in the future.

References

Allan, U. S., 1989, Model for hydrocarbon migration and entrapment within faulted structures: AAPG Bulletin, v. 73, p. 803–811, doi:10.1306/94885962-1704-11D7-8645000102C1865D.

Anell, I., H. Thybo, and E. Rasmussen, 2012, A synthesis of Cenozoic sedimentation in the North Sea: Basin Research, v. 24, p. 154–179, doi:10.1111/j.1365-2117.2011.00517.x.

Asquith, G., and D. Krygowski, 2004, Gamma Ray, *in* G. Asquith and D. Krygowski, eds., Basic well log analysis: AAPG Methods in Exploration 16, p. 31–35.

Bachu, S., 2003, Screening and ranking of sedimentary basins for sequestration of CO_2 in geological media in response to climate change: Environmental Geology, v. 44, p. 277–289, doi:10.1007/s00254-003-0762-9.

Bachu, S., and M. A. Celia, 2009, Assessing the potential for CO_2 leakage, particularly through wells, from geological storage sites, *in* J. B. Mcpherson and E. T. Sundquist, eds., Carbon sequestration and its role in the global carbon cycle: AGU Geophysical Monograph Series 183, p. 203–216, doi:10.1029/2005GM000338.

Badley, M. E., J. D. Price, C. Rambech Dahl, and T. Agdestein, 1988, The structural evolution of the northern Viking Graben and its bearing upon extensional modes of basin formation: Journal of the Geological Society of London, v. 145, p. 455–472, doi:10.1144/gsjgs.145.3.0455.

Bartholomew, I. D., J. M. Peters, and C. M. Powell, 1993, Regional structural evolution of the North Sea: oblique slip and the reactivation of basement lineaments, *in* J. R. Parker, ed., Petroleum geology of Northwest Europe: Geological Society of London Petroleum Geology Conference Series 4, p. 1109–1122, doi:10.1144/0041109.

Bell, R. E., C. A.-L. Jackson, P. S. Whipp, and B. Clements, 2014, Strain migration during multiphase extension: observations from the northern North Sea: Tectonics, v. 33, p. 1936–1963, doi:10.1002/2014TC003551.

Bense, V. F., and R. Van Balen, 2004, The effect of fault relay and clay smearing on groundwater flow patterns in the Lower Rhine Embayment: Basin Research, v. 16, p. 397–411, doi:10.1111/j.1365-2117.2004.00238.x.

Bergmo, P. E. S., E. Lindeberg, F. Riis, and W. T. Johansen, 2009, Exploring geological storage sites for CO_2 from Norwegian gas power plants: Johansen Formation: Energy Procedia, v. 1, p. 2945–2952, doi:10.1016/j.egypro.2009.02.070.

Bergmo, P. E. S., A.-A. Grimstad, and K. Kurtev, 2018, Mapping of paleo residual oil zones on the NCS and the potential for production by CO_2-EOR: International Journal of Greenhouse Gas Control, v. 75, p. 254–261, doi:10.1016/j.ijggc.2018.06.005.

Bjerkeli, Å., 2019, Tectonostratigraphy and fault analysis of the Øygarden Fault Complex footwall, northern Horda Platform, northern North Sea, Master’s thesis, University of Oslo, Oslo, Norway, 131 p.

Bolle, L., 1992, Troll field: Norway’s giant offshore gas field, *in* M. T. Halbouty, ed., Giant oil and gas fields of the decade 1978–1988: AAPG Memoir 54, p. 447–458, doi:10.1306/M54555C27.

Bretan, P., G. Yielding, and H. Jones, 2003, Using calibrated shale gouge ratio to estimate hydrocarbon column heights: AAPG Bulletin, v. 87, p. 397–413, doi:10.1306/08010201128.

Bretan, P., G. Yielding, O. M. Mathiassen, and T. Thorsnes, 2011, Fault-seal analysis for CO_2 storage: an example from the Troll area, Norwegian Continental Shelf: Petroleum Geoscience, v. 17, p. 181–192, doi:10.1144/1354-079310-025.

Briseid, H. C., T. Dreyer, R. Færseth, K. O. Hager, and A. Groth, 1998, Middle to Upper Jurassic syn-rift development on the Horda Platform, Lomre and Uer terraces, northern North Sea: implications for prospectivity, *in* G. Berge, ed., Seminar on Improving the Exploration Process by Learning from the Past: Norwegian Petroleum Society, p. 31–32.

Brunstad, H., F. M. Gradstein, J. E. Lie, Ø. Hammer, D. Munsterman, G. Ogg, and M. Hollerbach, 2013, Stratigraphic guide to the Rogaland Group, Norwegian North Sea: Newsletters on Stratigraphy, v. 46, p. 137–286, doi:10.1127/0078-0421/2013/0032.

Bugge, T., B. Tveiten, and S. Backstrom, 2001, The depositional history of the Cretaceous in the northeastern North Sea, *in* O. J. Martinsen, and T. Dreyer, eds., Sedimentary environments Offshore Norway – Palaeozoic to Recent: Norwegian Petroleum Society Special Publication 10, p. 279–291, doi:10.1016/S0928-8937(01)80018-7.

Chamock, M. A., I. Kristiansen, A. Ryseth, and J. P. G. Fenton, 2001, Sequence Stratigraphy of the Lower Jurassic Dunlin Group, Northern North Sea, *in* O. J. Martinsen, and T. Dreyer, eds., Sedimentary environments Offshore Norway – Palaeozoic to Recent: Norwegian Petroleum Society Special Publication 10, p. 145–174, doi:10.1016/S0928-8937(01)80012-6.

Childs, C., J. J. Walsh, T. Manzocchi, J. Strand, A. Nicol, M. Tomasso, M. P. J. Schöpfer, and A. C. Aplin, 2007, Definition of a fault permeability predictor from outcrop studies of a faulted turbidite sequence, Taranaki, New Zealand, *in* S. J. Jolley, D. Barr, J. J. Walsh, and R. J.

Knipe, eds., Structurally complex reservoirs: Geological Society of London Special Publication 292, p. 235–258, doi:10.1144/SP292.14.

Clausen, J. A., R. H. Gabrielsen, P. A. Reksnes, and E. Nysæther, 1999, Development of intraformational (Oligocene–Miocene) faults in the northern North Sea: Influence of remote stresses and doming of Fennoscandia: Journal of Structural Geology, v. 21, no. 10, p. 1457–1475, doi:10.1016/S0191-8141(99)00083-8.

Coward, M. P., J. Dewey, M. A. Mange, M. Hempton, and J. Holroyd, 2003, Tectonic evolution, *in* D. Evans, C. Graham, A. Armour, and P. Bathurst, eds., The millennium atlas: petroleum geology of the central and northern North Sea: Geological Society of London, p. 26–65.

Crameri, F., G. E. Shephard, and P. J. Heron, 2020, The misuse of colour in science communication: Nature Communications, v. 11, p. 1–10, doi:10.1038/s41467-020-19160-7.

Crameri, F., 2021, Scientific colour maps, Zenodo, v. 7.0.0, https://zenodo.org/record/4491293#.YOFBF-gzY2w (accessed July, 3, 2021), doi:10.5281/zenodo.4491293.

Deng, C., H. Fossen, R. L. Gawthorpe, A. Rotevatn, C. A.-L. Jackson, and H. Fazlikhani, 2017, Influence of fault reactivation during multiphase rifting: the Oseberg area, northern North Sea rift: Marine and Petroleum Geology, v. 86, p. 1252–1272, doi:10.1016/j.marpetgeo.2017.07.025.

Dmitrieva, E., C. A.-L. Jackson, M. Huuse, and A. McCarthy, 2012, Paleocene deep-water depositional systems in the North Sea Basin: a 3D seismic and well data case study, offshore Norway: Petroleum Geoscience, v. 18, p. 97–114, doi:10.1144/1354-079311-027.

Dmitrieva, E., C. A.-L. Jackson, M. Huuse, and I. A. Kane, 2018, Regional distribution and controls on the development of post-rift turbidite systems: insights from the Paleocene of the eastern North Viking Graben, offshore Norway, *in* M. Bowman, and B. Levell, eds., Petroleum geology of NW Europe: Geological Society of London Petroleum Geology Conference Series 8, p. 147–170, doi:10.1144/PGC8.31.

Domínguez, R., 2007, Structural evolution of the Penguins Cluster, UK northern North Sea, *in* S. J. Jolley, D. Barr, J. J. Walsh, and R. J. Knipe, eds., Structurally complex reservoirs: Geological Society of London Special Publication 292, p. 25–48, doi:10.1144/sp292.2.

Downey, M. W., 1984, Evaluating seals for hydrocarbon accumulations: AAPG Bulletin, v. 68, p. 1752–1763, doi:10.1306/AD461994-16F7-11D7-8645000102C1865D.

Downey, M. W., 1994, Hydrocarbon seal rocks, *in* L. B. Magoon, and W. G. Dow, eds., The petroleum system—from source to trap: AAPG Memoir 60, p. 159–164, doi:10.1306/M60585C8.

Dreyer, T., M. Whitaker, J. Dexter, and H. Flesche, 2005, From spit system to tide-dominated delta: integrated reservoir model of the Upper Jurassic Sognefjord Formation on the Troll West field, *in* A. G. Doré, and B. A. Vining, eds., Petroleum geology of Northwest Europe and global perspectives: Geological Society of London Petroleum Geology Conference Series 6, p. 423–448, doi:10.1144/0060423.

Duffy, O. B., R. E. Bell, C. A.-L. Jackson, R. L. Gawthorpe, and P. S. Whipp, 2015, Fault growth and interactions in a multiphase rift fault network: Horda Platform, Norwegian North Sea: Journal of Structural Geology, v. 80, p. 99–119, doi:10.1016/j.jsg.2015.08.015.

Eidvin, T., and Y. Rundberg, 2007, Post-Eocene strata of the southern Viking Graben, northern North Sea; integrated biostratigraphic, strontium isotopic and lithostratigraphic study: Norwegian Journal of Geology, v. 87, p. 391–450.

Eidvin, T., F. Riis, and E. S. Rasmussen, 2014, Oligocene to Lower Pliocene deposits of the Norwegian Continental Shelf, Norwegian Sea, Svalbard, Denmark and their relation to the uplift of Fennoscandia: a synthesis: Marine and Petroleum Geology, v. 56, p. 184–221, doi:10.1016/j.marpetgeo.2014.04.006.

Faleide, J. I., R. Kyrkjebø, T. Kjennerud, R. H. Gabrielsen, H. Jordt, S. Fanavoll, and M. D. Bjerke, 2002, Tectonic impact on sedimentary processes during Cenozoic evolution of the northern North Sea and surrounding areas, *in* A. G. Doré, J. A. Cartwright, M. S. Stoker, J. P. Turner, and N. White, eds., Exhumation of the North Atlantic Margin: timing, mechanisms, and implications for petroleum exploration: Geological Society of London Special Publication 196, p. 235–269, doi:10.1144/GSL.SP.2002.196.01.14.

Fawad, M., M. J. Rahman, and N. H. Mondol, 2021a, Seismic reservoir characterization of potential CO_2 storage reservoir sandstones in Smeaheia area, northern North Sea: Journal of Petroleum Science and Engineering, v. 205, p. 108812, doi:10.1016/j.petrol.2021.108812.

Fawad, M., M. J. Rahman, and N. H. Mondol, 2021b, Seismic-derived geomechanical properties of potential CO_2 storage reservoir and cap rock in Smeaheia area, northern North Sea: The Leading Edge, v. 40, p. 254–260, doi:10.1190/tle40040254.1.

Fazlikhani, H., H. Fossen, R. L. Gawthorpe, J. I. Faleide, and R. E. Bell, 2017, Basement structure and its influence on the structural configuration of the northern North Sea rift: Tectonics, v. 36, p. 1151–1177, doi:10.1002/2017TC004514.

Fazlikhani, H., S. S. Aagotnes, M. A. Refvem, J. Hamilton-Wright, R. E. Bell, H. Fossen, R. L. Gawthorpe, C. A.-L. Jackson, and A. Rotevatn, 2020, Strain migration during multiphase extension, Stord Basin, northern North Sea rift: Basin Research, v. 33, p. 1–23, doi:10.1111/bre.12522.

Fisher, Q. J., S. D. Harris, E. McAllister, R. J. Knipe, and A. J. Bolton, 2001, Hydrocarbon flow across faults by capillary leakage revisited: Marine and Petroleum Geology, v. 18, p. 251–257, doi:10.1016/S0264-8172(00)00064-7.

Fisher, Q. J., and R. J. Knipe, 2001, The permeability of faults within siliciclastic petroleum reservoirs of the North Sea and Norwegian Continental Shelf: Marine and Petroleum Geology, v. 18, p. 1063–1081, doi:10.1016/S0264-8172(01)00042-3.

Fjellanger, E., T. R. Olsen, and J. L. Rubino, 1996, Sequence stratigraphy and palaeogeography of the Middle Jurassic Brent and Vestland deltaic systems, northern North Sea: Norwegian Geological Survey Bulletin, v. 76, p. 75–106.

Forsberg, C. F., S. Planke, T. I. Tjelta, G. Svanø, J. M. Strout, and H. Svensen, 2007, Formation of pockmarks in the Norwegian Channel: 6th International Offshore Site Investigation and Geotechnics Conference: Confronting New Challenges and Sharing Knowledge, Society of Underwater Technology, p. 221–230.

Fossen, H., 1992, The role of extensional tectonics in the Caledonides of southern Norway: Journal of Structural Geology, v. 14, p. 1033–1046, doi:10.1016/0191-8141(92)90034-T.

Fossen, H., G. Mangerud, J. Hesthammer, T. Bugge, and R. H. Gabrielsen, 1997, The Bjorøy Formation: a newly discovered occurrence of Jurassic sediments in the Bergen Arc System: Norwegian Journal of Geology, v. 77, p. 269–287.

Fossen, H., and C. A. Hurich, 2005, The Hardangerfjord Shear Zone in SW Norway and the North Sea: a large-scale low-angle shear zone in the Caledonian crust: Journal of the Geological Society of London, v. 162, p. 675–687, doi:10.1144/0016-764904-136.

Fossen, H., H. F. Khani, J. I. Faleide, A. K. Ksienzyk, and W. J. Dunlap, 2017, Post-Caledonian extension in the West Norway-northern North Sea region: the role of structural inheritance, *in* C. Childs, R. E. Holdsworth, C. A.-L. Jackson, T. Manzocchi, J. J. Walsh, and G. Yielding, eds., The geometry and growth of normal faults: Geological Society of London Special Publication 439, p. 465–486, doi:10.1144/SP439.6.

Fredman, N., J. Tveranger, S. Semshaug, A. Braathen, and E. Sverdrup, 2007, Sensitivity of fluid flow to fault core architecture and petrophysical properties of fault rocks in siliciclastic reservoirs: a synthetic fault model study: Petroleum Geoscience, v. 13, p. 305–320, doi:10.1144/1354-079306-721.

Freeman, B., G. Yielding, D. T. Needham, and M. E. Badley, 1998, Fault seal prediction: the gouge ratio method, *in* M. P. Coward, T. S. Daltaban, and H. Johnson, eds., Structural geology in reservoir characterization: Geological Society of London Special Publication 127, p. 19–25, doi:10.1144/GSL.SP.1998.127.01.03.

Frost, R. T. C., F. J. Fitch, and J. A. Miller, 1981, The age and nature of the crystalline basement of the North Sea Basin, *in* L. V. Illing, and G. D. Hobson, eds., Petroleum geology of the continental shelf of North-West Europe: London Institute of Petroleum, p. 43–57.

Furre, A. K., O. Eiken, H. Alnes, J. N. Vevatne, and A. F. Kiær, 2017, 20 Years of Monitoring CO_2-injection at Sleipner: Energy Procedia, v. 114, p. 3916–3926, doi:10.1016/j.egypro.2017.03.1523.

Furre, A.-K., R. Meneguolo, P. Ringrose, and S. Kassold, 2019, Building confidence in CCS : From Sleipner to the Northern Lights Project: First Break, v. 37, p. 81–87, doi:10.3997/1365-2397.n0038.

Furre, A.-K., R. Meneguolo, L. Pinturier, and K. Bakke, 2020, Planning deep subsurface CO_2 storage monitoring for the Norwegian full-scale CCS project: First Break, v. 38, p. 55–60, doi:10.3997/1365-2397.fb2020074.

Fyfe, J. A., I. Abbotts, and A. Crosby, 1981, The subcrop of the mid-Mesozoic unconformity in the UK area, *in* L. V. Illing, and G. D. Hobson, eds., Petroleum Geology of the Continental Shelf of North-West Europe: The Geological Society of London, p. 236–244.

Færseth, R. B., R. H. Gabrielsen, and C. A. Hurich, 1995, Influence of basement in structuring of the North Sea Basin, offshore southwest Norway: Norwegian Journal of Geology, v. 75, p. 105–119.

Færseth, R. B., 1996, Interaction of Permo-Triassic and Jurassic extensional fault-blocks during the development of the northern North Sea: Journal of the Geological Society of London, v. 153, p. 931–944, doi:10.1144/gsjgs.153.6.0931.

Gabrielsen, R. H., R. Kyrkjebø, J. I. Faleide, W. Fjeldskaar, and T. Kjennerud, 2001, The Cretaceous post-rift basin configuration of the northern North Sea: Petroleum Geoscience, v. 7, p. 137–154, doi:10.1144/petgeo.7.2.137.

Gabrielsen, R. H., J. P. Nystuen, E. M. Jarsve, and A. M. Lundmark, 2015, The sub-Cambrian peneplain in southern Norway: its geological significance and its implications for post-Caledonian faulting, uplift and denudation: Journal of the Geological Society of London, v. 172, p. 777–791, doi:10.1144/jgs2014-154.

Gawthorpe, R. L., and M. R. Leeder, 2000, Tectono-sedimentary evolution of active extensional basins: Basin Research, v. 12, p. 195–218, doi:10.1111/j.1365-2117.2000.00121.x.

Gee, D. G., H. Fossen, N. Henriksen, and A. K. Higgins, 2008, From the early Paleozoic platforms of Baltica and Laurentia to the Caledonide Orogen of Scandinavia and Greenland: Episodes, v. 31, p. 44–51, doi:10.18814/epiiugs/2008/v31i1/007.

Glennie, K. W., 1990, Outline of North Sea history and structural framework, *in* K. W. Glennie, ed., Introduction to the petroleum geology of the North Sea: Blackwell Scientific Publications, p. 34–77.

GCCSI, 2020, Global Status of CCS: Global CCS Institute Report, 44 p.

Goldsmith, P. J., 2000, Exploration potential east of the Troll field, offshore Norway, after dry well 32/4-1, *in* K. Ofstad, J. E. Kittilsen, and P. Alexander-Marrack, eds., Improving the exploration process by learning from the past: Norwegian Petroleum Society Special Publication 9, p. 65–97, doi:10.1016/S0928-8937(00)80010-7.

Gradstein, F. M., and C. N. Waters, 2016, Stratigraphic guide to the Cromer Knoll, Shetland and Chalk groups, North Sea and Norwegian Sea: Newsletters on Stratigraphy, v. 49, p. 71–280, doi:10.1127/nos/2016/0071.

Gray, I., 1987, Troll, *in* A. M. Spencer, E. Holter, C. J. Campbell, S. Hanslien, P. H. H. Nelson, E. Nysæther, and E. Ormaasen, eds., Geology of the Norwegian oil and gas fields: Graham & Trotman, p. 389–401.

Gudmestad, O. T., 2019, Management of challenges during the construction of offshore facilities: International Journal of Energy Production and Management, v. 4, p. 187–197, doi:10.2495/EQ-V4-N3-187-197.

Hagen, J., and B. Kvalheim, 1992, Oseberg field, *in* M. T. Halbouty, ed., Giant oil and gas fields of the decade 1978–1988: AAPG Memoir 54, p. 417–428, doi:10.1306/m54555c25.

Harris, D., G. Yielding, P. Levine, G. Maxwell, P. T. Rose, and P. A. R. Nell, 2002, Using shale gouge ratio (SGR) to model faults as transmissibility barriers in reservoirs: an example from the Strathspey field, North Sea: Petroleum Geoscience, v. 8, p. 167–176, doi:10.1144/petgeo.8.2.167.

Helland-Hansen, W., M. Ashton, L. Lømo, and R. J. Steel, 1992, Advance and retreat of the Brent delta: recent contributions to the depositional model, *in* A. C. Morton, R. S. Haszeldine, M. R. Giles, and S. Broom, eds., Geology of the Brent Group: Geological Society of London Special Publications 61, p. 109–127, doi:10.1144/GSL.SP.1992.061.01.07.

Heum, O. R., 1996, A fluid dynamic classification of hydrocarbon entrapment: Petroleum Geoscience, v. 2, p. 145–158, doi:10.1144/petgeo.2.2.145.

Holden, N., 2021, Structural characterization and across-fault seal assessment of the Aurora CO_2 storage site, northern North Sea, Master's thesis, University of Oslo, Oslo, Norway, 171 p.

Holgate, N. E., C. A.-L. Jackson, G. J. Hampson, and T. Dreyer, 2013, Sedimentology and sequence stratigraphy of the Middle–Upper Jurassic Krossfjord and Fensfjord formations, Troll field, northern North Sea: Petroleum Geoscience, v. 19, p. 237–258, doi:10.1144/petgeo2012-039.

Horstad, I., and S. R. Larter, 1997, Petroleum migration, alteration, and remigration within Troll field, Norwegian North Sea: AAPG Bulletin, v. 81, p. 222–248, doi:10.1306/522B42F3-1727-11D7-8645000102C1865D.

Hovland, M., 2007, Discovery of prolific natural methane seeps at Gullfaks, northern North Sea: Geo-Marine Letters, v. 27, p. 197–201, doi:10.1007/s00367-007-0070-6.

Høye, T., E. Damsleth, and K. Hollund, 1994, Stochastic structural modeling of Troll West, with special emphasis on the thin oil zone, *in* J. M. Yarus, and R. L. Chambers, eds., Stochastic modeling and geostatistics: AAPG Computer Applications 3, p. 217–239, doi:10.1306/CA3590C17.

Husmo, T., G. P. Hamar, O. Høiland, E. P. Johannessen, A. Rømuld, A. Spenser, and R. Titterton, 2002, Lower and Middle Jurassic, *in* D. Evans, C. Graham, A. Armour, and P. Bathurst, eds., The millennium atlas: petroleum geology of the central and northern North Sea: Geological Society of London, p. 129–155.

Ide, S. T., S. J. Friedmann, and H. J. Herzog, 2006, CO_2 leakage through existing wells: current technology and regulations, *in* N. Rokke, O. Bolland, and J. Gale, eds., 8th International Conference on Greenhouse Gas Control Technologies: Elsevier, 6 p.

IEA, 2015, Carbon capture and storage: the solution for deep emissions reductions: International Energy Agency Publications.

IPCC, 2005, Carbon dioxide capture and storage: Intergovernmental Panel on Climate Change Special Report, Cambridge University Press, 443 p.

IPCC, 2014, Mitigation of climate change: Working Group III contribution to the Fifth Assessment Report of the Intergovernmental Panel on Climate Change: Cambridge University Press, 1454 p., doi:10.1017/cbo9781107415416.

IPCC, 2018, Global warming of 1.5°C: Intergovernmental Panel on Climate Change Special Report, 630 p., doi:10.1038/291285a0.

Isaksen, D., and K. Tonstad, 1989, A revised Cretaceous and Tertiary lithostratigraphic nomenclature for the Norwegian North Sea: Norwegian Petroleum Directorate, 79 p.

Jarsve, E. M., T. E. Maast, R. H. Gabrielsen, J. I. Faleide, P. Johan, and C. Sassier, 2014a, Seismic stratigraphic subdivision of the Triassic integrating seismic reflection and well data: Journal of the Geological Society of London, v. 171, p. 353–374, doi:10.1144/jgs2013-056.

Jarsve, E. M., J. I. Faleide, R. H. Gabrielsen, and J. P. Nystuen, 2014b, Mesozoic and Cenozoic basin configurations in the North Sea, *in* A. W. Martinius, R. B. Ravnås, J. A. Howell, R. J. Steel, and J. P. Wonham, eds., From depositional systems to sedimentary successions on the Norwegian Continental Margin: International Association of Sedimentologists Special Publication 1, p. 417–452, doi:10.1002/9781118920435.ch15.

Johnsen, J. R., H. Rutledal, and D. E. Nilsen, 1995, Jurassic reservoirs; field examples from the Oseberg and Troll fields: Horda Platform area, *in* S. Hanslien, ed., Petroleum exploration and exploitation in Norway: Norwegian Petroleum Society Special Publication 4, p. 199–234, doi:10.1016/S0928-8937(06)80043-3.

Jones, R. M., and R. R. Hillis, 2003, An integrated, quantitative approach to assessing fault-seal risk: AAPG Bulletin, v. 87, p. 507–524, doi:10.1306/10100201135.

Jordt, H., B. I. Thyberg, and A. Nøttvedt, 2000, Cenozoic evolution of the central and northern North Sea with focus on differential vertical movements of the basin floor and surrounding clastic source areas, *in* A. Nøttvedt, B. T. Larsen, R. H. Gabrielsen, S. Olaussen, H. Brekke, B. Tørudbakken, Ø. Birkeland, and J. Skogseid, eds., Dynamics of the Norwegian Margin: Geological Society of London Special Publication 167, p. 219–243, doi:10.1144/GSL.SP.2000.167.01.09.

Karolytė, R., G. Johnson, G. Yielding, and S. M. V. Gilfillan, 2020, Fault seal modelling – the influence of fluid properties on fault sealing capacity in hydrocarbon and CO_2: Petroleum Geoscience, v. 26, p. 610–612, doi:10.1144/petgeo2019-126.

Knag, G., D. South, and A. M. Spencer, 1995, Exploration trends in the northern North Sea (60–62°N), *in* S. Hanslien, ed., Petroleum exploration and exploitation in Norway: Norwegian

Petroleum Society Special Publications 4, p. 115–134, doi:10.1016/S0928-8937(06)80040-8.

Kombrink, H., and S. Patruno, 2020, The integration of public domain lithostratigraphic data into a series of cross-border North Sea well penetration maps, *in* S. Patruno, S. G. Archer, D. Chiarella, J. A. Howell, C. A.-L. Jackson, and H. Kombrink, eds., Themes in petroleum geology I, Geological Society of London Special Publication 494, p. 32, doi:10.1144/sp494-2020-25.

Kristensen, T. B., A. Rotevatn, D. C. P. Peacock, G. A. Henstra, I. Midtkandal, and S. A. Grundvåg, 2016, Structure and flow properties of syn-rift border faults: the interplay between fault damage and fault-related chemical alteration (Dombjerg Fault, Wollaston Forland, NE Greenland): Journal of Structural Geology, v. 92, p. 99–115, doi:10.1016/j.jsg.2016.09.012.

Kyrkjebø, R., R. H. Gabrielsen, and J. I. Faleide, 2004, Unconformities related to the Jurassic–Cretaceous syn-rift–post-rift transition of the northern North Sea: Journal of the Geological Society of London, v. 161, p. 1–17, doi:10.1144/0016-764903-051.

Lauritsen, H., S. Kassold, R. Meneguolo, and A.-K. Furre, 2018, Assessing potential influence of nearby hydrocarbon production on CO_2 storage a Smeaheia: 5th EAGE CO_2 Geological Storage Workshop, European Association of Geoscientists & Engineers, p. 5, doi:10.3997/2214-4609.201802970.

Lepercq, J. Y., and J. M. Gaulier, 1996, Two-stage rifting in the North Viking Graben area (North Sea): inferences from a new three-dimensional subsidence analysis: Marine and Petroleum Geology, v. 13, p. 129–148, doi:10.1016/0264-8172(95)00031-3.

Lervik, K.-S., 2006, Triassic lithostratigraphy of the northern North Sea Basin: Norwegian Journal of Geology, v. 86, p. 93–116.

Lothe, A. E., P. E. S. Bergmo, and A.-A. Grimstad, 2019, Storage resources for future European CCS deployment; a roadmap for a Horda CO_2 storage hub, offshore Norway, *in* N. A. Røkke, and H. Knuutila, eds., 10th Trondheim Conference on CO_2 Capture, Transport and Storage, SINTEF Academic Press, p. 39–48.

Lothe, A. E., P. E. S. Bergmo, B. U. Emmel, A.-A. Grimstad, and P. Eliasson, 2021, How to evaluate and quantify safe CO_2 storage? Workflow demonstration on the Smeaheia area, offshore Norway, 15th International Conference on Greenhouse Gas Control Technologies: Social Science Research Network, p. 9, doi:10.2139/ssrn.3811556.

Lyon, P. J., P. J. Boult, R. R. Hillis, and S. D. Mildren, 2005, Sealing by shale gouge and subsequent seal breach by reactivation: a case study of the Zema prospect, Otway Basin, *in* P. J. Boult, and J. Kaldi, eds., Evaluating fault and cap rock seals: AAPG Hedberg Series 2, p. 179–197, doi:10.1306/1060764H23169.

Magoon, L. B., and W. G. Dow, 1994, The petroleum system, *in* L. B. Magoon, and W. G. Dow, eds., The petroleum system—from source to trap: AAPG Memoir 60, p. 3–24, doi:10.1306/M60585C1.

Marjanac, T., and R. J. Steel, 1997, Dunlin Group sequence stratigraphy in the northern North Sea: A model for Cook Sandstone deposition: AAPG Bulletin, v. 81, p. 276–292, doi:10.1306/522B4307-1727-11D7-8645000102C1865D.

Martinsen, O. J., T. Lien, and C. A.-L. Jackson, 2005, Cretaceous and Palaeogene turbidite systems in the North Sea and Norwegian Sea basins: source, staging area and basin physiography controls on reservoir development, *in* A. G. Doré, and B. A. Vining, eds., Petroleum geology of North-West Europe and global perspectives: Geological Society of London Petroleum Geology Conference Series 6, p. 1147–1164, doi:10.1144/0061147.

Mazzini, A., H. H. Svensen, S. Planke, C. F. Forsberg, and T. I. Tjelta, 2016, Pockmarks and methanogenic carbonates above the giant Troll gas field in the Norwegian North Sea: Marine Geology, v. 373, p. 26–38, doi:10.1016/j.margeo.2015.12.012.

Meckel, T. A., A. P. Bump, S. D. Hovorka, and R. H. Trevino, 2021, Carbon capture, utilization, and storage hub development on the Gulf Coast: Greenhouse Gases: Science and Technology, v. 14, p. 1–14, doi:10.1002/ghg.2082.

Mazzini, A., H. H. Svensen, C. F. Forsberg, H. Linge, S. E. Lauritzen, H. Haflidason, Ø. Hammer, S. Planke, and T. I. Tjelta, 2017, A climatic trigger for the giant Troll pockmark field in the northern North Sea: Earth and Planetary Science Letters, v. 464, p. 24–34, doi:10.1016/j.epsl.2017.02.014.

Miocic, J. M., G. Johnson, and C. E. Bond, 2019, Uncertainty in fault seal parameters: implications for CO_2 column height retention and storage capacity in geological CO_2 storage projects: Solid Earth, v. 10, p. 951–967, doi:10.5194/se-10-951-2019.

Miocic, J. M., G. Johnson, and S. M. V. Gilfillan, 2020, Stress field orientation controls on fault leakage at a natural CO_2 reservoir: Solid Earth, v. 11, p. 1361–1374, doi:10.5194/se-11-1361-2020.

Mulrooney, M. J., J. L. Osmond, E. Skurtveit, L. Wu, and A. Braathen, 2018, Smeaheia, a potential northern North Sea CO_2 storage site: structural description and de-risking strategies: 5th EAGE CO_2 Geological Storage Workshop, European Association of Geoscientists & Engineers, p. 5, doi:10.3997/2214-4609.201802957.

Mulrooney, M. J., J. L. Osmond, E. Skurtveit, J. I. Faleide, and A. Braathen, 2020, Structural analysis of the Smeaheia fault block, a potential CO_2 storage site, northern Horda Platform, North Sea: Marine and Petroleum Geology, v. 121, p. 104598, doi:10.1016/j.marpetgeo.2020.104598.

Naruk, S. J., J. G. Solum, J. P. Brandenburg, P. Origo, and D. E. Wolf, 2019, Effective stress constraints on vertical flow in fault zones: Learnings from natural CO_2 reservoirs: AAPG Bulletin, v. 103, p. 1979–2008, doi:10.1306/12181817393.

Nipen, O., 1987, Oseberg, *in* A. M. Spencer, E. Holter, C. J. Campbell, S. Hanslien, P. H. H. Nelson, E. Nysæther, and E. Ormaasen, eds., Geology of the Norwegian oil and gas fields: Graham & Trotman, p. 379–387.

Nøttvedt, A., R. H. Gabrielsen, and R. J. Steel, 1995, Tectonostratigraphy and sedimentary architecture of rift basins, with reference to the northern North Sea: Marine and Petroleum Geology, v. 12, p. 881–901, doi:10.1016/0264-8172(95)98853-W.

Norton, M. G., 1986, Late Caledonide extension in western Norway: a response to extreme crustal thickening: Tectonics, v. 5, p. 195–204, doi:10.1029/TC005i002p00195.

NMPE, 2020, Longship – carbon capture and storage: Norwegian Ministry of Petroleum and Energy Meld. St. 33, 92 p.

NPD, 2011, CO_2 storage atlas: Norwegian North Sea: Norwegian Petroleum Directorate, 72 p.

NPD, 2014, Lithostratigraphic chart - Norwegian North Sea: Norwegian Petroleum Directorate, 1 p.

Odinsen, T., P. Christiansson, R. H. Gabrielsen, J. I. Faleide, and A. M. Berge, 2000, The geometries and deep structure of the northern North Sea rift system, *in* A. Nøttvedt, B. T. Larsen, S. Olaussen, B. Tørudbakken, J. Skogseid, R. H. Gabrielsen, H. Brekke, and Ø.

Birkeland, eds., Dynamics of the Norwegian Margin: Geological Society of London Special Publication 167, p. 41–57, doi:10.1144/GSL.SP.2000.167.01.03.

Orsini, P., D. Ponting, D. Stone, and B. Nazarian, 2020, An assessment of the CO_2 fate at Smeaheia, a potential large-scale storage site in Norway: EAGE Annual Conference & Exhibition, European Association of Geoscientists & Engineers, p. 5, doi:10.3997/2214-4609.202011099.

Ottesen, D., C. L. Batchelor, J. A. Dowdeswell, and H. Løseth, 2018, Morphology and pattern of Quaternary sedimentation in the North Sea Basin (52–62°N): Marine and Petroleum Geology, v. 98, p. 836–859, doi:10.1016/j.marpetgeo.2018.08.022.

Osmond, J. L., and T. A. Meckel, 2020, Enhancing trap and fault seal analyses by integrating observations from HR3D seismic data with well logs and conventional 3D seismic data, Texas inner shelf, *in* S. R. Ogilvie, S. J. Dee, R. W. Wilson, and W. R. Bailey, eds., Integrated fault seal analysis: Geological Society of London Special Publication 496, p. 253–279, doi:10.1144/sp496-2018-142.

Osmond, J. L., M. J. Mulrooney, E. Skurtveit, and A. Braathen, 2020, Distribution of faulted Mesozoic and Tertiary seals for CCS in the Horda Platform, northern North Sea: 82nd EAGE Annual Conference & Exhibition, European Association of Geoscientists & Engineers, p. 5, doi:10.3997/2214-4609.202012027.

Patruno, S., G. J. Hampson, C. A.-L. Jackson, and T. Dreyer, 2015, Clinoform geometry, geomorphology, facies character and stratigraphic architecture of a sand-rich subaqueous delta: Jurassic Sognefjord Formation, offshore Norway: Sedimentology, v. 62, p. 350–388, doi:10.1111/sed.12153.

Pei, Y., D. A. Paton, R. J. Knipe, and K. Wu, 2015, A review of fault sealing behaviour and its evaluation in siliciclastic rocks: Earth-Science Reviews, v. 150, p. 121–138, doi:10.1016/j.earscirev.2015.07.011.

Phillips, T. B., H. Fazlikhani, R. L. Gawthorpe, H. Fossen, C. A.-L. Jackson, R. E. Bell, J. I. Faleide, and A. Rotevatn, 2019, The influence of structural inheritance and multiphase extension on rift development, the northern North Sea: Tectonics, v. 38, p. 4099–4126, doi:10.1029/2019TC005756.

Prosser, S., 1993, Rift-related linked depositional systems and their seismic expression, *in* G. D. Williams, and A. Dobb, eds., Tectonics and seismic sequence stratigraphy: Geological Society of London Special Publication 71, p. 35–66, doi:10.1144/GSL.SP.1993.071.01.03.

Rahman, M. J., M. Fawad, and N. H. Mondol, 2020, Organic-rich shale caprock properties of potential CO_2 storage sites in the northern North Sea, offshore Norway: Marine and Petroleum Geology, v. 122, p. 25, doi:10.1016/j.marpetgeo.2020.104665.

Rahman, M. J., J. C. Choi, M. Fawad, and N. H. Mondol, 2021, Probabilistic analysis of Vette fault stability in potential CO_2 storage site Smeaheia, offshore Norway: International Journal of Greenhouse Gas Control, v. 108, p. 103315, doi:10.1016/j.ijggc.2021.103315.

Randen, T., and L. Sønneland, 2005, Atlas of 3D seismic attributes, *in* A. Iske, and L. Sønneland, eds., Mathematical methods and modelling in hydrocarbon exploration and production: Springer, p. 23–46, doi:10.1007/3-540-26493-0_2.

Rattey, R. P., and A. B. Hayward, 1993, Sequence stratigraphy of a failed rift system: the Middle Jurassic to Early Cretaceous basin evolution of the central and northern North Sea, *in* J. R. Parker, ed., Petroleum geology of Northwest Europe: Geological Society of London Petroleum Geology Conference Series 4, p. 215–249, doi:10.1144/0040215.

Ravnås, R., A. Nøttvedt, R. J. Steel, and J. Windelstad, 2000, Syn-rift sedimentary architectures in the Northern North Sea, *in* A. Nøttvedt, B. T. Larsen, S. Olaussen, B. Tørudbakken, J. Skogseid, R. H. Gabrielsen, H. Brekke, and Ø. Birkeland, eds., Dynamics of the Norwegian Margin: Geological Society of London Special Publications 167, p. 133–177, doi:10.1144/GSL.SP.2000.167.01.07.

Rawson, P. F., and L. A. Riley, 1982, Latest Jurassic–Early Cretaceous events and the "late Cimmerian unconformity" in North Sea area: AAPG Bulletin, v. 66, p. 2628–2648, doi:10.1306/03b5ac87-16d1-11d7-8645000102c1865d.

Riis, F., 1996, Quantification of Cenozoic vertical movements of Scandinavia by correlation of morphological surfaces with offshore data: Global and Planetary Change, v. 12, p. 331–357, doi:10.1016/0921-8181(95)00027-5.

Riis, F., 2018, Norway CCS Demonstration Project: evaluation of Jurassic reservoirs for safe CO_2 injection and storage: 5th EAGE CO_2 Geological Storage Workshop, European Association of Geoscientists & Engineers, p. 5, doi:10.3997/2214-4609.201802954.

Ringrose, P. S., and T. A. Meckel, 2019, Maturing global CO_2 storage resources on offshore continental margins to achieve 2DS emissions reductions: Scientific Reports, v. 9, p. 1–10, doi:10.1038/s41598-019-54363-z.

Ringrose, P. S., A. K. Furre, S. M. V. Gilfillan, S. Krevor, M. Landroslash, R. Leslie, T. Meckel, B. Nazarian, and A. Zahid, 2021, Storage of carbon dioxide in saline aquifers: physicochemical processes, key constraints, and scale-up potential: Annual Review of Chemical and Biomolecular Engineering, v. 12, p. 471–494, doi:10.1146/annurev-chembioeng-093020-091447.

Roberts, A. M., N. J. Kusznir, G. Yielding, and H. Beeley, 2019, Mapping the bathymetric evolution of the northern North Sea: from Jurassic synrift archipelago through Cretaceous–Tertiary post-rift subsidence: Petroleum Geoscience, v. 25, p. 306–321, doi:10.1144/petgeo2018-066.

Røe, S.-L., and R. J. Steel, 1985, Sedimentation, sea-level rise and tectonics at the Triassic-Jurassic boundary (Statfjord Formation), Tampen Spur, northern North Sea: Journal of Petroleum Geology, v. 8, p. 163–186, doi:10.1111/j.1747-5457.1985.tb01009.x.

Sales, J. K., 1997, Seal strength vs. trap closure — fundamental control on the distribution of oil and gas, *in* R. C. Surdam, ed., Seals, traps, and the petroleum system: AAPG Memoir 67, p. 57–83, doi:10.1306/M67611C5.

Sejrup, H. P., I. Aarseth, H. Haflidason, R. Løvlie, Å. Bratten, G. Tjøstheim, C. F. Forsberg, and K. L. Ellingsen, 1995, Quaternary of the Norwegian Channel: glaciation history and palaeoceanography: Norwegian Journal of Geology, v. 75, p. 65–87, doi:0029-196X.

Skurtveit, E., J. C. Choi, J. L. Osmond, M. J. Mulrooney, and A. Braathen, 2018, 3D fault integrity screening for Smeaheia CO_2 injection site, 14th International Conference on Greenhouse Gas Control Technologies: Social Science Research Network, p. 10, doi:10.2139/ssrn.3366335.

Sneider, J. S., P. de Clarens, and P. R. Vail, 1995, Sequence stratigraphy of the Middle to Upper Jurassic, Viking Graben, North Sea, *in* R. J. Steel, V. Felt, E. P. Johannessen, and C. Mathieu, eds., Sequence stratigraphy of the Northwest European Margin: Norwegian Petroleum Society Special Publication 5, p. 167–197, doi:10.1016/S0928-8937(06)80068-8.

Spencer, A. M., and V. B. Larsen, 1990, Fault traps in the northern North Sea, *in* R. F. P. Hardman, and J. Brooks, eds., Tectonic events responsible for Britain's oil and gas reserves:

Geological Society of London Special Publications 55, p. 281–298, doi:10.1144/GSL.SP.1990.055.01.13.

Sperrevik, S., P. A. Gillespie, Q. J. Fisher, T. Halvorsen, and R. J. Knipe, 2002, Empirical estimation of fault rock properties, *in* A. G. Koestler, and R. Hundsdale, eds., Hydrocarbon seal quantification: Norwegian Petroleum Society Special Publication 11, p. 109–125, doi:10.1016/S0928-8937(02)80010-8.

Steel, R. J., and A. Ryseth, 1990, The Triassic -- early Jurassic succession in the northern North Sea: megasequence stratigraphy and intra-Triassic tectonics, *in* R. F. P. Hardman, and J. Brooks, eds., Petroleum geology of Northwest Europe: Geological Society of London Petroleum Geology Conference Series 4, p. 139–168, doi:10.1144/GSL.SP.1990.055.01.07.

Steel, R. J., 1993, Triassic–Jurassic megasequence stratigraphy in the northern North Sea: rift to post-rift evolution, *in* J. R. Parker, ed., Geological Society of London Petroleum Geology Conference Series 4, p. 299–315, doi:10.1144/0040299.

Stewart, D. J., M. Schwander, and L. Bolle, 1995, Jurassic depositional systems of the Horda Platform, Norwegian North Sea: practical consequences of applying sequence stratigraphic techniques, *in* R. J. Steel, ed., Sequence stratigraphy on the Northwest European Margin: Norwegian Petroleum Society Special Publication 5, p. 291–323, doi:10.1016/S0928-8937(06)80073-1.

Sundal, A., J. P. Nystuen, K. L. Rørvik, H. Dypvik, and P. Aagaard, 2016, The Lower Jurassic Johansen Formation, northern North Sea – depositional model and reservoir characterization for CO_2 storage: Marine and Petroleum Geology, v. 77, p. 1376–1401, doi:10.1016/j.marpetgeo.2016.01.021.

Sundal, A., and H. Hellevang, 2019, Using reservoir geology and petrographic observations to improve CO_2 mineralization estimates; examples from the Johansen Formation, North Sea, Norway: Minerals, v. 9, p. 23, doi:10.3390/min9110671.

Tillmans, F., R. L. Gawthorpe, C. A.-L. Jackson, and A. Rotevatn, 2021, Syn-rift sediment gravity flow deposition on a Late Jurassic fault-terraced slope, northern North Sea: Basin Research, v. 33, p. 1844–1879, doi:10.1111/bre.12538.

Torabi, A., B. Alaei, and T. S. S. Ellingsen, 2018, Faults and fractures in basement rocks, their architecture, petrophysical and mechanical properties: Journal of Structural Geology, v. 117, p. 256–263, doi:10.1016/j.jsg.2018.07.001.

Underhill, J. R., and M. A. Partington, 1993, Jurassic thermal doming and deflation in the North Sea: implications of the sequence stratigraphic evidence, *in* J. R. Parker, ed., Petroleum geology of Northwest Europe: Geological Society of London Petroleum Geology Conference Series 4, p. 337–345, doi:10.1144/0040337.

USGS, 2000, U.S. Geological Survey World Petroleum Assessment: DDS-60, https://energy.usgs.gov/OilGas/AssessmentsData/WorldPetroleumAssessment.aspx (accessed July 3, 2021).

van Ojik, K., A. Silvius, Y. Kremer, and Z. K. Shipton, 2020, Fault seal behaviour in Permian Rotliegend reservoir sequences: case studies from the Dutch Southern North Sea, *in* S. R. Ogilvie, S. J. Dee, R. W. Wilson, and W. R. Bailey, eds., Integrated fault seal analysis: Geological Society of London Special Publication 496, p. 9–38, doi:10.1144/sp496-2018-189.

Vetti, V. V., and H. Fossen, 2012, Origin of contrasting Devonian supradetachment basin types in the Scandinavian Caledonides: Geology, v. 40, p. 571–574, doi:10.1130/G32512.1.

Vollset, J., and A. G. Doré, 1984, A revised Triassic and Jurassic lithostratigraphic nomenclature for the Norwegian North Sea: Norwegian Petroleum Directorate, 53 p.

Watts, N. L., 1987, Theoretical aspects of cap-rock and fault seals for single- and two-phase hydrocarbon columns: Marine and Petroleum Geology, v. 4, p. 274–307, doi:10.1016/0264-8172(87)90008-0.

Whipp, P. S., C. A.-L. Jackson, R. L. Gawthorpe, T. Dreyer, and D. Quinn, 2014, Normal fault array evolution above a reactivated rift fabric; a subsurface example from the northern Horda Platform, Norwegian North Sea: Basin Research, v. 26, p. 523–549, doi:10.1111/bre.12050.

Wibberley, C. A. J., J. Gonzalez-Dunia, and O. Billon, 2017, Faults as barriers or channels to production-related flow: insights from case studies: Petroleum Geoscience, v. 23, p. 134–147, doi:10.1144/petgeo2016-057.

Wiest, J. D., T. Wrona, M. S. Bauck, H. Fossen, R. L. Gawthorpe, P. T. Osmundsen, and J. I. Faleide, 2020, From Caledonian collapse to North Sea rift: the extended history of a metamorphic core complex: Tectonics, v. 39, p. 15, doi:10.1029/2020TC006178.

Wrona, T., C. Magee, C. A.-L. Jackson, M. Huuse, and K. G. Taylor, 2017, Kinematics of polygonal fault systems: observations from the northern North Sea: Frontiers in Earth Science, v. 5, p. 21, doi:10.3389/feart.2017.00101.

Wu, L., R. Thorsen, S. Ottesen, R. Meneguolo, K. Hartvedt, P. Ringrose, and B. Nazarian, 2021a, Significance of fault seal in assessing CO_2 storage capacity and containment risks – an example from the Horda Platform, northern North Sea: Petroleum Geoscience, v. 27, petgeo2020-12, doi:10.1144/petgeo2020-102.

Wu, L., H. Fossen, R. Thorsen, P. Ringrose, and B. Nazarian, 2021b, Advances in understanding the Øygarden Fault System—insights from offshore seismic interpretation and onshore Bjorøy Fault Zone: 10th Trondheim Conference on CO_2 Capture, Transport and Storage, SINTEF Academic Press.

Würtzen, C. L., J. L. Osmond, J. I. Faleide, J. P. Nystuen, I. M. Anell, and I. Midtkandal, In review, Syn- to post-rift alluvial basin fill: seismic stratigraphic analysis of the Permian-Triassic deposition in the Horda Platform, Norway: Basin Research, p. 43, doi:10.31223/X5K32G.

Yielding, G., 1990, Footwall uplift associated with Late Jurassic normal faulting in the northern North Sea: Journal of the Geological Society of London, v. 147, p. 219–222, doi:10.1144/gsjgs.147.2.0219.

Yielding, G., B. Freeman, and D. T. Needham, 1997, Quantitative fault seal prediction: AAPG Bulletin, v. 81, p. 897–917, doi:10.1306/522B498D-1727-11D7-8645000102C1865D.

Yielding, G., 2002, Shale gouge ratio - calibration by geohistory, *in* A. G. Koestler, and R. Hunsdale, eds., Hydrocarbon seal quantification: Norwegian Petroleum Society Special Publication 11, p. 1–15, doi:10.1016/S0928-8937(02)80003-0.

Yielding, G., P. Bretan, and B. Freeman, 2010, Fault seal calibration: a brief review, *in* S. J. Jolly, Q. J. Fisher, R. B. Ainsworth, P. J. Vrolijk, and S. Delisle, eds., Reservoir compartmentalization: Geological Society of London Special Publication 347, p. 243–255, doi:10.1144/SP347.14.

Zahasky, C., and S. Krevor, 2020, Global geologic carbon storage requirements of climate change mitigation scenarios: Energy & Environmental Science, v. 13, p. 1561–1567, doi:10.1039/D0EE00674B.

Zhong, X., and A. Escalona, 2020, Evidence of rift segmentation and controls of Middle to Late Jurassic synrift deposition in the Ryggsteinen Ridge area, northern North Sea: AAPG Bulletin, v. 104, p. 1531–1565, doi:10.1306/03172018173.

Ziegler, P. A., 1975, Geologic evolution of North Sea and its tectonic framework: AAPG Bulletin, v. 59, p. 1073–1097, doi:10.1306/83D91F2E-16C7-11D7-8645000102C1865D.

Ziegler, P. A., 1982, Triassic rifts and facies pattern in Western and Central Europe: International Journal of Earth Sciences, v. 71, p. 747–772, doi: 10.1007/BF01821101.

Ziegler, P. A., 1990, Geological atlas of western and central Europe: Shell International Petroleum, 239 p.

Figure captions

1. Figure 1. Regional map of the northern Horda Platform area of the North Sea along West Norway highlighting the location of regional structures, hydrocarbon exploration wells and discoveries, CCS exploitation licenses and infrastructure, as well as data utilized for this study. All maps herein are displayed using European Datum 1950 UTM Zone 31N projected coordinate system. DK = Denmark; HNFZ = Horda North Fault Zone; LT = Lomre Terrace; ØFZ = Øygarden Fault Zone; SFB; Smeaheia fault block; SVFZ = Svartalv Fault Zone; SVFB = Svartalv fault block; TRFZ = Troll Fault Zone; TFZ = Tusse Fault Zone; TFB = Tusse fault block; UT = Uer Terrace; VFZ = Vette Fault Zone.
2. Figure 2. Regional structure and local stratigraphy of the northern Horda Platform. (A) Map of structural elements of the northern North Sea Rift Basin compiled from Roberts et al. (1995), Færseth et al. (1995), and Domínguez (2007), and modified after Whipp et al., 2014. (B) Chronostratigraphic chart of the Horda Platform modified after the NPD

(2014) and gamma-ray well log correlation with data from CO_2 exploitation well 31/5-7 (Eos). Key stratigraphic units representing potential storage aquifers, intermediate aquifers, and seals are indicated and grouped into corresponding Lower and Upper Jurassic CO_2 storage complexes (dark and light blue annotation, respectively).

3. Figure 3. Composite seismic section A–A’ running approximately west to east from left to right through the northern Horda Platform study area. (A) Uninterpreted seismic section. (B) Corresponding interpreted section with stratigraphic units and faults. (C) Corresponding interpreted section with Lower and Upper Jurassic CO_2 storage complex aquifers and seals, as well as faults. See Figure 1 for explanation of abbreviations. Scientific color bar (version 7.0.0) sourced from Crameri (2021). Wellbore intersections and section kinks indicated along the top of the section. Distance shown in kilometers and depth in meters TVDSS. Section location (red lines) shown in inset map. VE = vertical exaggeration.
4. Figure 4. Gamma-ray log correlation section B–B’ running west to east from left to right through the northern Horda Platform study area. Lower and Upper Jurassic CO_2 storage aquifers and seals are indicated, along with pertinent stratigraphic tops. Depth datum and log curves are hung at the top Sognefjord Formation and corresponding fault block locations are indicated at the bottom. Wellbores are spaced relative to one another with depth shown in meters TVDSS. Section location (red lines) shown in inset map.
5. Figure 5. Gross storage aquifer isochore thickness maps (m) for the (A) Lower and (B) Upper Jurassic storage complexes based on 3D seismic interpretation. Individual maps are plotted at different scales. Scientific color bar (version 7.0.0) sourced from Crameri

(2021). Distance shown in kilometers. CI = contour interval (bolded at increments of five).

6. Figure 6. Top storage aquifer structure maps (m TVDSS) for the (A) Lower and (B) Upper Jurassic storage complexes based on 3D seismic interpretation. Maps are plotted at the same scale. Scientific color bar (version 7.0.0) sourced from Crameri (2021). Distance shown in kilometers. CI = contour interval (bolded at increments of five).
7. Figure 7. Top storage aquifer seismic variance attribute maps for the (A) Lower and (B) Upper Jurassic storage complexes. Attribute values extracted from along the corresponding top storage aquifer structure surfaces shown in Figure 6. Scientific color bar (version 7.0.0) sourced from Crameri (2021). Distance shown in kilometers.
8. Figure 8. Gross seal isochore thickness maps (m) for the (A) Lower and (B) Upper Jurassic storage complexes based on 3D seismic interpretation. Individual maps are plotted at different scales. Scientific color bar (version 7.0.0) sourced from Crameri (2021). Distance shown in kilometers. CI = contour interval (bolded at increments of five).
9. Figure 9. Structural traps within the northern Horda Platform study area. (A, C) Lower and (B, D) Upper Jurassic trap closure area polygons overlaid on (A, B) top storage aquifer structure maps (m TVDSS; Figure 6) and (C, D) seal isochore thickness maps (m; Figure 8). 50 Lower Jurassic traps and 28 Upper Jurassic traps. Traps derived from structural surfaces shown in Figure 6. Hydrocarbon discoveries are also overlaid on maps corresponding to the Upper Jurassic CO_2 storage complex (B, C). Note the greater Troll field polygon approximately correlates with the largest trap closure area

10. Figure 10. Plots of trap closure statistics for Lower and Upper Jurassic storage complex traps. (A) Scatter plot of closure height (m) versus basal closure area (km^2), log/log scale. Insets for the 50 Lower Jurassic traps (upper; dark blue polygons) and 28 Upper Jurassic traps (lower; light blue polygons) are down in the left side of the figure. (B) Bar chart of trap gross-rock-volume (GRV; m^3), log scale. Detailed trap locations shown in Figure 9.
11. Figure 11. Composite seismic section C–C' running approximately west to east from left to right through the northern Horda Platform study area. (A) Uninterpreted seismic section. (B) Corresponding interpreted section with Lower and Upper Jurassic CO_2 storage complex aquifers and seals, trap closure bases, as well as faults. See Figure 1 for explanation of abbreviations. Scientific color bar (version 7.0.0) sourced from Crameri (2021). Wellbore intersections and section kinks indicated along the top of the section. Distance shown in kilometers and depth in meters TVDSS. Section location (red lines) shown in inset map. VE = vertical exaggeration.
12. Figure 12. Composite seismic section D–D' running approximately west to east from left to right through the northern Horda Platform study area. (A) Uninterpreted seismic section. (B) Corresponding interpreted section with Lower and Upper Jurassic CO_2 storage complex aquifers and seals, trap closure bases, as well as faults. Generalized northward migration of injected CO_2 from wellbore 31/5-7 show with the dashed dark blue arrow. See Figure 1 for explanation of abbreviations. Scientific color bar (version 7.0.0) sourced from Crameri (2021). Wellbore intersections and section kinks indicated along the top of the section. Distance shown in kilometers and depth in meters TVDSS. Section location (red lines) shown in inset map. Dashed vertical lines are projected wellbores. VE = vertical exaggeration.

13. Figure 13. Composite seismic section E–E' running approximately west to east from left to right through the northern Horda Platform study area. (A) Uninterpreted seismic section. (B) Corresponding interpreted section with interpreted Lower and Upper Jurassic CO_2 storage complex aquifers and seals, trap closure bases, as well as faults. See Figure 1 for explanation of abbreviations. Scientific color bar (version 7.0.0) sourced from Crameri (2021). Wellbore intersections and section kinks indicated along the top of the section. Distance shown in kilometers and depth in meters TVDSS. Section location (red lines) shown in inset map. VE = vertical exaggeration.
14. Figure 14. Allan diagrams for illustrating aquifer and seal juxtaposition contacts only against Lower and Upper Jurassic storage aquifers in the footwall. (A) Svartalv Fault Zone. (B) Tusse Fault Zone. Note that the southern tip of the fault is located outside the available 3D seismic data coverage (see Figure 1), and this model is incomplete. (C) Vette Fault Zone segments 1 and 2. Horizon cutoff lines and trap closure bases are also indicated. Three-dimensional perspective view from the northwest of unfiltered models and fault location (red lines) maps shown in separate insets. VE = vertical exaggeration.
15. Figure 15. Formation pressure data plots for wellbores 31/5-7, 31/3-4, and 32/4-3 S within Svartalv, Tusse, and Smeaheia fault blocks, respectively. Plots are overlaid on a schematic cross-section indicating their structural position of Lower and Upper Jurassic CO_2 storage complex aquifers and seals within each fault block. Storage aquifer juxtapositions along the Tusse and Vette fault zones are also indicated. Pressure data are plotted at the same scale and hydrostatic gradient (ρ_w = 1.03 g/cm^3). Wellbore locations (red dots) shown in inset map.

16. Figure 16. Allan diagrams for illustrating calculated shale gouge ratio (SGR) values only against Lower and Upper Jurassic storage aquifers in the footwall. (A) Svartalv Fault Zone. (B) Tusse Fault Zone. Note that the southern tip of the fault is located outside the available 3D seismic data coverage (see Figure 1), and this model is incomplete. (C) Vette Fault Zone segments 1 and 2. Horizon cutoff lines and trap closure bases are also indicated. Note discrete SGR scaling. Three-dimensional perspective view from the northwest of unfiltered models, as well as fault (red lines) and well data (yellow dots) location maps shown in separate insets. Not that SGR values are plotted discretely. VE = vertical exaggeration.

Table captions

1. Table 1. Summary of aquifer and seal attributes for Lower and Upper Jurassic storage complexes in the northern Horda Platform. Attributes have been partitioned with respect to fault block location. P = primary seal unit; S = secondary seal unit; T = tertiary seal unit.
2. Table 2. Summary of fault seal attributes for analyzed faults displacing Upper and Lower Jurassic storage complexes. Attributes have been partitioned with respect to individual fault zones, and pertain to their footwall sides. AFPD = across fault pressure differential; SGR = shale gouge ratio; HWC = hydrocarbon-water contact.

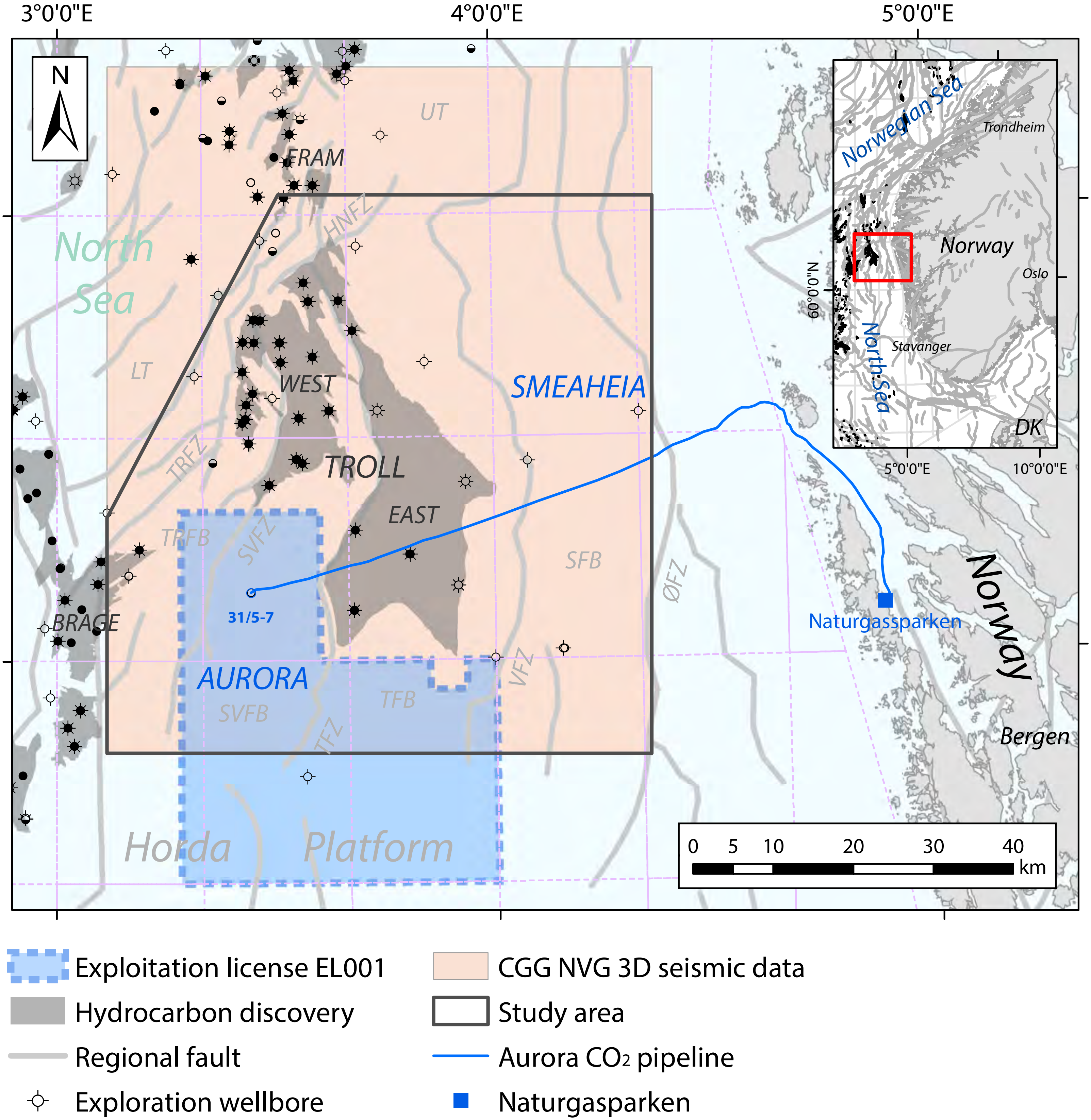
3°0'0"E
4°0'0"E
5°0'0"E
61°0'0"N
60°30'0"N
N
North Sea
UT
FRAM
HNFZ
LT
WEST
TROLL
EAST
TRFZ
TRFB
SVFZ
SMEAHEIA
SFB
ØFZ
BRAGE
31/5-7
AURORA
SVFB
TFB
TFZ
VFZ
Horda Platform
Naturgassparken
Norway
Bergen
Norwegian Sea
Trondheim
Norway
Oslo
60°0'0"N
North Sea
Stavanger
DK
5°0'0"E
10°0'0"E
0 5 10 20 30 40 km
Exploitation license EL001
Hydrocarbon discovery
Regional fault
Exploration wellbore
CGG NVG 3D seismic data
Study area
Aurora CO2 pipeline
Naturgasparken

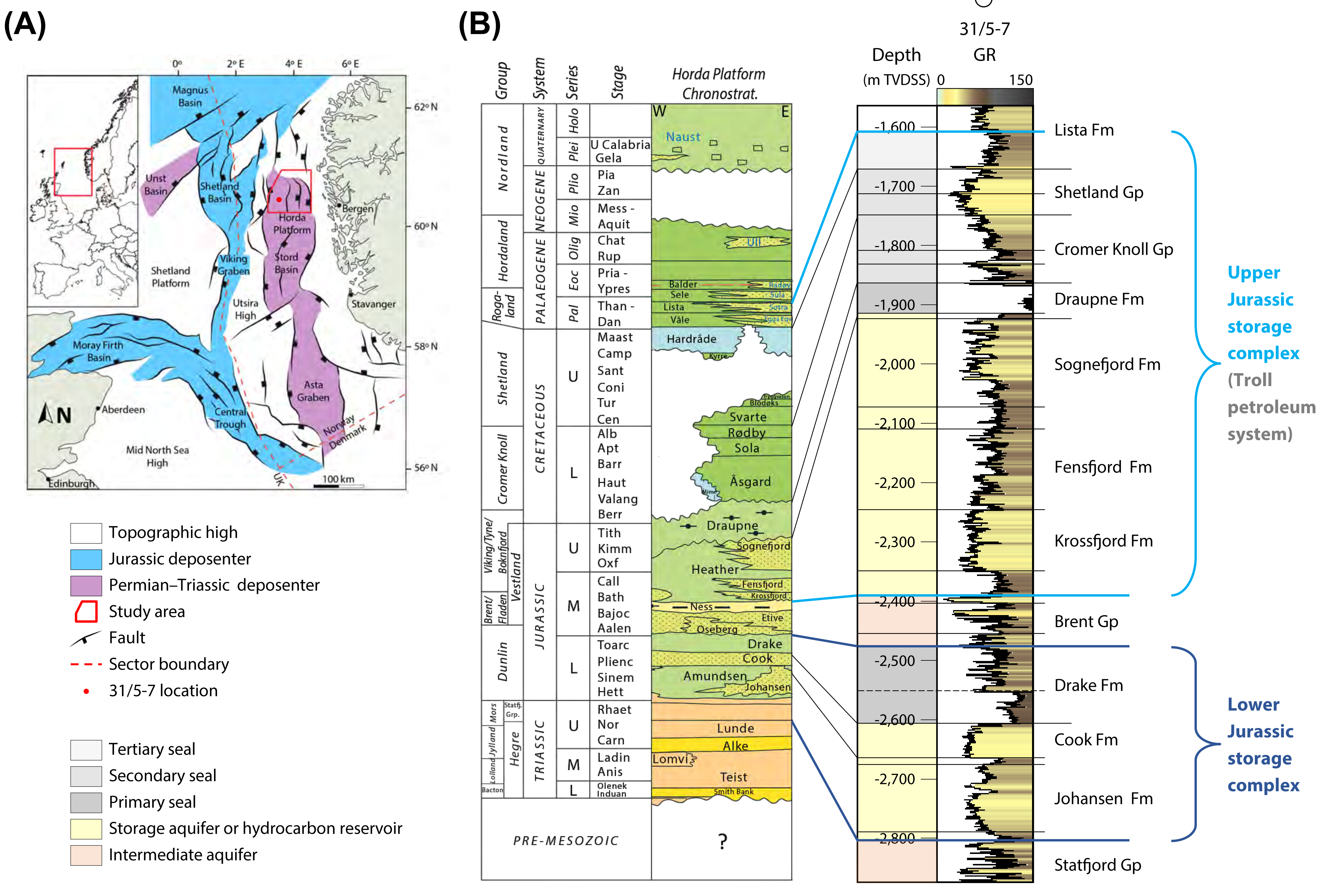

(A)
(B)
0°
2° E
4° E
6° E
62° N
60° N
58° N
56° N
Magnus Basin
Unst Basin
Shetland Basin
Horda Platform
Bergen
Viking Graben
Stord Basin
Shetland Platform
Utsira High
Stavanger
Moray Firth Basin
Asta Graben
N
Aberdeen
Central Trough
Norway
Denmark
Mid North Sea High
UK
100 km
Edinburgh
Topographic high
Jurassic deposenter
Permian–Triassic deposenter
Study area
Fault
Sector boundary
31/5-7 location
Tertiary seal
Secondary seal
Primary seal
Storage aquifer or hydrocarbon reservoir
Intermediate aquifer
Group
System
Series
Stage
Horda Platform Chronostrat.
W
E
Nordland
Hordaland
Rogaland
Shetland
Cromer Knoll
Viking/Tyne/Boknfjord
Brent/Fladen
Vestland
Dunlin
Statfj. Grp.
Mors
Jylland
Lolland
Bacton
Hegre
QUATERNARY
NEOGENE
PALAEOGENE
CRETACEOUS
JURASSIC
TRIASSIC
PRE-MESOZOIC
Holo
Plei
Plio
Mio
Olig
Eoc
Pal
U
L
M
U Calabria
Gela
Pia
Zan
Mess - Aquit
Chat
Rup
Pria - Ypres
Than - Dan
Maast
Camp
Sant
Coni
Tur
Cen
Alb
Apt
Barr
Haut
Valang
Berr
Tith
Kimm
Oxf
Call
Bath
Bajoc
Aalen
Toarc
Plienc
Sinem
Hett
Rhaet
Nor
Carn
Ladin
Anis
Olenek
Induan
Naust
Utsira
Balder
Sele
Lista
Våle
Hardråde
Kyrre
Svarte
Rødby
Sola
Åsgard
Draupne
Sognefjord
Heather
Fensfjord
Krossfjord
Ness
Etive
Oseberg
Drake
Cook
Amundsen
Johansen
Lunde
Alke
Lomvi
Teist
Smith Bank
?
31/5-7
Depth
(m TVDSS)
GR
0
150
-1,600
-1,700
-1,800
-1,900
-2,000
-2,100
-2,200
-2,300
-2,400
-2,500
-2,600
-2,700
-2,800
Lista Fm
Shetland Gp
Cromer Knoll Gp
Draupne Fm
Sognefjord Fm
Fensfjord Fm
Krossfjord Fm
Brent Gp
Drake Fm
Cook Fm
Johansen Fm
Statfjord Gp
Upper Jurassic storage complex
(Troll petroleum system)
Lower Jurassic storage complex

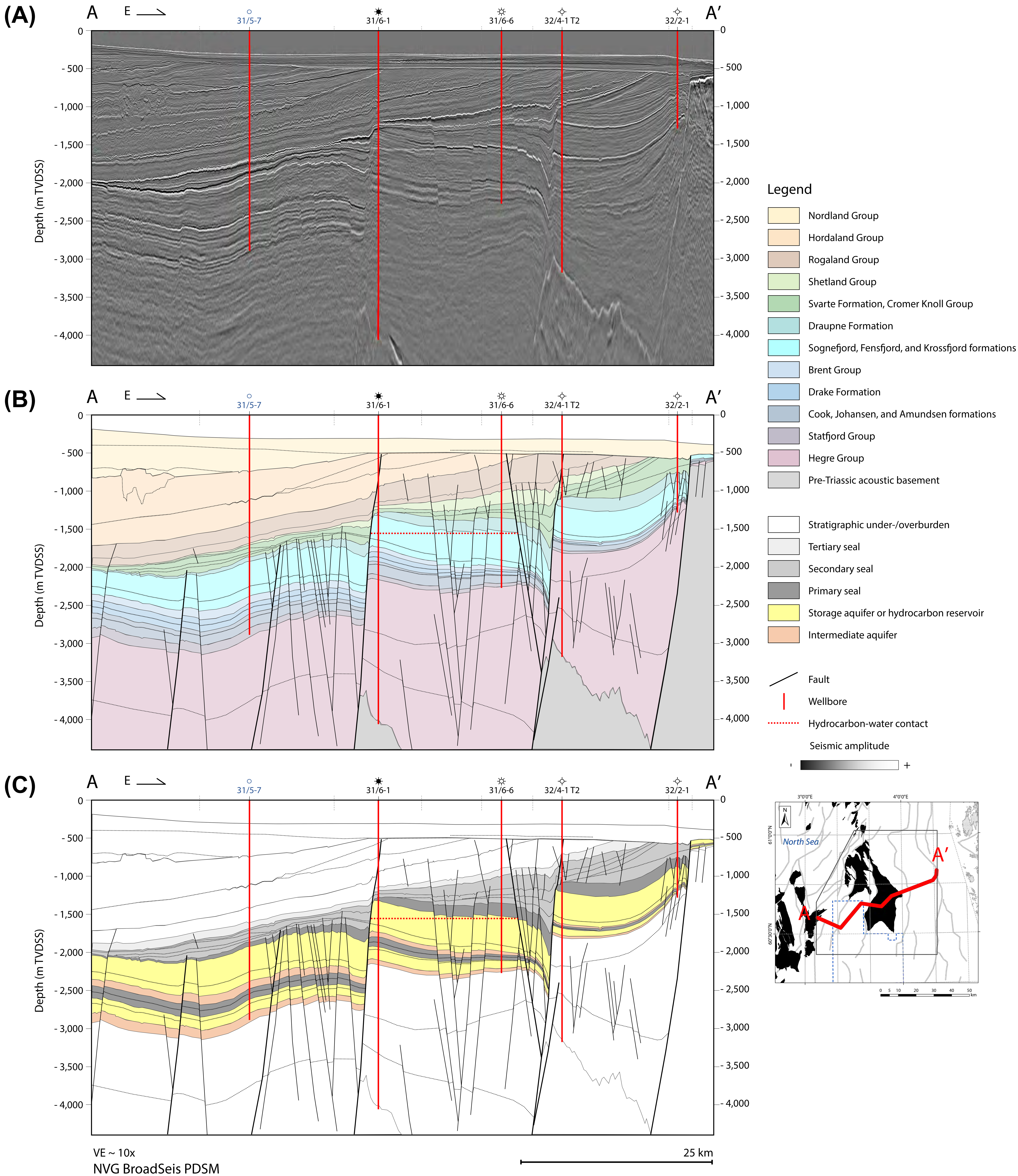
(A)
(B)
(C)
A
E
A′
31/5-7
31/6-1
31/6-6
32/4-1 T2
32/2-1
Depth (m TVDSS)
0
- 500
- 1,000
- 1,500
- 2,000
- 2,500
- 3,000
- 3,500
- 4,000
Legend
Nordland Group
Hordaland Group
Rogaland Group
Shetland Group
Svarte Formation, Cromer Knoll Group
Draupne Formation
Sognefjord, Fensfjord, and Krossfjord formations
Brent Group
Drake Formation
Cook, Johansen, and Amundsen formations
Statfjord Group
Hegre Group
Pre-Triassic acoustic basement
Stratigraphic under-/overburden
Tertiary seal
Secondary seal
Primary seal
Storage aquifer or hydrocarbon reservoir
Intermediate aquifer
Fault
Wellbore
Hydrocarbon-water contact
Seismic amplitude
-
+
North Sea
3°0'0"E
4°0'0"E
VE ~ 10x
NVG BroadSeis PDSM
25 km

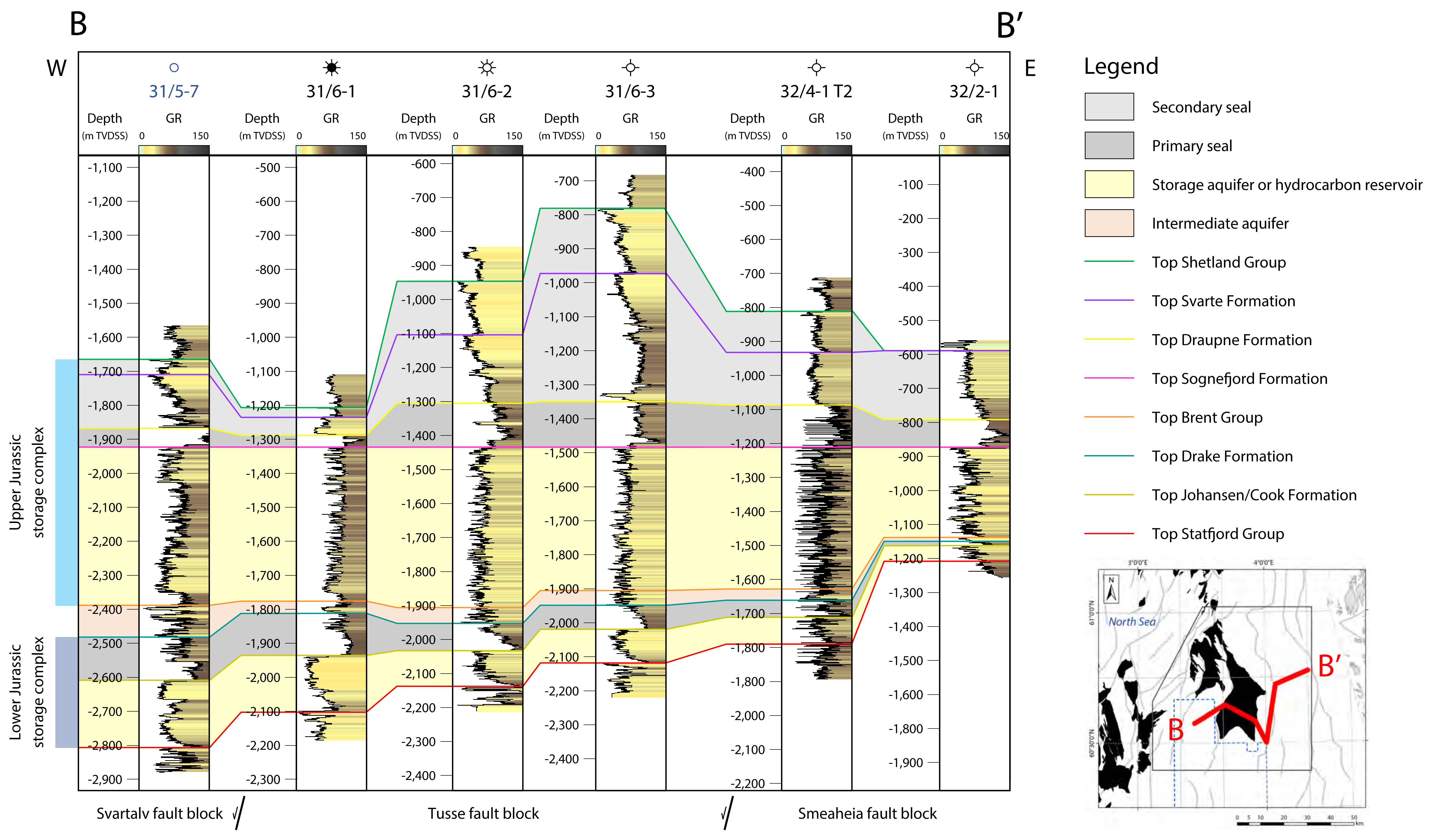
B
B′
W
E
31/5-7
31/6-1
31/6-2
31/6-3
32/4-1 T2
32/2-1
Depth (m TVDSS)
GR 0 150
-1,100 -1,200 -1,300 -1,400 -1,500 -1,600 -1,700 -1,800 -1,900 -2,000 -2,100 -2,200 -2,300 -2,400 -2,500 -2,600 -2,700 -2,800 -2,900
-500 -600 -700 -800 -900 -1,000 -1,100 -1,200 -1,300 -1,400 -1,500 -1,600 -1,700 -1,800 -1,900 -2,000 -2,100 -2,200 -2,300
-600 -700 -800 -900 -1,000 -1,100 -1,200 -1,300 -1,400 -1,500 -1,600 -1,700 -1,800 -1,900 -2,000 -2,100 -2,200 -2,300 -2,400
-700 -800 -900 -1,000 -1,100 -1,200 -1,300 -1,400 -1,500 -1,600 -1,700 -1,800 -1,900 -2,000 -2,100 -2,200 -2,300 -2,400
-400 -500 -600 -700 -800 -900 -1,000 -1,100 -1,200 -1,300 -1,400 -1,500 -1,600 -1,700 -1,800 -1,800 -2,000 -2,100 -2,200
-100 -200 -300 -400 -500 -600 -700 -800 -900 -1,000 -1,100 -1,200 -1,300 -1,400 -1,500 -1,600 -1,800 -1,900
Upper Jurassic storage complex
Lower Jurassic storage complex
Svartalv fault block
Tusse fault block
Smeaheia fault block
Legend
Secondary seal
Primary seal
Storage aquifer or hydrocarbon reservoir
Intermediate aquifer
Top Shetland Group
Top Svarte Formation
Top Draupne Formation
Top Sognefjord Formation
Top Brent Group
Top Drake Formation
Top Johansen/Cook Formation
Top Statfjord Group
North Sea
3°0'0"E
4°0'0"E
61°0'0"N
60°30'0"N
N
0 5 10 20 30 40 50 km

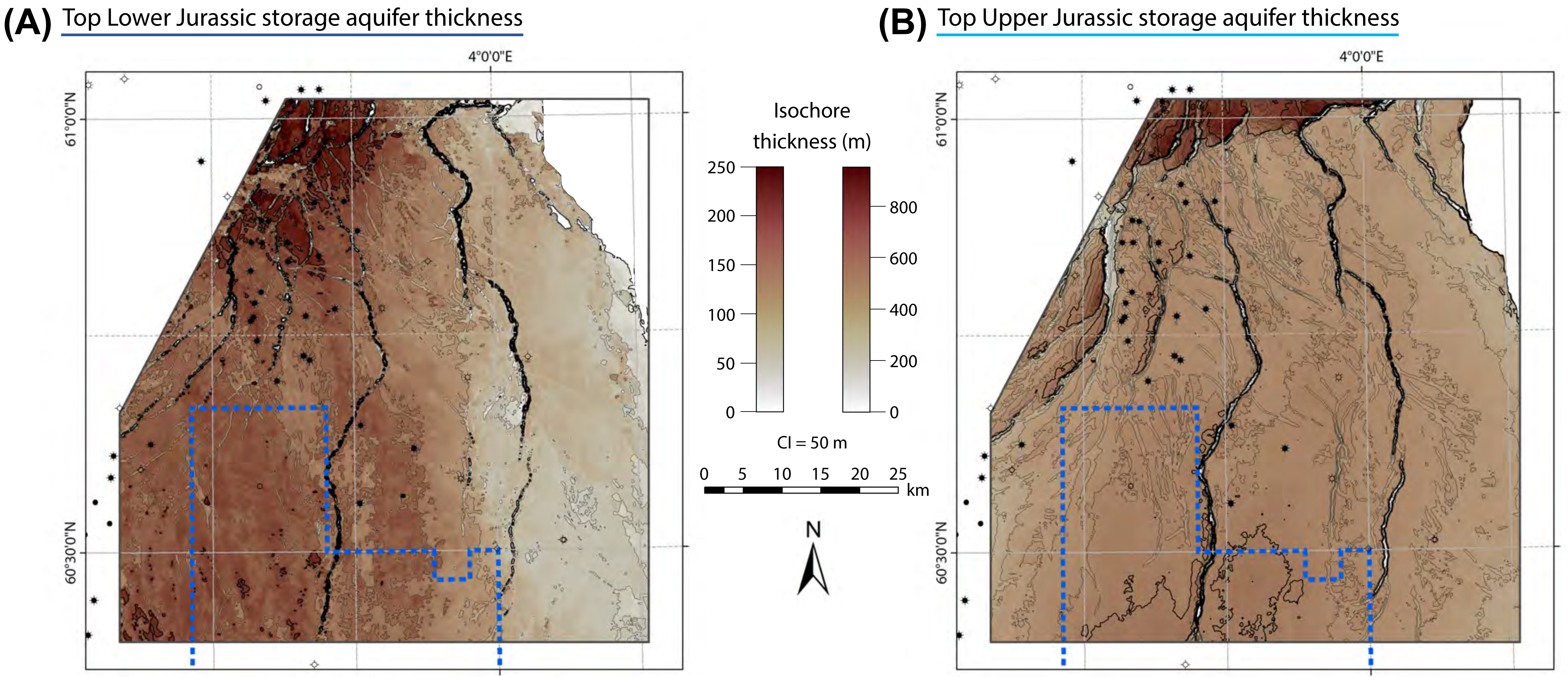
(A) Top Lower Jurassic storage aquifer thickness
(B) Top Upper Jurassic storage aquifer thickness
4°0'0"E
61°0'0"N
60°30'0"N
Isochore thickness (m)
250
200
150
100
50
0
800
600
400
200
0
CI = 50 m
0 5 10 15 20 25 km
N

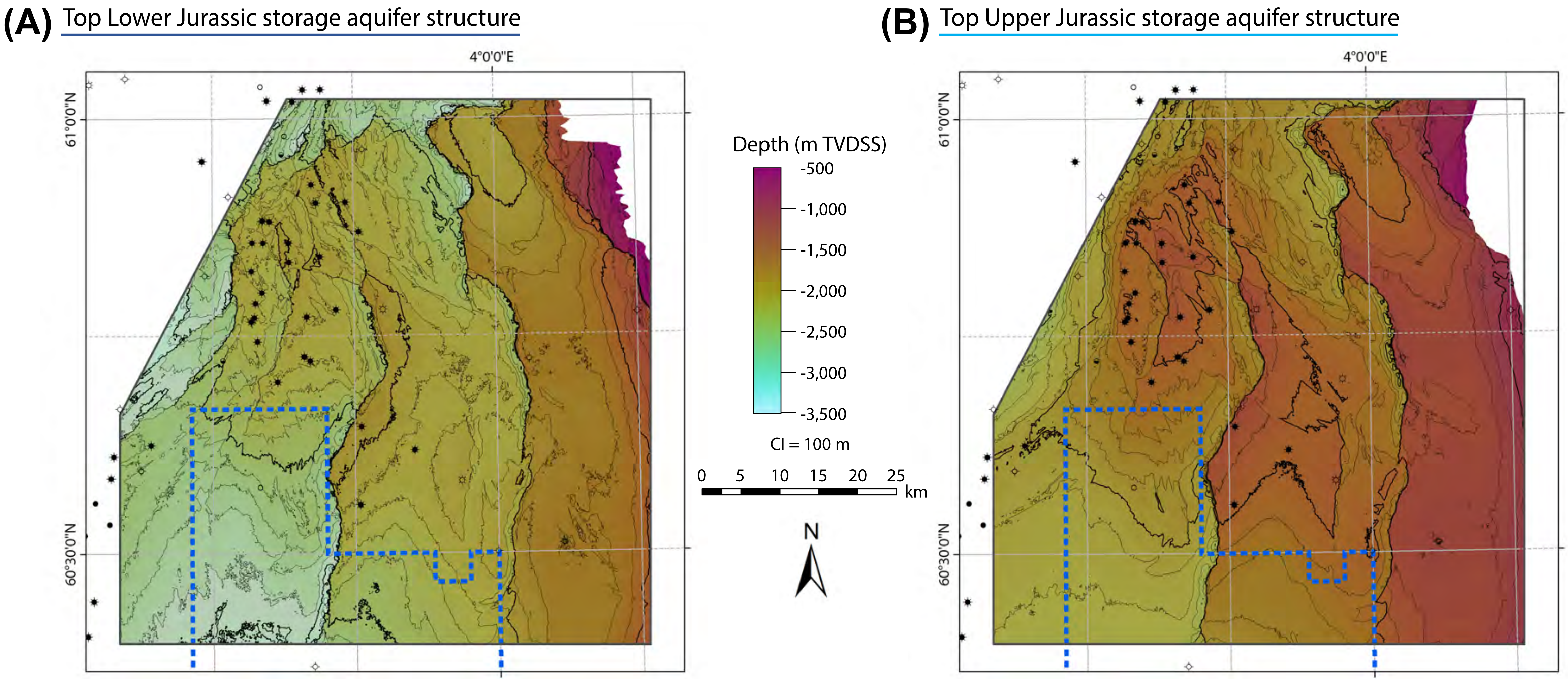

(A)
Top Lower Jurassic storage aquifer structure
(B)
Top Upper Jurassic storage aquifer structure
4°0'0"E
61°0'0"N
60°30'0"N
Depth (m TVDSS)
-500
-1,000
-1,500
-2,000
-2,500
-3,000
-3,500
CI = 100 m
0 5 10 15 20 25
km
N

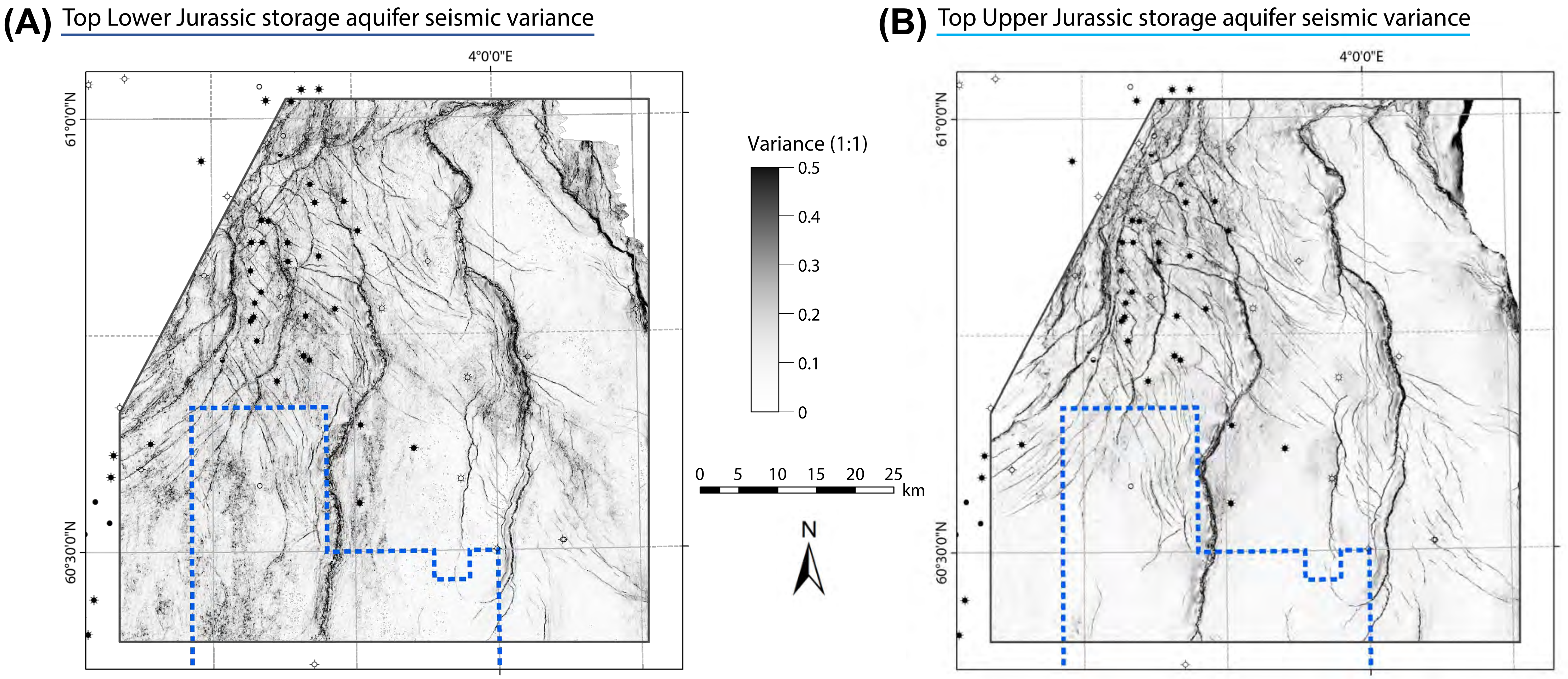
(A) Top Lower Jurassic storage aquifer seismic variance
4°0'0"E
61°0'0"N
60°30'0"N
(B) Top Upper Jurassic storage aquifer seismic variance
4°0'0"E
61°0'0"N
60°30'0"N
Variance (1:1)
0.5
0.4
0.3
0.2
0.1
0
0 5 10 15 20 25
km
N

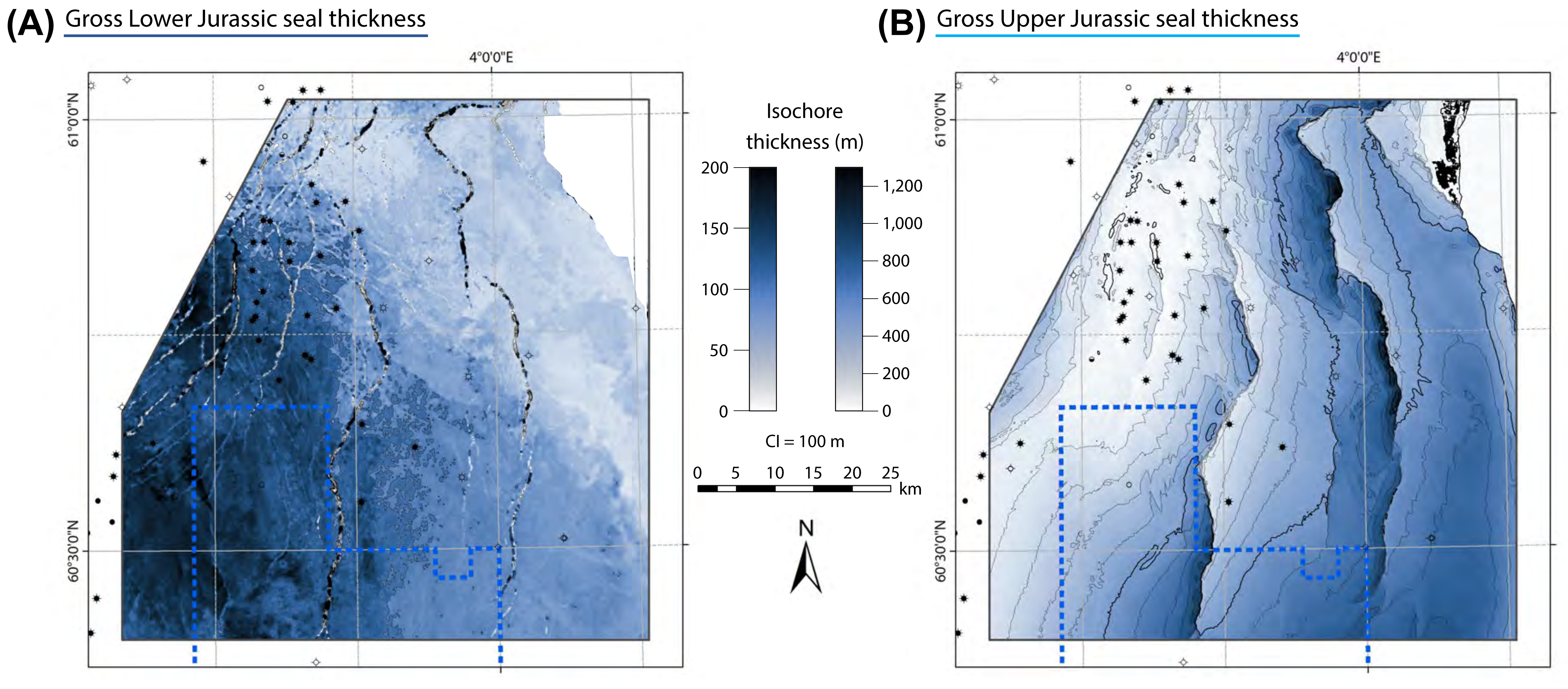

(A) Gross Lower Jurassic seal thickness
(B) Gross Upper Jurassic seal thickness
4°0'0"E
61°0'0"N
60°30'0"N
Isochore thickness (m)
200
150
100
50
0
1,200
1,000
800
600
400
200
0
CI = 100 m
0 5 10 15 20 25
km
N

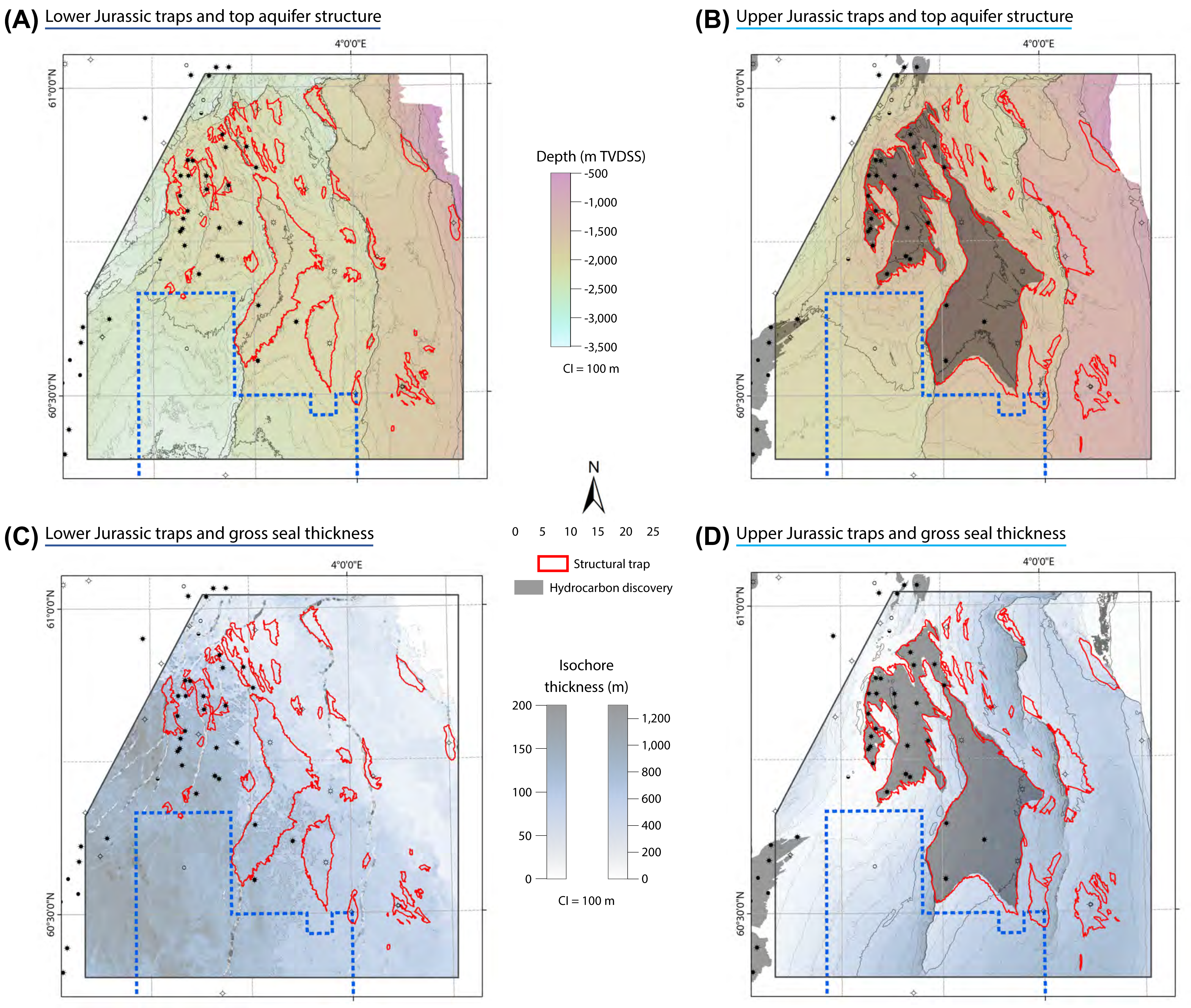

(A) Lower Jurassic traps and top aquifer structure
(B) Upper Jurassic traps and top aquifer structure
(C) Lower Jurassic traps and gross seal thickness
(D) Upper Jurassic traps and gross seal thickness
4°0'0"E
61°0'0"N
60°30'0"N
Depth (m TVDSS)
-500
-1,000
-1,500
-2,000
-2,500
-3,000
-3,500
CI = 100 m
N
0 5 10 15 20 25
Structural trap
Hydrocarbon discovery
Isochore thickness (m)
200
150
100
50
0
1,200
1,000
800
600
400
200
0
CI = 100 m

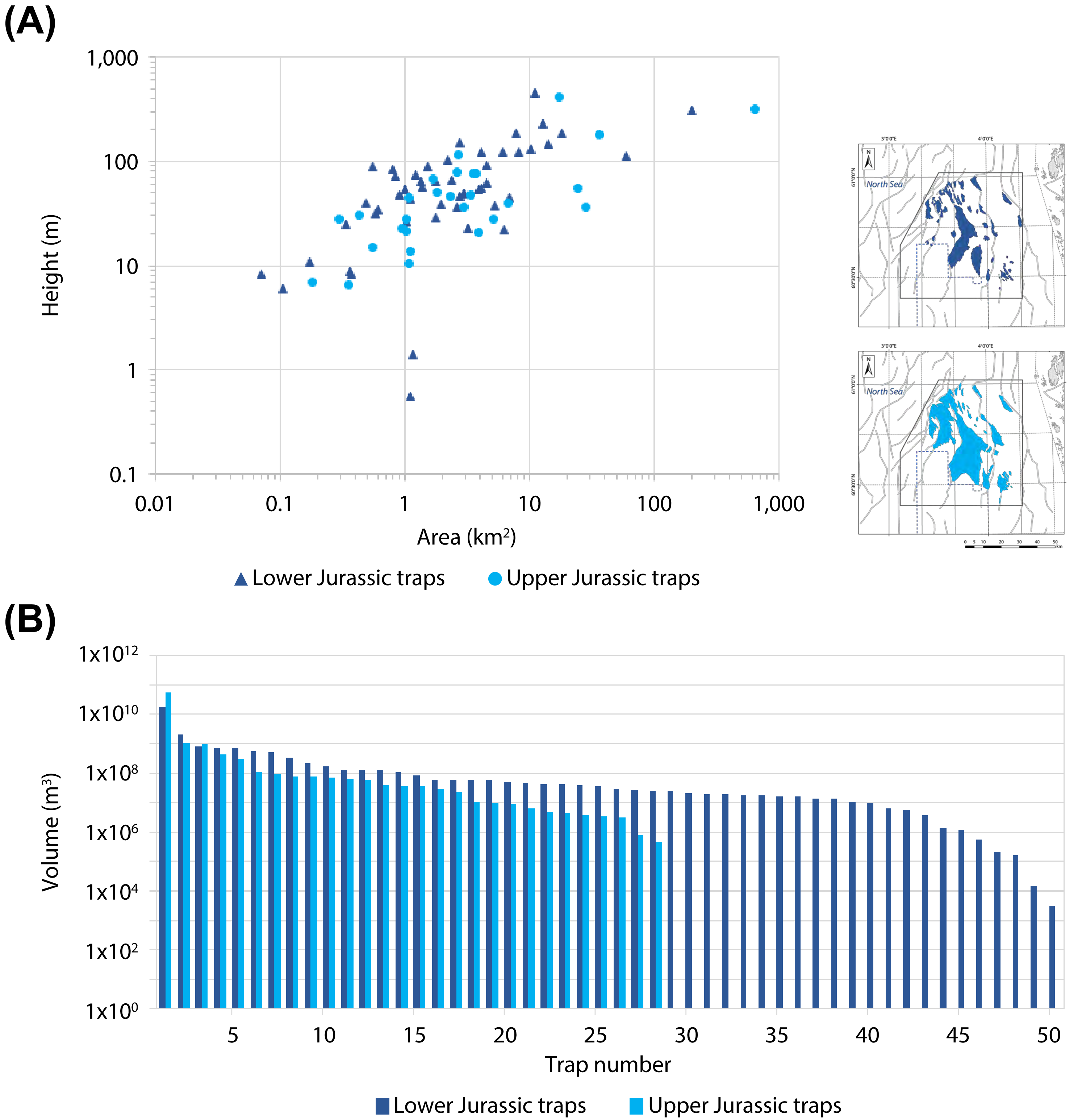

(A)
1,000
100
10
1
0.1
Height (m)
0.01
0.1
1
10
100
1,000
Area (km²)
Lower Jurassic traps
Upper Jurassic traps
North Sea
North Sea
(B)
1x10¹²
1x10¹⁰
1x10⁸
1x10⁶
1x10⁴
1x10²
1x10⁰
Volume (m³)
5
10
15
20
25
30
35
40
45
50
Trap number
Lower Jurassic traps
Upper Jurassic traps

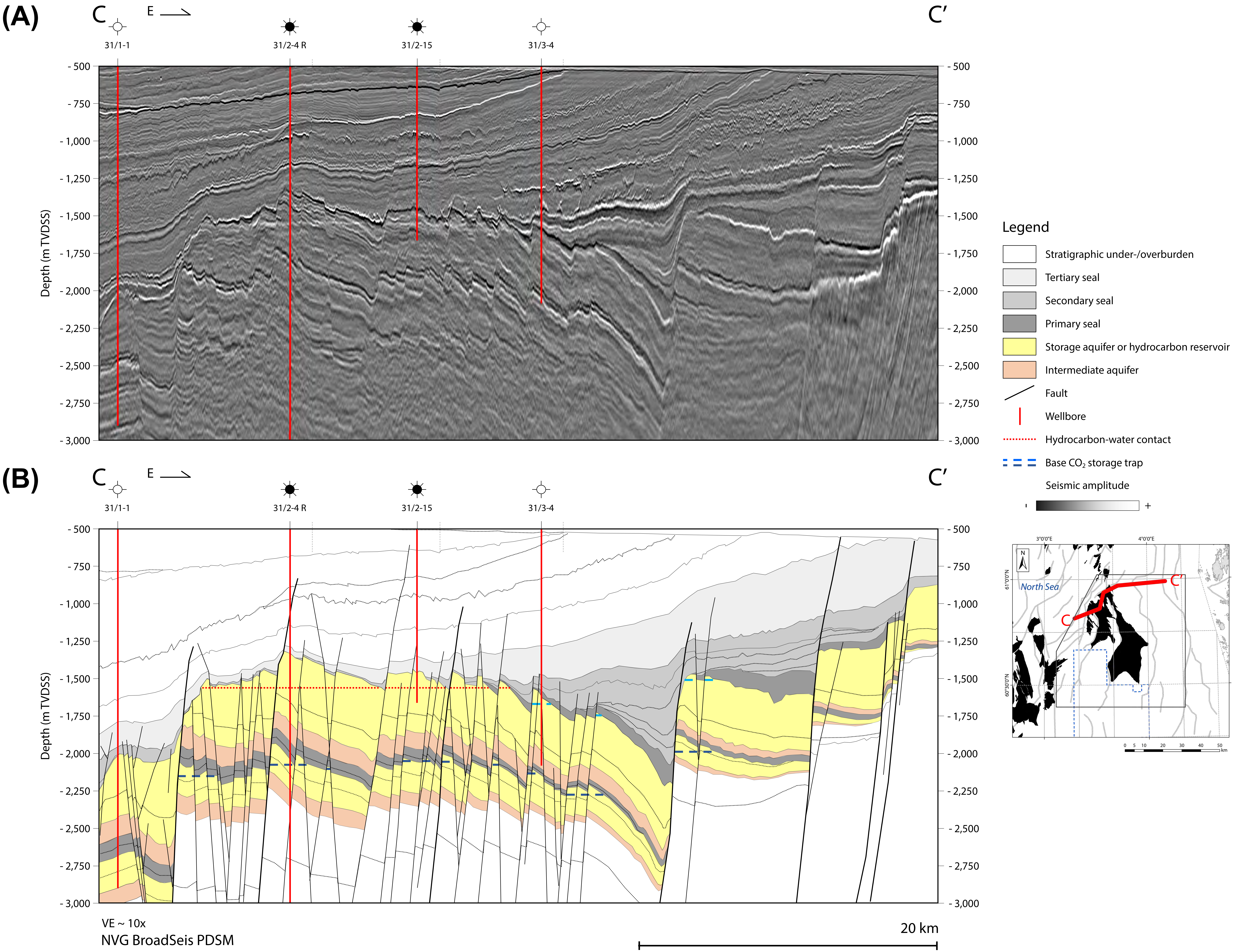
(A)
C
E
C'
31/1-1
31/2-4 R
31/2-15
31/3-4
Depth (m TVDSS)
- 500
- 750
- 1,000
- 1,250
- 1,500
- 1,750
- 2,000
- 2,250
- 2,500
- 2,750
- 3,000
(B)
VE ~ 10x
NVG BroadSeis PDSM
20 km
Legend
Stratigraphic under-/overburden
Tertiary seal
Secondary seal
Primary seal
Storage aquifer or hydrocarbon reservoir
Intermediate aquifer
Fault
Wellbore
Hydrocarbon-water contact
Base CO_2 storage trap
Seismic amplitude
-
+
North Sea
3°0'0"E
4°0'0"E
61°0'0"N
60°30'0"N
0 5 10 20 30 40 50
km

(A)
D
E
D′
31/5-7
31/5-5
31/2-1
31/2-2 R
31/3-1
31/3-3
Depth (m TVDSS)
- 500
- 750
- 1,000
- 1,250
- 1,500
- 1,750
- 2,000
- 2,250
- 2,500
- 2,750
- 3,000
(B)
D
E
D′
31/5-7
31/5-5
31/2-1
31/2-2 R
31/3-1
31/3-3
Depth (m TVDSS)
VE ~ 10x
NVG BroadSeis PDSM
20 km
Legend
Stratigraphic under-/overburden
Tertiary seal
Secondary seal
Primary seal
Storage aquifer or hydrocarbon reservoir
Intermediate aquifer
Fault
Wellbore
Hydrocarbon-water contact
Base CO_2 storage trap
Seismic amplitude
-
+
North Sea
D′
D

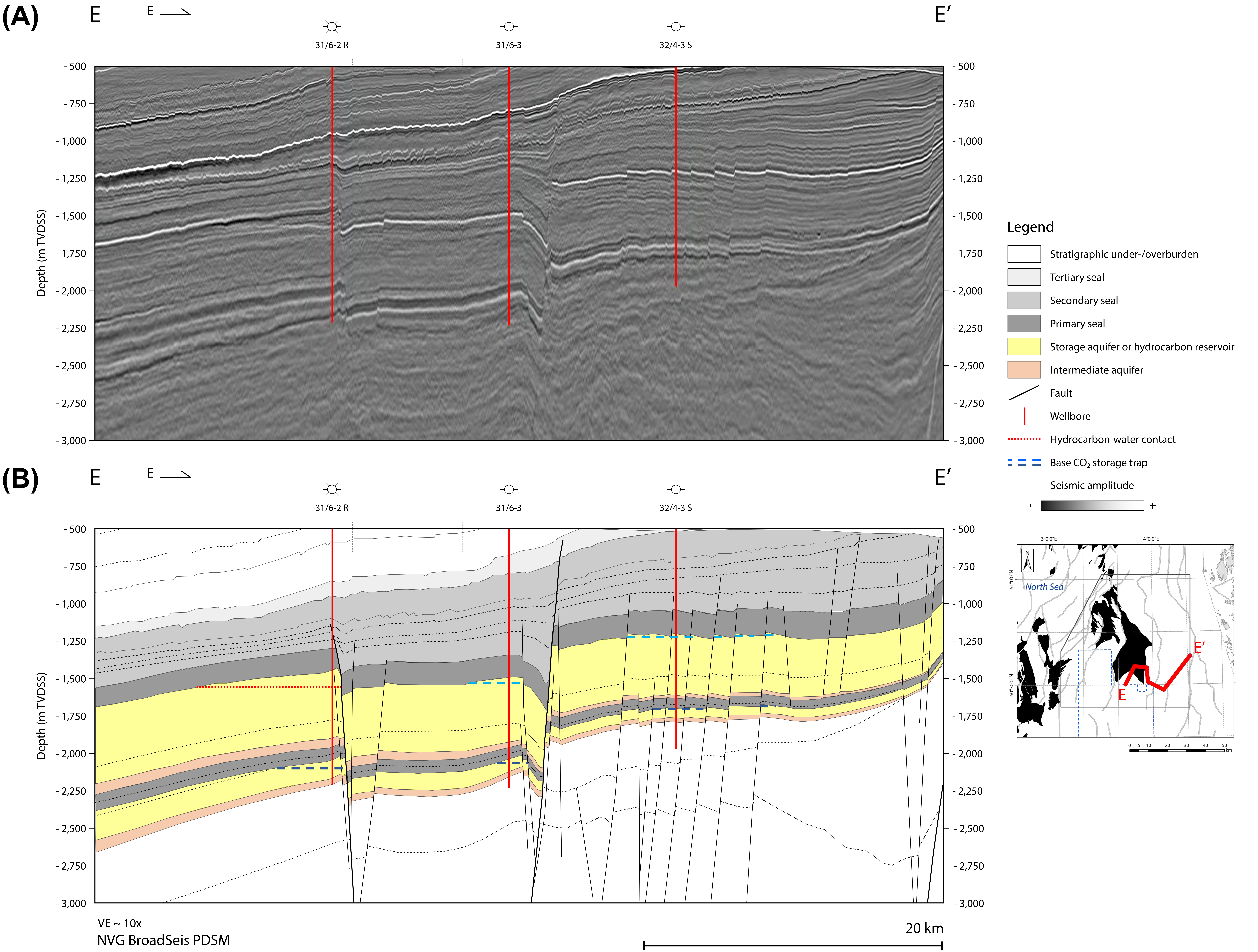
(A)
E
E
E′
31/6-2 R
31/6-3
32/4-3 S
Depth (m TVDSS)
- 500
- 750
- 1,000
- 1,250
- 1,500
- 1,750
- 2,000
- 2,250
- 2,500
- 2,750
- 3,000
(B)
Legend
Stratigraphic under-/overburden
Tertiary seal
Secondary seal
Primary seal
Storage aquifer or hydrocarbon reservoir
Intermediate aquifer
Fault
Wellbore
Hydrocarbon-water contact
Base CO_2 storage trap
Seismic amplitude
North Sea
VE ~ 10x
NVG BroadSeis PDSM
20 km

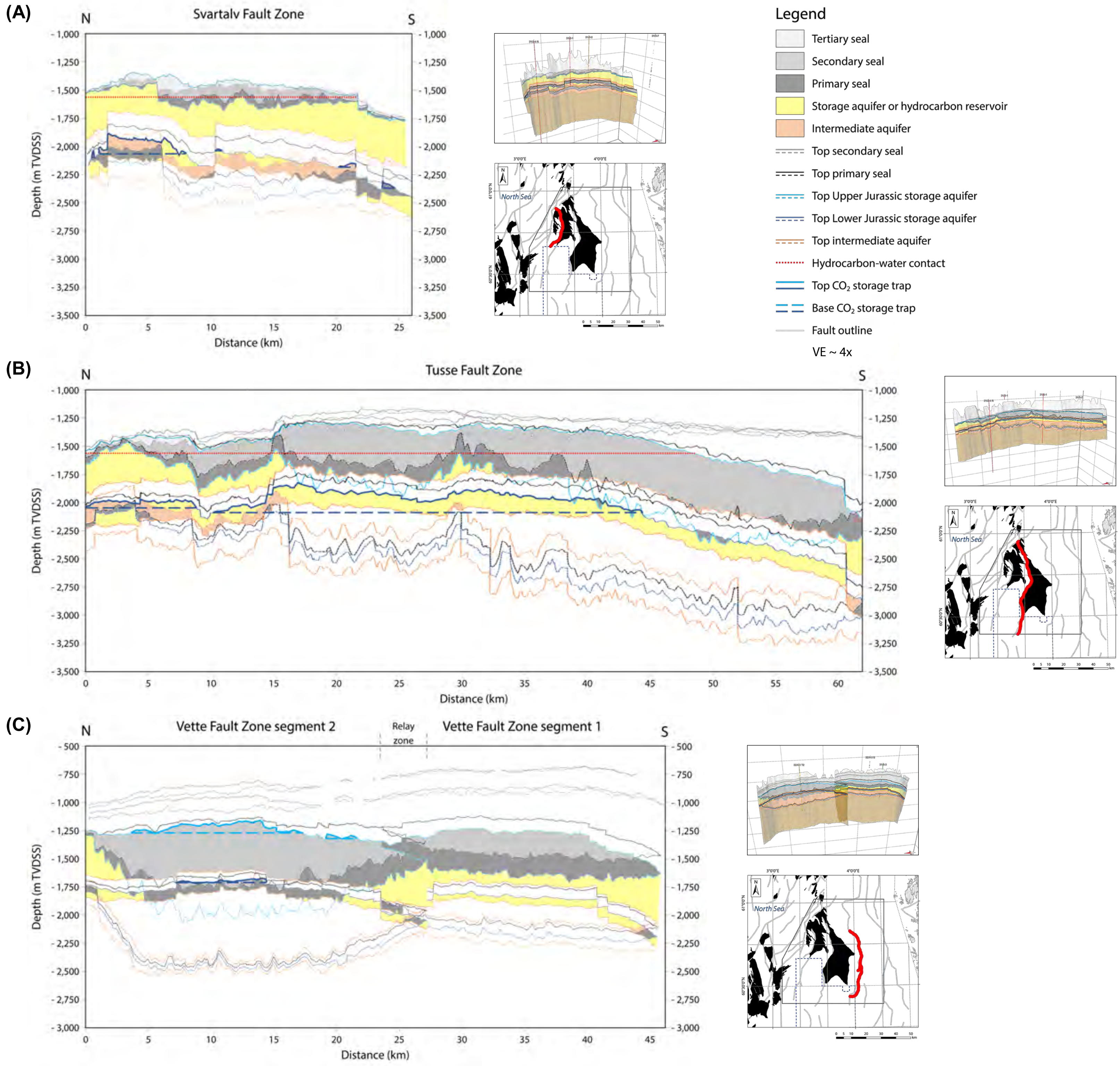

(A)
N
Svartalv Fault Zone
S
Depth (m TVDSS)
Distance (km)
North Sea
Legend
Tertiary seal
Secondary seal
Primary seal
Storage aquifer or hydrocarbon reservoir
Intermediate aquifer
Top secondary seal
Top primary seal
Top Upper Jurassic storage aquifer
Top Lower Jurassic storage aquifer
Top intermediate aquifer
Hydrocarbon-water contact
Top CO_2 storage trap
Base CO_2 storage trap
Fault outline
VE ~ 4x
(B)
N
Tusse Fault Zone
S
Depth (m TVDSS)
Distance (km)
North Sea
(C)
N
Vette Fault Zone segment 2
Relay zone
Vette Fault Zone segment 1
S
Depth (m TVDSS)
Distance (km)
North Sea

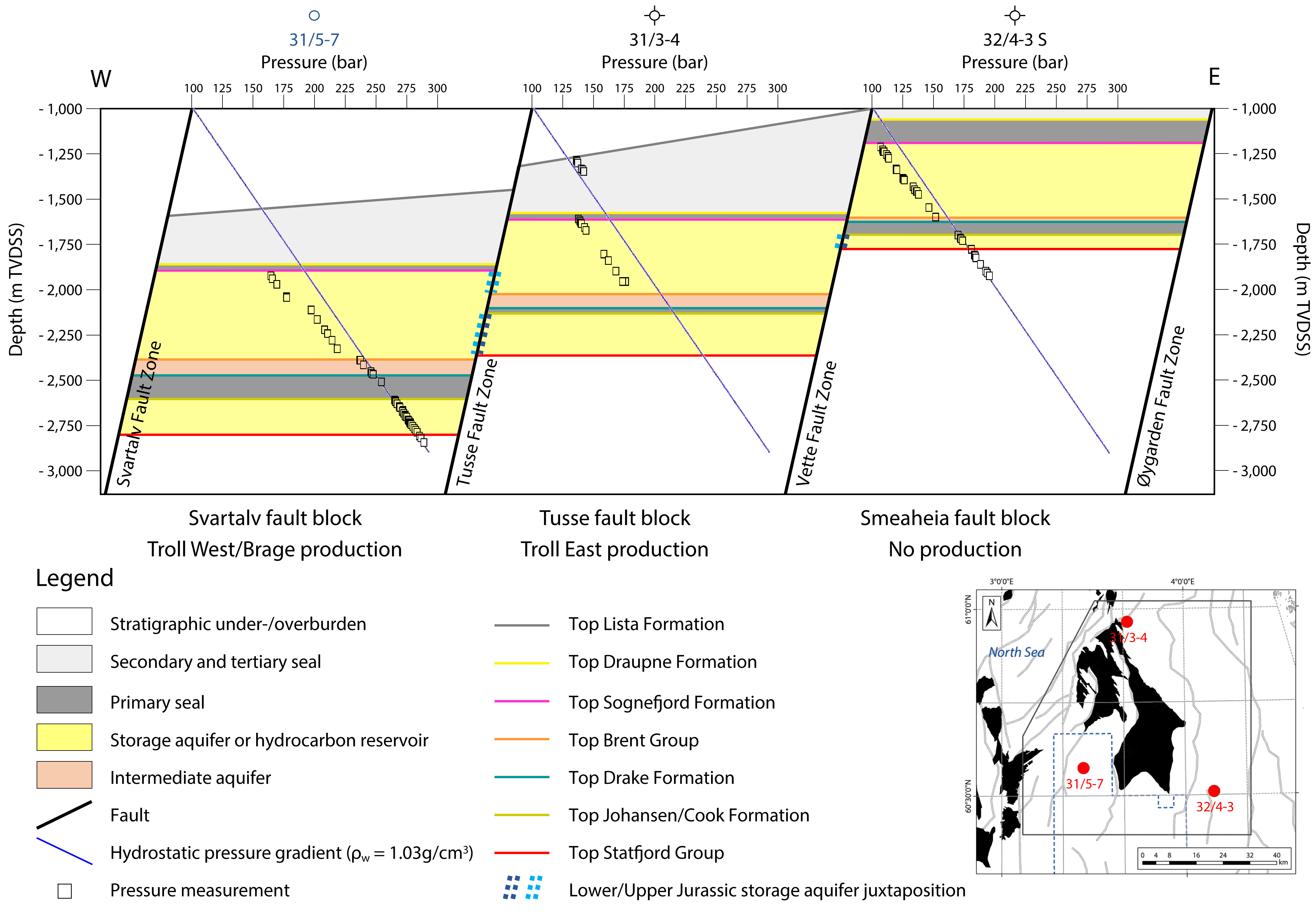
31/5-7
Pressure (bar)
31/3-4
Pressure (bar)
32/4-3 S
Pressure (bar)
W
E
100 125 150 175 200 225 250 275 300
Depth (m TVDSS)
- 1,000
- 1,250
- 1,500
- 1,750
- 2,000
- 2,250
- 2,500
- 2,750
- 3,000
Svartalv Fault Zone
Tusse Fault Zone
Vette Fault Zone
Øygarden Fault Zone
Svartalv fault block
Troll West/Brage production
Tusse fault block
Troll East production
Smeaheia fault block
No production
Legend
Stratigraphic under-/overburden
Secondary and tertiary seal
Primary seal
Storage aquifer or hydrocarbon reservoir
Intermediate aquifer
Fault
Hydrostatic pressure gradient (ρ_w = 1.03g/cm³)
Pressure measurement
Top Lista Formation
Top Draupne Formation
Top Sognefjord Formation
Top Brent Group
Top Drake Formation
Top Johansen/Cook Formation
Top Statfjord Group
Lower/Upper Jurassic storage aquifer juxtaposition
3°0'0"E
4°0'0"E
61°0'0"N
60°30'0"N
N
North Sea
31/3-4
31/5-7
32/4-3
0 4 8 16 24 32 40
km

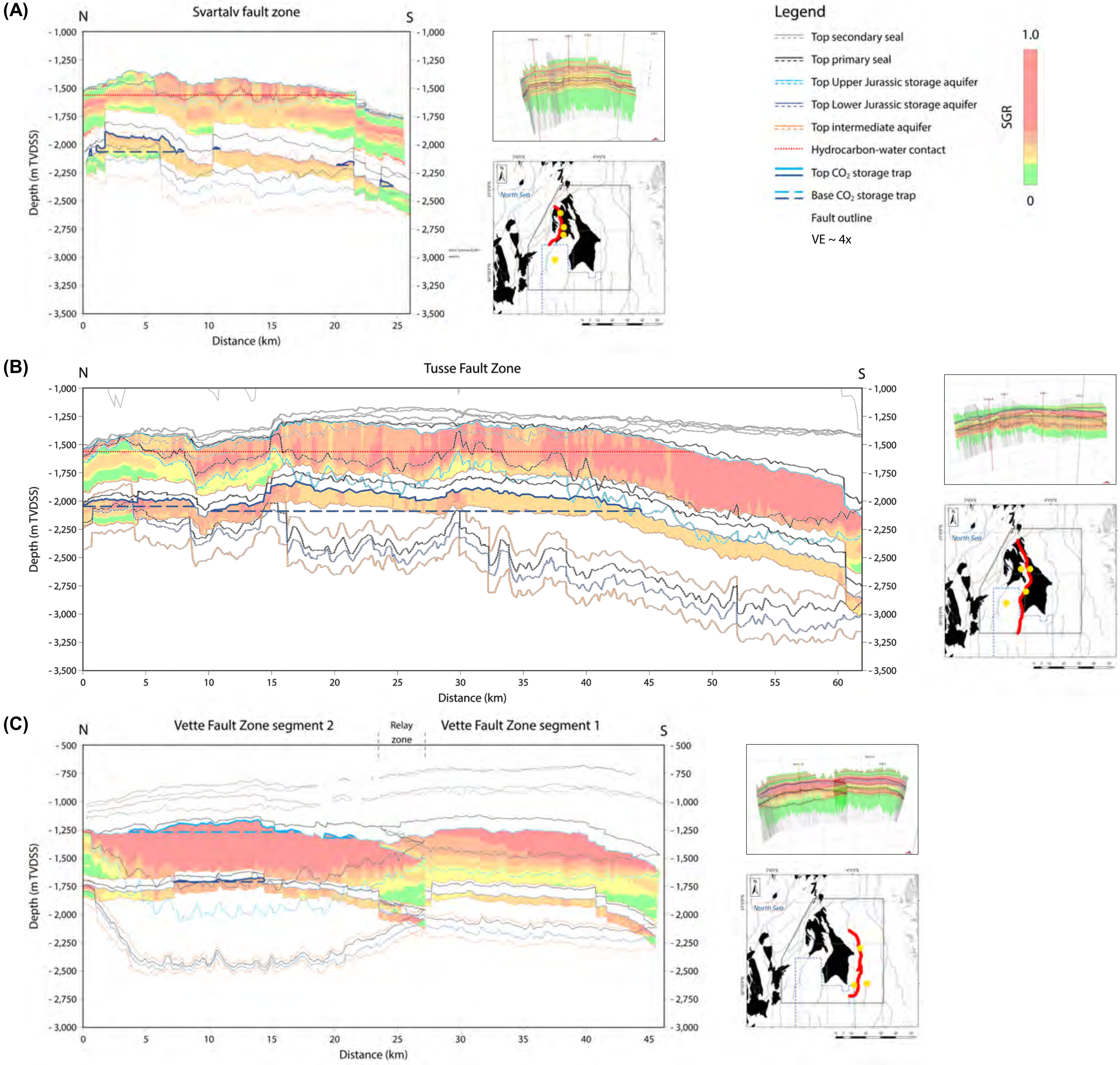

(A)
Svartalv fault zone
N
S
Depth (m TVDSS)
Distance (km)
Legend
Top secondary seal
Top primary seal
Top Upper Jurassic storage aquifer
Top Lower Jurassic storage aquifer
Top intermediate aquifer
Hydrocarbon-water contact
Top CO_2 storage trap
Base CO_2 storage trap
Fault outline
VE ~ 4x
SGR
1.0
0
North Sea
(B)
Tusse Fault Zone
(C)
Vette Fault Zone segment 2
Relay zone
Vette Fault Zone segment 1

Table 1

Storage complex	Attribute	Troll	Svartalv	Tusse	Smeaheia
Upper Jurassic	Gross storage aquifer thickness (m)	<10–540	300–530	340–510	215–445
	Relative aquifer pressure conditions	Depleation likely	High depleation	High depleation	Moderate depleation
	Primary and secondary seal thickness (m)	0–175	0–960	15–1260	150–735
	Required top seal units	P, S, T	P, S, T	P, S	P, S
	Top seal pressure barrier	Unknown	Unknown	Yes	Unknown
	Number of structural traps	1	1	16	12
	Total structural trap GRV (m^3)	5.39×10^{10}	5.39×10^{10}	5.49×10^{10}	2.53×10^{9}
Lower Jurassic	Gross storage aquifer thickness (m)	110–235	100–270	30–255	<10–145
	Relative aquifer pressure conditions	Unknown	Hydrostatic	Unknown	Hydrostatic
	Primary top seal thickness (m)	65–215	30–195	20–170	<10–105
	Required top seal units	P	P	P	P
	Top seal pressure barrier	Unknown	Yes	Unknown	Yes
	Number of structural traps	4	13	17	16
	Total structural trap GRV (m^3)	8.48×10^{8}	1.16×10^{9}	2.08×10^{10}	2.14×10^{9}

Table 2

Storage complex	Attribute	Svartalv	Tusse	Vette 1	Vette 2
Upper Jurassic	Juxtaposition scenarios	1, 2	1, 2	1, 2	1, 2
	Relative scenario 1 AFPD	Unknown	Low	Moderate	Moderate
	Relative scenario 3 AFPD	n/a	n/a	n/a	n/a
	Minimum scenario 1 SGR	<0.15	<0.15	<0.15	<0.15
	Minimum scenario 3 SGR	n/a	n/a	n/a	n/a
	Nature of HWC	Throughgoing	Throughgoing	n/a	n/a
Lower Jurassic	Juxtaposition scenarios	1, 2, 3	1, 2, 3, 4	1, 2, 3	1, 2, 3, 4
	Relative scenario 1 AFPD	Unknown	Unknown	Unknown	Unknown
	Relative scenario 3 AFPD	Unknown	Unknown	High	High
	Minimum scenario 1 SGR	<0.15	<0.15	<0.15	<0.15
	Minimum scenario 3 SGR	>0.15	>0.2	>0.15	~0.15
	Nature of HWC	n/a	n/a	n/a	n/a